



Title	Strategies to Use Frustrated Lewis Pairs Based on Conformational Isomerization of Lewis Acids or Lewis Bases
Author(s)	櫻羽, 真熙
Citation	大阪大学, 2024, 博士論文
Version Type	VoR
URL	https://doi.org/10.18910/96030
rights	
Note	

The University of Osaka Institutional Knowledge Archive : OUKA

<https://ir.library.osaka-u.ac.jp/>

The University of Osaka

Doctoral Dissertation

**Strategies to Use Frustrated Lewis Pairs Based on
Conformational Isomerization of Lewis Acids or
Lewis Bases**

Mahiro Sakuraba

December 2023

**Graduate School of Engineering
Osaka University**

Preface and Acknowledgements

The study in this thesis has been carried out under the direction of Professor Dr. Sensuke Ogoshi at the Department of Applied Chemistry, Graduate School of Engineering, Osaka University from April 2017 to March 2020 and from April 2021 to March 2024. This thesis describes the strategies to use frustrated Lewis pairs based on conformational isomerization of Lewis acids or Lewis bases.

Firstly, I would like to express my gratitude to Professor Dr. Sensuke Ogoshi for invaluable suggestions, discussions, and heartfelt encouragement throughout my Ph.D. study and related research. I would like to thank the rest of my thesis committee: Professor Dr. Koji Hirano and Professor Dr. Makoto Yasuda for their insightful comments and encouragement, but also for the hard question which invented me to widen my research from various perspectives.

I would like to express my grateful thanks to associate Professor Dr. Yoichi Hoshimoto for a great number of suggestions not only about my research but also my life, heartfelt encouragement for my research and laboratory life, and meaningful discussions. I would like to extend my gratitude to the group staffs: Assistant Professor Dr. Ryohei Doi, Professor Dr. Masato Ohashi (Osaka Metropolitan University), Assistant Professor Dr. Hiroaki Iwamoto, Assistant Professor Dr. Kotaro Kikushima (Ritsumeikan University), postdoctoral fellow Dr. Amit Kumar Jaiswal, and postdoctoral fellow Dr. Sunit Hazra for their continuous guidance, advice and assistance. I am also deeply grateful to the secretaries: Ms. Yukiko Mori, Chika Sugiki, Yuri Kishimoto, and Noriko Fujimoto for their kind help and heart-warming encouragement.

I thank my fellow labmates: Mr. Hiroto Imiya, Mr. Junu Kim, Ms. Anna Shigaki, Ms. Chika Nishimura, and Mr. Kodai Fukudome for the heartfelt encouragements to each other, improving together, and for all the fun we have had in our laboratory life and private time. I am deeply indebted to my respectful seniors in the Ogoshi Group: Dr. Hironobu Sakaguchi, Dr. Takuya Kinoshita, Dr. Takuya Kawashima, Dr. Hiroshi Shirataki, Dr. Takahiro Asada, Dr. Keita Ashida, Mr. Takaya Hinogami, Dr. Naoyoshi Ishida, Mr. Kazuya Ishimoto, Dr. Yasuhiro Yamauchi, Mr. Kota Ando, Mr. Yu Hashimoto, Ms. Shiori Kusaka, Mr. Takafumi Ono, Mr. Yugo Ueda, Ms. Tinghui Yu, Mr. Hideki Ito, Mr. Takahiro Kawakita, Mr. Wataru Sahashi, Ms. Emi Dennise Sunagawa, Mr. Nozomi Yasui, Ms. Inas Wafiya, Ms. Chiharu Akatsuka, Mr. Takuya Tsuruta, Shun Nagai, Mr. Taiki Hashimoto, Ms. Reina Okamoto, Mr. Koki Kajiwara, Mr. Daiki Kitazoe, Mr. Lueangratana Pacharapaul, Mr. Naoki Kajita, Mr. Yuyang Zhou, Mr. Taiki Negoro, Mr. Keisuke Nozaki, Mr. Yutaka Mondori, Mr. Kenta Koh, Ms. Setsuka Homma, Mr. Nobutaka Mito, Mr. Taichi Morishita, Mr. Genki Yamaguchi, and Mr. Chihiro Yamaguchi for their helpful advice and kind encouragements. I thank all of my juniors in the Ogoshi Group: Mr. Koki Kambe, Mr. Yusuke Goto, Mr. Yusuke Tokura, and Mr. Ryosuke Harada for their helpful assistance and heartfelt communications. I also thank the visiting research students: Mr. David Scott, Mr. Nicholas Andrella, Mr. Andy, and Mr. Coco for sharing good times.

I have also received a lot of advice from other groups for my Ph.D. study. I explain my gratitude to Professor Dr. Jun-ya Hasegawa (Hokkaido University), Mr. Masaki Ohbo (Hokkaido University), and Mr. Manussada Ratanasak (Hokkaido University) for meaningful suggestions to theoretical studies in Chapter 1. I am grateful to Professor Dr. Takashi Hayashi, associate Professor Dr. Koji Oohora, and Assistant Professor Dr. Shunsuke Kato for their helpful advice for the electrospray ionization mass spectroscopy analyses. I would like to express my special thanks to the Analytical Instrumentation Facility, Graduate School of Engineering, Osaka University, for the measurement of spectral and analytical data. Especially, I am grateful to Assistant Professor Dr. Kyoko Inoue for her advice for the nuclear magnetic resonance analyses, and technical specialist Mr. Hiroaki Tanaka for his advice for the mass spectrometry.

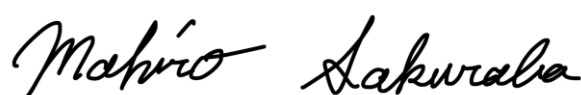
I thank AIR WATER INC. for providing the gaseous mixture mentioned in Chapter 2 as industrial crude H₂ and Kuraray Co. Ltd. for providing 4-methyltetrahydropyran (MTHP).

My sincere thanks also go to Professor Dr. Cathleen Crudden (Queen's University), who provided me an opportunity to join her group as a visiting research student (from April 2023 to July 2023 in Kingston, Canada). I am also grateful to her labmates: Dr. Tetyana Levchenko, Dr. Ahmadreza Nezamzadeh, Dr. Rob Nolla-Saltiel, Dr. Zeng Rong, Dr. Kumar Siddhant, Dr. Monika, Dr. Emily Albright, Mr. Mark Aloisio, Ms. Jana Alpin, Ms. Alannah Constable, Mr. Aaron Erlich, Mr. Florian Handel, Mr. Andrew Laluk, Ms. Viv Kulkarni, Dr. Dianne S. Lee, Ms. Dana Nanan, Ms. Anastasia Messina, Mr. Angus Sullivan, Ms. Stefanie Schiele, and Ms. Salma Elmallah for sharing wonderful time and their grateful help. I am also deeply grateful to the Crudden group's secretary: Ms. Megan Bruce for her heartfelt help.

I acknowledge a JST SPRING grant (September 2021–March 2023) and a Grant-in-Aid for Japan Society for the Promotion of Science (JSPS) Research Fellow (April 2023–March 2024).

Finally, I would like to express my utmost gratitude to my parents, Mr. Ichiro Sakuraba and Ms. Keiko Sakuraba for their attentive support and warm encouragement.

January 2024

A handwritten signature in black ink, reading "Mahiro Sakuraba". The signature is fluid and cursive, with the first name "Mahiro" and the last name "Sakuraba" clearly distinguishable.

Mahiro Sakuraba

Contents

General Introduction	1
Chapter 1	6
Mechanistic Studies on Thermal-Responsive Generation of FLPs from PoxIm–BAr ₃ Adducts by Phosphinoyl Rotation	
Chapter 2	37
Remote Back Strain for Catalytic Hydrogenation of Carbonyl Compounds Using Crude H ₂	
Chapter 3	58
Studies on Details of Remote Back Strain	
Conclusion	90
List of Publications	91

Abbreviations

The following abbreviations are used in this thesis.

Ac	acetate
acac	acetylacetonate
AIM	atoms in molecules
atm	atmospheric pressure
aq.	aqueous
Ar	aryl
BAr ₃	triarylborane
br	broad
Bu	butyl
calcd	calculated
cat.	catalyst
cf.	confer
CH ₄	methane
CLA	classical Lewis adduct
CO	carbon monoxide
CO ₂	carbon dioxide
conv.	conversion
COSY	correlation spectroscopy
°C	degrees Celsius
d	doublet
δ	chemical shift of NMR signal in ppm
DCE	1,2-dichloroethane
DFT	density functional theory
Dipp	2,6-diisopropylphenyl
DMF	<i>N,N</i> -dimethylformamide
Dtbp	3,5-di- <i>tert</i> -butylphenyl
EI	electron ionization
equiv	equivalent
ESI	electrospray ionization
Et	ethyl
Eqn.	Equation
FLP	frustrated Lewis pair
GC	gas chromatography
GPC	Gel permeation chromatography
h	hour(s)
H ₂	molecular hydrogen
HMBC	hetero-nuclear multiple-bond connectivity
HMQC	hetero-nuclear multiple quantum coherence
HPLC	high performance liquid chromatography
HRMS	high-resolution mass spectra
Hz	hertz
<i>i</i>	iso
IRC	intrinsic reaction coordinate
<i>J</i>	coupling constant in NMR
k	kilo

LA	Lewis acid
LB	Lewis base
LDA	lithium diisopropylamine
LUMO	lowest unoccupied molecular orbital
M	mega
m	multiplet
<i>m</i>	meta
Me	methyl
Mes	mesityl
min	minute(s)
mL	milliliter
μL	microliter
MS	mass spectrometry
MS	molecular sieves
MTHP	4-methyltetrahydropyrane
<i>n</i>	normal
NCI	non covalent interaction
NHC	<i>N</i> -heterocyclic carbene
NMR	nuclear magnetic resonance
<i>o</i>	ortho
ref.	reference
<i>p</i>	para
Ph	phenyl
pin	pinacolato
Pr	propyl
q	quartet
rt	room temperature
s	singlet
s	second
SC	single crystal
sec	second
sept	septet
SI	supporting information
t	triplet
<i>t</i>	tertiary
Tf	trifluoromethylsulfonyl
<i>tert</i>	tertiary
THF	tetrahydrofuran
TMS	trimethylsilyl
TOF	time-of-flight
Tol	tolyl
TON	turn over number
TS	transition state
UV	ultraviolet
vs	versus
VT	variable temperature
XRD	X-ray diffraction

General Introduction

Frustrated Lewis pairs (FLPs) have attracted much attention over the past two decades due to their high reactivity toward small molecules, e.g. molecular hydrogen (H_2), carbon monoxide (CO), and carbon dioxide (CO_2).¹⁻⁴ In particular, FLPs have been widely applied to catalytic molecular transformations such as the catalytic hydrogenation of unsaturated molecules.^{1,2} Currently, chemists are continuously devoting their efforts to develop practical and sustainable (catalytic) molecular transformations using less-toxic main-group elements.

FLPs are recognized as transient encounter complexes stabilized by noncovalent interactions (NCIs) between Lewis acids (LAs) and Lewis bases (LBs), while the formation of classical Lewis adducts (CLAs) was effectively prevented by steric repulsion between them.¹ Moreover, FLPs often tend to decompose quickly under ambient conditions,¹⁻³ which should restrict their facile use in organic synthesis. It should be thus worthwhile to establish a strategy to generate FLPs from isolable and shelf-stable CLAs effectively, as such a 'frustration revival strategy' can further expand the utility and hence applications of FLPs in organic chemistry (Figure 1).⁵

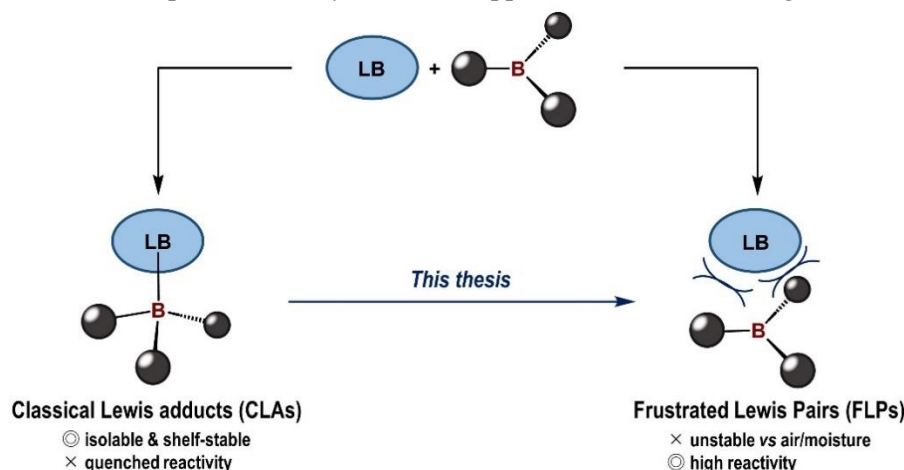


Figure 1. Generation of classical Lewis adducts (CLAs) and frustrated Lewis pairs (FLPs) through the reaction between Lewis acids (LAs) and Lewis bases (LBs).

In the context of the frustration revival strategy, an external-stimuli-responsive reaction system is a practical method.⁵⁻⁸ For example, it has been reported that $B(C_6F_5)_3$ and 2,6-dimethylpiperidine form CLA at room temperature, and heterolytic cleavage of H_2 is proceeded through generation of FLP when CLA is heating (Figure 2a).^{6b} It has also been reported that the silylium complex $[^iPr_3Si-P^tBu_3]^+[B(C_6F_5)_4]^-$ generates FLP at 90 °C and cleaves H_2 heterolytically (Figure 2b).^{6c}

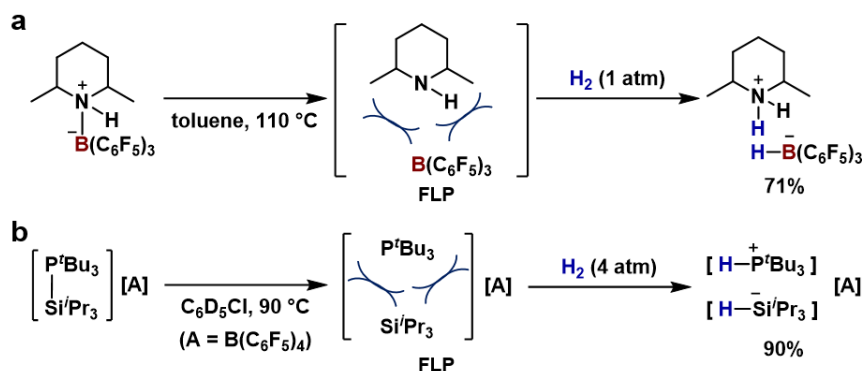


Figure 2. Thermally induced FLPs from CLAs comprising (a) B(C₆F₅)₃ and 2,6-dimethylpiperidine, (b) The system between silylium and P⁺tBu₃.

On the other hand, an external-stimuli-responsive conformational isomerization has been also used for generating FLPs from CLAs. As a pioneering example, our group has developed the thermal revival system of FLPs from *N*-phosphine-oxide-substituted imidazolyidenes (PoxIm)s–borane adduct by rotation of the *N*-phosphinoyl moiety. (Figure 3).^{5,7} PoxIm)s have syn (C–N–P–O: ca. 20°) and anti (C–N–P–O: ca. 180°) conformers based on the relative orientation of the carbene carbon and phosphinoyl oxygen atoms with respect to the N–P bonds, and their interconversion occurs through the rotation of the phosphinoyl group ($\Delta E^\ddagger \sim 12 \text{ kcal mol}^{-1}$). However, details on reaction mechanisms for the generation of FLP species from the PoxIm–borane adduct remained unclear. Based on these backgrounds, I have studied the detailed reaction mechanism on revival of FLPs from PoxIm–borane adducts shown in Figure 1.5 in Chapter 1.

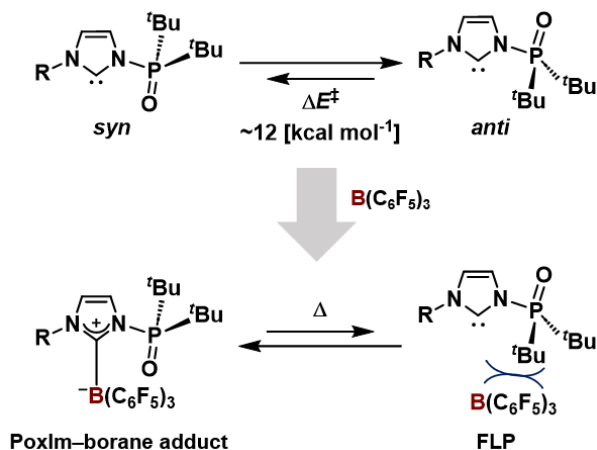
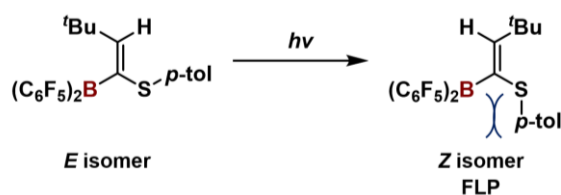


Figure 3. Interconversion between syn- and anti-conformers in PoxIm)s (top), and between PoxIm–borane adducts and FLP species comprising PoxIm)s and B(C₆F₅)₃.

It should be noted that the group of Stephan also reported an FLP-generation system driven by a light-induced *E/Z* isomerization of (C₆F₅)₂B(*p*-Tol)S)C=CCH(^tBu) (Figure 4).⁸ In this system FLP is generated from *E* isomer, in which the distance of B⋯S is closer than *Z* isomer due to the steric repulsion of ^tBu group.



So far, I discussed the frustration revival strategy based on the thermal-responsive conformational isomerization of Lewis bases (i.e. PoxIms) included in CLAs. In the following Chapters, I have studied a strategy to effectively generate FLP species from the CLAs derived from triarylboranes based on the geometrical variation of triarylboranes. Triarylboranes are representative LAs and thus widely used as catalysts, activators, and core structures in π -conjugated materials.⁹ Especially in the field of main-group catalysis, recent progress on FLPs has gathered the attention of the structural diversifications of halogenated triarylboranes beyond the archetypal $B(C_6F_5)_3$.¹⁻⁴ Consequently, several strategies have been demonstrated to control the reactivity, especially Lewis acidity, of triarylboranes.^{10,11} These strategies generally focus on modulating energy (a thermodynamic aspect) and the accessibility (a kinetic aspect) of the empty p orbitals at the boron center. In the former case, more- or less-electrophilic triarylborane derivatives have been prepared using the strategy that involves modifying *meta*-F and/or *para*-F atoms in $B(C_6F_5)_3$ to more- or less- electron-withdrawing substituents (i.e. their intrinsic Lewis acidity).^{1c,9a,b,10,12} In the latter case, the intermolecular steric repulsion between the boron center and LBs is regulated by the size of *ortho*-substituents on the Ar groups in triarylborane (front strain) (Figure 5; right).^{13,14} On the other hand, the Lewis acidity of triarylboranes has rarely been modified by regulating the intramolecular steric repulsion between the Ar groups of tetrahedral LB-borane adducts (back strain) (Figure 5; left).

Figure 5. A schematic representation of the front strain and back strain generated between triarylborane and LBs.

This thesis consists of this General Introduction and the following three Chapters. In Chapter 1, the

detailed mechanism on the revival of FLPs from PoxIm–borane adducts has been clarified by experimental and theoretical studies. In Chapter 2, the hydrogenation of carbonyl compounds under a 1:1:1 molar ratio of a gaseous mixture of H₂, CO, and CO₂ has been achieved efficiently by using an FLP catalyst comprising ethereal LB and triarylborane that was newly designed based on the concept of the remote back strain. In Chapter 3, the remote back strain has been clarified by experimental and theoretical studies. Finally, this thesis is summarized in Conclusion.

References and notes

- For selected reviews on FLP, see: (a) Jupp, A. R.; Stephan, D. W. *Trends Chem.* **2019**, *1*, 35. (b) Fasano, V.; Ingleson, M. J. *Synthesis* **2018**, *50*, 1783. (c) Carden, J. L.; Dasgupta, A.; Melen, R. L. *Chem. Soc. Rev.* **2020**, *49*, 1706. (d) Weicker, S. A.; Stephan, D. W. *Bull. Chem. Soc. Jpn.* **2015**, *88*, 1003.
- (a) Stephan, D. W. *J. Am. Chem. Soc.* **2021**, *143*, 20002. (b) Scott, D. J.; Fuchter, M. J.; Ashley, A. E. *Chem. Soc. Rev.* **2017**, *46*, 5689. (c) Paradies, J. *Acc. Chem. Res.* **2023**, *56*, 821. (d) Zhou, R.; Tavandashti, Z. P.; Paradies, J. *SynOpen* **2023**, *7*, 46. (e) Oestreich, M.; Hermeke, J.; Mohr, J. *Chem. Soc. Rev.* **2015**, *44*, 2202. (f) Hoshimoto, Y.; Ogoshi, S. *ACS Catal.* **2019**, *9*, 5439.
- (a) Stephan, D. W. *Chem. Soc. Rev.* **2023**, *52*, 4632. (b) Stephan, D. W.; Erker, G. *Chem. Sci.* **2014**, *5*, 2625. (c) Stephan, D. W.; Erker, G. *Angew. Chem., Int. Ed.* **2010**, *49*, 46.
- (a) Ashley, A. E.; Thompson, A. L.; O'Hare, D. *Angew. Chem., Int. Ed.* **2009**, *48*, 9839. (b) Mömmling, C. M.; Otten, E.; Kehr, G.; Fröhlich, R.; Grimme, S.; Stephan, D. W.; Erker, G. *Angew. Chem., Int. Ed.* **2009**, *48*, 6643. (c) Tran, S. D.; Tronic, T. A.; Kaminsky, W.; Heinekey, D. M.; Mayer, J. M. *Inorg. Chim. Acta* **2011**, *369*, 126. (d) Voss, T.; Mahdi, T.; Otten, E.; Fröhlich, R.; Kehr, G.; Stephan, D. W.; Erker, G. *Organometallics* **2012**, *31*, 2367. (e) Liu, Y.-L.; Kehr, G.; Daniliuc, C. G.; Erker, G. *Chem. Sci.* **2017**, *8*, 1097. (f) Jian, Z.; Kehr, G.; Daniliuc, C. G.; Wibbeling, B.; Erker, G. *Dalton Trans.* **2017**, *46*, 11715. (g) Jie, X.; Sun, Q.; Daniliuc, C. G.; Knitsch, R.; Hansen, M. R.; Eckert, H.; Kehr, G.; Erker, G. *Chem.-Eur. J.* **2020**, *26*, 1269.
- (a) Rokob, T. A.; Hamza, A.; Stirling, A.; Pápai, I. *J. Am. Chem. Soc.* **2009**, *131*, 2029. (b) Jiang, C.; Blacque, O.; Fox, T.; Berke, H. *Organometallics* **2011**, *30*, 2117. (c) Herrington, T. J.; Ward, B. J.; Doyle, L. R.; McDermott, J.; White, A. J. P.; Hunt, P. A.; Ashley, A. E. *Chem. Commun.* **2014**, *50*, 12753. (d) Wu, L.; Chitnis, S. S.; Jiao, H.; Annibale, V. T.; Manners, I. *J. Am. Chem. Soc.* **2017**, *139*, 16780. (e) Han, Y.; Zhang, S.; He, J.; Zhang, Y. *ACS Catal.* **2018**, *8*, 8765. (f) Wang, X.; Kehr, G.; Daniliuc, C. G.; Erker, G. *J. Am. Chem. Soc.* **2014**, *136*, 3293. (g) Holtrichter-Rößmann, T.; Rösener, C.; Hellmann, J.; Uhl, W.; Würthwein, E.-U.; Fröhlich, R.; Wibbeling, B. *Organometallics* **2012**, *31*, 3272. (h) Mömmling, C. M.; Kehr, G.; Wibbeling, B.; Fröhlich, R.; Erker, G. *Dalton Trans.* **2010**, *39*, 7556. (i) Spies, P.; Kehr, G.; Bergander, K.; Wibbeling, B.; Fröhlich, R.; Erker, G. *Dalton Trans.* **2009**, 1534. (j) Spies, P.; Erker, G.; Kehr, G.; Bergander, K.; Fröhlich, R.; Grimme, S.; Stephan, D. W. *Chem. Commun.* **2007**, 5072. (k) Kolychev, E. L.; Bannenberg, T.; Freytag, M.; Daniliuc, C. G.; Jones, P. G.; Tamm, M.; *Chem.-Eur. J.* **2012**, *18*, 16938. (l) Geier, S. J.; Stephan, D. W. *J. Am. Chem. Soc.* **2009**, *131*, 3476.
- Hoshimoto, Y.; Kinoshita, T.; Ohashi, M.; Ogoshi, S. *Angew. Chem. Int. Ed.* **2015**, *54*, 11666.
- Hoshimoto, Y.; Ogoshi, S. *Bull. Chem. Soc. Jpn.* **2021**, *94*, 327.
- Fan, L.; Jupp, A. R.; Stephan, D. W. *J. Am. Chem. Soc.* **2018**, *140*, 8119.
- (a) Berger, S. M.; Ferger, M.; Marder, T. B. *Chem.-Eur. J.* **2021**, *27*, 7043. (b) Berionni, G. *Chem. Synth.* **2021**, *1*, 10. (c) He, J.; Rauch, F.; Finze, M.; Marder, T. B. *Chem. Sci.* **2021**, *12*, 128. (d) Lawson, J. R.; Melen, R. L. *Inorg. Chem.* **2017**, *56*, 8627.

10. Recently, Greb *et al.* have proposed that Lewis acidity could be classified as global, effective, or intrinsic. These labels refer to the thermodynamic energy change during adduct formation ($\Delta E/\Delta G$), the spectroscopic changes observed on the Lewis base (e.g. the Gutmann-Beckett method) upon forming an adduct, and intrinsic properties of the free boranes (e.g. the energy level of the empty p orbitals and its electron affinity), respectively, for details, see: (a) Erdmann, P.; Greb, L. *Angew. Chem., Int. Ed.* **2022**, *61*, e202114550. (b) Greb, L. *Chem.-Eur. J.* **2018**, *24*, 17881. (c) Rodrigues Silva, D.; de Azevedo Santos, L.; P. Freitas, M.; Fonseca Guerra, C.; Hamlin, T. A. *Chem.-Asian. J.* **2020**, *15*, 4043. (d) Muller, P. *Pure Appl. Chem.* **1994**, *66*, 1077.
11. Sivaev, I. B.; Bregadze, V. I. *Coord. Chem. Rev.* **2014**, *270–271*, 75.
12. (a) Zhang, Y. *Inorg. Chem.* **1982**, *21*, 3889. (b) Brown, I. D.; Skowron, A. *J. Am. Chem. Soc.* **1990**, *112*, 3401. (c) Chattaraj, P. K.; Sarkar, U.; Roy, D. R. *Chem. Rev.* **2006**, *106*, 2065. (d) Jupp, A. R.; Johunstone, T. C.; Stephan, D. W. *Dalton Trans.* **2018**, *47*, 7029.
13. For selected examples, see: (a) Morgan, M. M.; Marwitz, A. J. V; Piers, W. E.; Parvez, M. *Organometallics* **2013**, *32*, 317. (b) Ashley, A. E.; Herrington, T. J.; Wildgoose, G. G.; Zaher, H.; Thompson, A. L.; Rees, N. H.; Krämer, T.; Öhare, D. *J. Am. Chem. Soc.* **2011**, *133*, 14727. (c) Erős, G.; Mehdi, H.; Pápai, I.; Rokob, T. A.; Király, P.; Tárkányi, G.; Soós, T. *Angew. Chem. Int. Ed.* **2010**, *49*, 6559. (d) Erős, G.; Nagy, K.; Mehdi, H.; Pápai, I.; Nagy, P.; Király, P.; Tárkányi, G.; Soós, T. *Chem. -Eur. J.* **2012**, *18*, 574. (e) Dorkó, É.; Kótai, B.; Földes, T.; Gyömöre, Á.; Papai, I.; Soós, T. *J. Organomet. Chem.* **2017**, *847*, 258. (f) Hoshimoto, Y.; Kinoshita, T.; Hazra, S.; Ohashi, M.; Ogoshi, S. *J. Am. Chem. Soc.* **2018**, *140*, 7292.
14. Chase, P. A.; Henderson, L. D.; Piers, W. E.; Parvez, M.; Clegg, W.; Elsegood, M. R. *J. Organometallics* **2006**, *25*, 349.

Chapter 1

Mechanistic Studies on Thermal-Responsive Generation of FLPs from PoxIm-BAr₃ Adducts by Phosphinoyl Rotation

Abstract: Chemists have designed strategies that trigger the conformational isomerization of molecules in response to external stimuli, which can be further applied to regulate the complexation between Lewis acids and bases. Our group have recently developed a system in which frustrated carbene–borane pairs are revived from shelf-stable but external-stimuli-responsive carbene–borane adducts comprised of *N*-phosphine-oxide-substituted imidazolylienes (PoxIm)s and triarylboranes. Herein, I report the detailed mechanism on this revival process. A thermally induced borane-transfer process from the carbene carbon atom to the *N*-phosphinoyl oxygen atom initiates the transformation of the carbene–borane adduct. Subsequent conformational isomerization via the rotation of the *N*-phosphinoyl group in PoxIm moieties eventually leads to the revival of frustrated carbene–borane pairs that can cleave H₂. I believe that this work illustrates an essential role of dynamic conformational isomerization in the regulation of the reactivity of external-stimuli-responsive Lewis acid-base adducts that contain multifunctional substituents.

1.1. Introduction

There have been many recent developments in the chemistry of frustrated Lewis pairs (FLPs) that have been of note, for example, the activation of H₂ mediated by main-group elements.¹ In general, FLPs are transient and not shelf-stable species making their isolation challenging. Meanwhile, chemists have developed strategies that trigger the conformational isomerization of molecules in response to external-stimuli.² These strategies can also be used to generate transient FLP species from classical Lewis adducts (CLAs) that act like their shelf-stable precursors.^{3,4} In 2015, our group has demonstrated a strategy to generate FLPs from shelf-stable CLAs (**PoxIm·B¹** in Figure 1.1) that are comprised of *N*-phosphine-oxide-substituted imidazolylienes (PoxIm)s; **1**) and B(C₆F₅)₃ (**B¹**). Here, the revival of the FLP from the CLA is closely controlled by a thermally induced conformational isomerization of the *N*-phosphinoyl moiety.^{4c,5} In 2018, Stephan et al. reported a system to control the generation of FLPs from CLAs via a light-induced *E/Z* isomerization of (C₆F₅)₂B((*p*-Tol)S)C=CCH(^tBu).⁶ Nevertheless, such FLP revival systems, including external-stimuli-responsive conformational isomerizations, are still underdeveloped. Thus, clarifying the relationship between external-stimuli-responsive conformational isomerizations and the interconversion that occurs between frustrated and quenched Lewis pairs is of great importance. This would allow a significant expansion of different strategies to design and apply FLP species.^{4e}

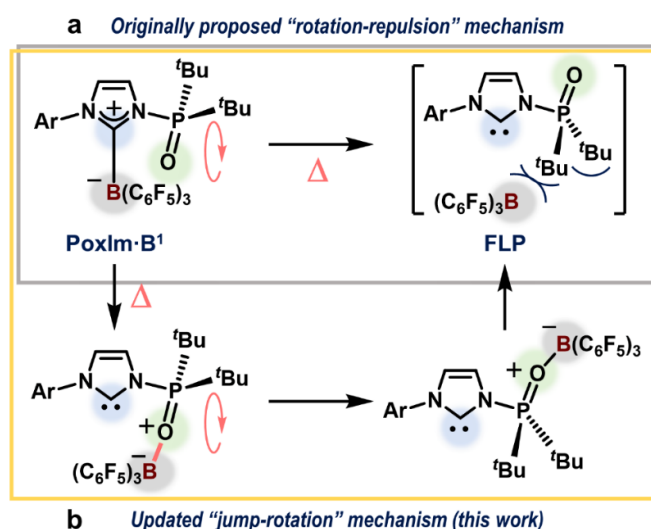


Figure 1.1. Revival of FLPs from **PoxIm·B¹** adducts, induced by thermally responsive molecular motions. (a) A previously proposed mechanism. (b) The updated mechanism proposed based on the results of this work.

In our system that uses PoxIm's, the revival mechanism has not been fully explained. A tentative mechanism in which a $\text{B}(\text{C}_6\text{F}_5)_3$ moiety is repelled by the *N*-phosphinoyl group via a thermally induced isomerization from the *syn* to *anti* conformation had been proposed. In this case the *syn/anti* conformation refers to the relative orientation of the carbene carbon atom and the *N*-phosphinoyl oxygen atom with respect to the N–P bond (Figure 1.1a).^{4c} Herein, I report the results of a combined experimental and theoretical mechanistic study that demonstrates the key role of a transfer step where the triarylborane (BAR_3) unit on the carbene carbon atom moves to the *N*-phosphinoyl oxygen atom (Figure 1.1b). In this study, PoxIm's with 2,6-*i*Pr₂-C₆H₃, 2,4,6-Me₃-C₆H₂, and 3,5-*t*Bu₂-C₆H₃ groups were studied and are herein referred to as **1a**, **1b**, and **1c**, respectively.

1.2 Results and discussion

1.2.1. Effects of Lewis acidity.

To explore the impact of the Lewis acidity of BAR_3 on the formation and reactivity of the carbene–borane adducts, the reaction between **1a** and $\text{B}(p\text{-HC}_6\text{F}_4)_3$ (**B²**)⁷ was undertaken (Figure 1.2a). Full consumption of **1a** was confirmed after 20 minutes, resulting in the formation of two CLAs, i.e., **2aB²**, which contains a *N*-phosphinoyl oxygen–boron bond, and **3aB²**, which contains a carbene–boron bond, in 61% and 29% yield, respectively. Previously, our group has reported that, even at –30 °C, **2aB¹** could be converted to **3aB¹** and that full identification of **2aB¹** could therefore be achieved using NMR analysis conducted at –90 °C.^{4c} In the present case, **2aB²** exhibited a longer life-time at room temperature than **2aB¹**, which enabled us to prepare single crystals of **2aB²** by recrystallization from the reaction mixture at –30 °C. The molecular structure of **2aB²** was unambiguously confirmed using single-crystal X-ray diffraction (SC-XRD) analysis. A set of (*R_a*) and (*S_a*) atropisomers of **2aB²** was identified in the asymmetric unit of the single crystal. The molecular structure of (*R_a*)-**2aB²** is shown in Figure 1.2b and demonstrates a rare example of complexation-induced N–P axial chirality.^{5c} As the reaction progressed, **2aB²** was converted to **3aB²** and **4a**; **2aB²** was fully consumed within 6 h to afford these compounds in 75% and 25% yield, respectively. It should be noted that **4a** is likely furnished via the migration of the *N*-phosphinoyl group from the nitrogen atom to the carbene carbon atom. However, in the absence of **B²**, this migration only proceeded to 9% at 100 °C, even after 25 h.^{5d} The formation of **4a** was

therefore promoted by the enhancement of the electrophilicity of the P center via the coordination of the *N*-phosphinoyl moiety to **B**². Regeneration of **B**² was observed along with the production of **4a**. The molecular structure of **3aB**² was also confirmed by SC-XRD analysis (Figure 1.2c). Comparison of the structural parameters between the solid-state structures of **3aB**² and **3aB**¹ shows their similarity. For example, the C1–B distances in **3aB**² and in **3aB**¹ are 1.710(3) Å and 1.696(3) Å, respectively. The interatomic distance of 3.257(3) Å between the O and B atoms in **3aB**² suggests the absence of a specific interaction between these atoms, similar to that in **3aB**¹ (3.234(3) Å).

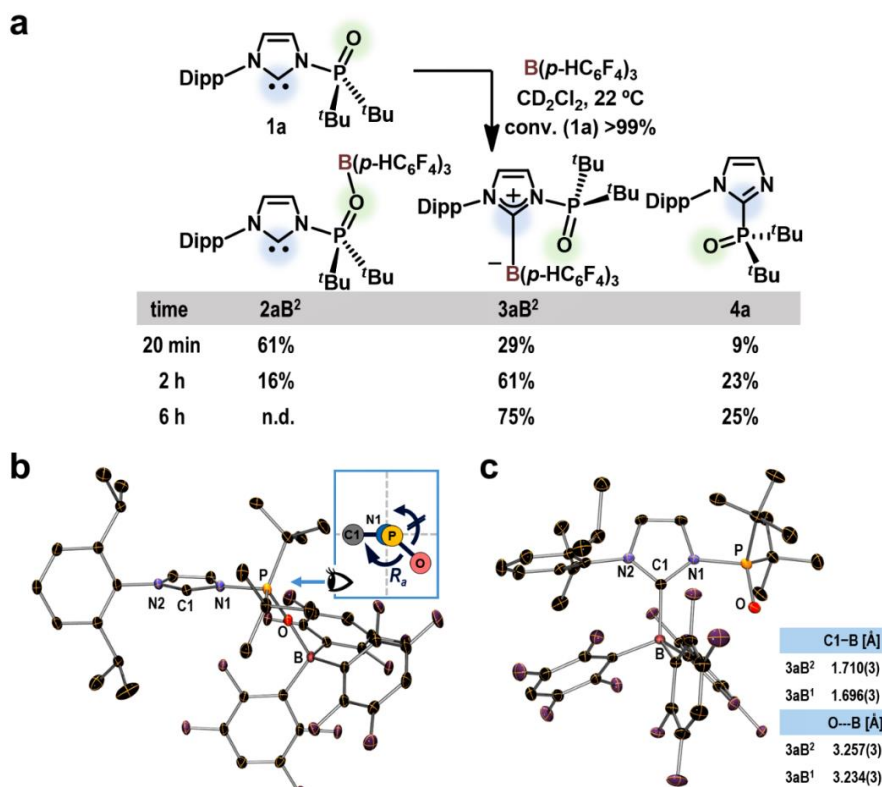


Figure 1.2. Reaction between **1a** and **B**(*p*-HC₆F₄)₃ (**B**²). (a) The reaction was monitored by NMR spectroscopy and the product yields were estimated based on ³¹P NMR analyses. (b) Molecular structure of (*R*_a)-**2aB**² with thermal ellipsoids at 30% probability; H atoms and solvated C₇H₈ molecules are omitted for clarity. Selected bond lengths [Å] and angles [°]: O–B 1.556(2), N1–P 1.707(2), P–O 1.513(1); P–O–B 165.2(1), C1–N1–P–O 128.0(1). (c) Molecular structure of **3aB**² with thermal ellipsoids at 30% probability; H atoms are omitted for clarity. For comparison with **3aB**¹ (*cf.* ref 4c), the carbene–boron bond lengths and interatomic distances between oxygen and boron atoms are shown; C1–N1–P–O: 15.3(2)°.

Thermolysis of **3aB**² at 60 °C for 3 h resulted in the generation of **4a** and **B**² in 77% and 73% yield, respectively, with concomitant formation of [**1a**–H][HO(**B**²)₂] in 4% yield (conversion of **3aB**² = 81%; Figure 1.3a). Although **2aB**² was not observed via NMR analysis of this reaction at 60 °C, the formation of **4a** and **B**² indicates the *in-situ* regeneration of **2aB**² (*vide supra*). The formation of [**1a**–H][HO(**B**²)₂] can be rationalized in terms of a reaction between contaminated H₂O and the FLP species regenerated from **3aB**² via **2aB**². The regeneration of the FLP species from **3aB**² was then clearly confirmed by treating **3aB**² with H₂ (5 atm) at 22 °C, resulting in the formation of [**1a**–H][H–**B**²] (**5aB**²) in 19% yield with concomitant formation of [**1a**–H][HO(**B**²)₂] (8%) and **1a** (6%) (Figure 1.3b). Under identical conditions, no reaction occurred when **3aB**¹ was

used.^{4c} At 60 °C, **5aB**² was generated in 90% yield after 3 h, which is almost comparable with the production of **5aB**¹ (89%) from **3aB**¹. Thus, the lower Lewis acidity of **B**² relative to **B**¹ allowed a more facile revival of the FLP species from **3aB**² than from **3aB**¹.⁸ However, the lower Lewis acidity did not affect the progress of the heterolytic cleavage of H₂ by FLPs at 60 °C.

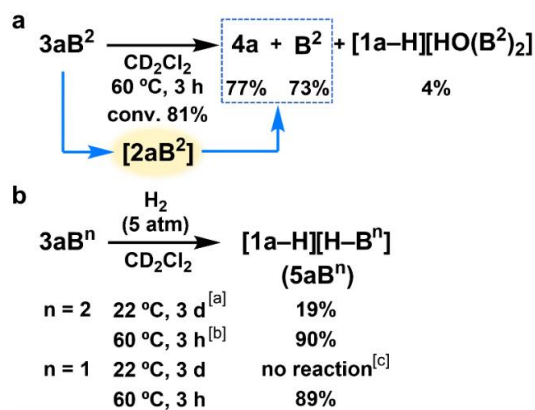


Figure 1.3. Reactivity of carbene–borane adducts **3aB**^{*n*} (*n* = 1, 2). (a) Thermolysis of **3aB**² monitored via NMR spectroscopy. Product yields were calculated based on ³¹P and ¹⁹F NMR analyses. (b) Reaction between **3aB**^{*n*} and H₂. Product yields were calculated based on ¹⁹F and ³¹P analysis. [a] [1a–H][HO(B²)₂] and **1a** were also observed in 8% and 6% yield, respectively. [b] [1a–H][HO(B²)₂] was also observed in 7% yield. ^cResults obtained using **3aB**¹ are reproduced from ref. 4c.

1.2.2. Kinetic studies

To gain further insight into the reaction mechanism, the initial rate constants for the generation of **5aB**¹, *k*_{int} [10^{–5} s^{–1}], from the reaction between **3aB**¹ and H₂ in 1,2-dichloroethane-*d*₄ (DCE-*d*₄) at 60 °C were estimated by varying the H₂ pressure from 0.5 to 5.0 atm (Figure 1.4a). It should be noted here that when H₂ was pressurized at 5.0 atm, an excess of H₂ (ca. 0.3 mmol) with respect to **3aB**¹ (0.010 mmol) was added to the pressure-tight NMR tube. The concentration of H₂ clearly influenced the progress of the reaction, suggesting that the heterolytic cleavage of H₂ by the FLP species is involved in the rate-determining events. Next, the reaction between **3aB**¹ and H₂ at 5.0 atm of pressure was monitored in DCE-*d*₄ whilst the temperature was varied from 50 to 80 °C (Figure 1.S27). Pseudo-first order rate constants, *k*_{obs} [10^{–5} s^{–1}], of 2.95(2), 11.2(8), 46.4(4) and 183(2) were estimated for the reactions at 50, 60, 70, and 80 °C, respectively. Thus, the activation energy and pre-exponential factor obtained from the plot based on the Arrhenius equation, $\ln k_{\text{obs}} = -(E_a/R)(1/T) + \ln A$, are *E*_a = 31.2 [kcal mol^{–1}] and *A* = 3.3(36)×10¹⁶ [s^{–1}] (Figure 1.4b). Given the close relation between *E*_a and Δ*H*[‡], the values obtained for *E*_a suggest that the formation of **5aB**¹ via the reaction between **3aB**¹ and H₂ only occurs at temperatures higher than 25 °C.⁹

Based on the results presented here and those previously reported,^{4c} the reaction between the carbene–borane adducts and H₂ to give [PoxIm–H][H–BAR₃] likely proceeds via the heterolytic cleavage of H₂ by the FLP species that are formed following the regeneration of the *N*-phosphinoyl oxygen–borane adducts. These steps are expected to be the rate-determining events because the concentration of H₂ (Figure 1.4a), the steric bulk of the *N*-aryl group^{4c} and the Lewis acidity of the BAR₃ moiety (Figure 1.3b) influence the reaction rates and/or the temperature required to initiate the reaction between the carbene–borane adducts and H₂.

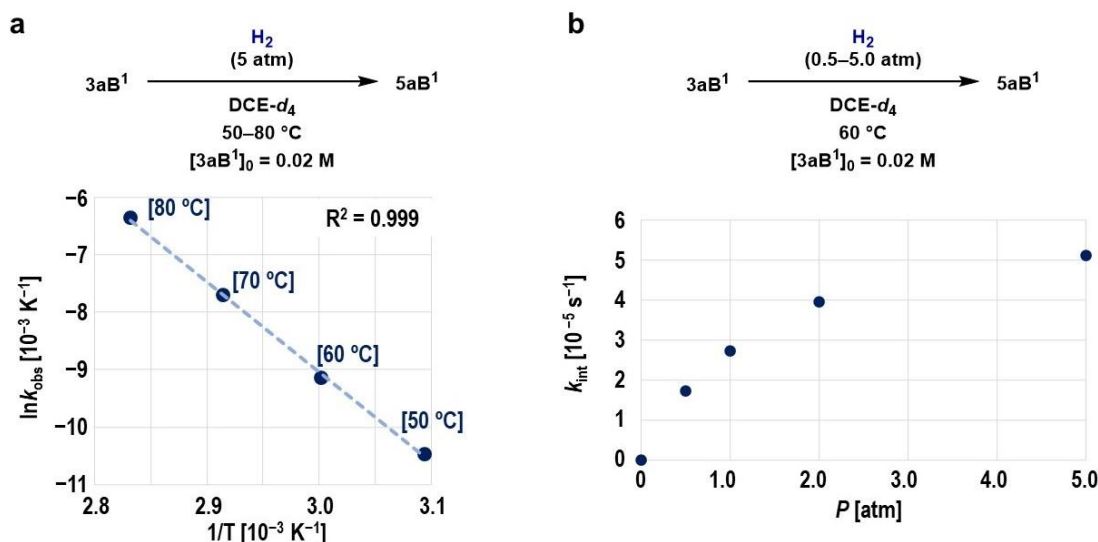


Figure 1.4. Kinetic studies for the reaction between **3aB¹** and H₂. (a) Plot of the H₂ pressure, P [atm], as a function of the initial reaction rate constants, k_{int} [10^{-5} s^{-1}]. (b) Plot of $1/T$ [10^{-3} K^{-1}] as a function of $\ln k_{obs}$ [s^{-1}]. The k_{obs} values are the pseudo-first order rate constants for the formation of **5aB¹** obtained from the reaction of **1a** ($2.0 \times 10^{-2} \text{ M}$ in DCE- d_4) and H₂ (5 atm).

1.2.3. Theoretical studies

Density-functional theory (DFT) calculations were carried out for **3aB¹** at the ω B97X-D/6-311G(d,p), PCM (DCE)// ω B97X-D/6-311G(d,p) for H₂ and 6-311G(d) for all other atoms level of theory (Figure 1.5a). The relative Gibbs free energies with respect to [**1a** + **B¹**] (0.0 kcal·mol⁻¹) are shown. During the transformation of **3aB¹** (−17.2 kcal·mol⁻¹) to **2aB¹** (−9.8 kcal·mol⁻¹), both of which were experimentally confirmed, the formation of an intermediate **2a'B¹** (−7.7 kcal·mol⁻¹) was predicted via a C-to-O transfer of **B¹** in **3aB¹**. This distinctive boron-transfer process takes place via saddle point **TS1a** (+7.3 kcal·mol⁻¹), while the potential energy surface around **TS1a** is very flat (Figure 1.S34 for details). The subsequent rotation of the *N*-phosphinoyl moiety via **TS2a** (+7.5 kcal·mol⁻¹) affords **2aB¹**. Next, the dissociation of the B–O bond occurs to regenerate [**1a** + **B¹**]. The optimized molecular structures of **TS1a** and **2a'B¹** are shown in Figure 1.5c. In **TS1a**, the interatomic distances C1...B and O...B are 4.24 and 3.34 Å, respectively, while **B¹** adopts a planar geometry. Thus, **B¹** is dissociated from both the carbene carbon and phosphinoyl oxygen atoms in **TS1a**, while the formation of the O–B bond (1.59 Å) is confirmed in **2a'B¹**. Based on the quantum theory of atoms in molecule (AIM) method, neither bond paths nor bond critical points were confirmed between the B and C1/O atoms in **TS1a** (Figure 1.S37).¹⁰ This AIM analysis demonstrates that several non-covalent interactions, including π - π and H...F interactions, exist between the **1a** and **B¹** moieties to stabilize **TS1a**.

Two plausible mechanisms were evaluated for the FLP-mediated cleavage of H₂ on the basis that the Lewis-basic center reacts with H₂ via cooperation with **B¹** (Figure 1.5b). One possibility is that the carbene carbon atom works as a Lewis base (path I; the right path in Figure 1.5b),^{1,11} while the other is that the *N*-phosphinoyl oxygen functions as a Lewis base (path II; the left path in Figure 1.5b).¹² In path I, the heterolytic cleavage of H₂ takes places via **TS4a** (+11.4 kcal·mol⁻¹), which arises from the insertion of H₂ into the reaction field around the carbene carbon and boron atoms in **FLP-1aB¹**, affording **5aB¹** (−34.8 kcal·mol⁻¹), a species more thermodynamically stable than **3aB¹**. In the optimized structure of **TS4a** (Figure 5d), the dissociation of

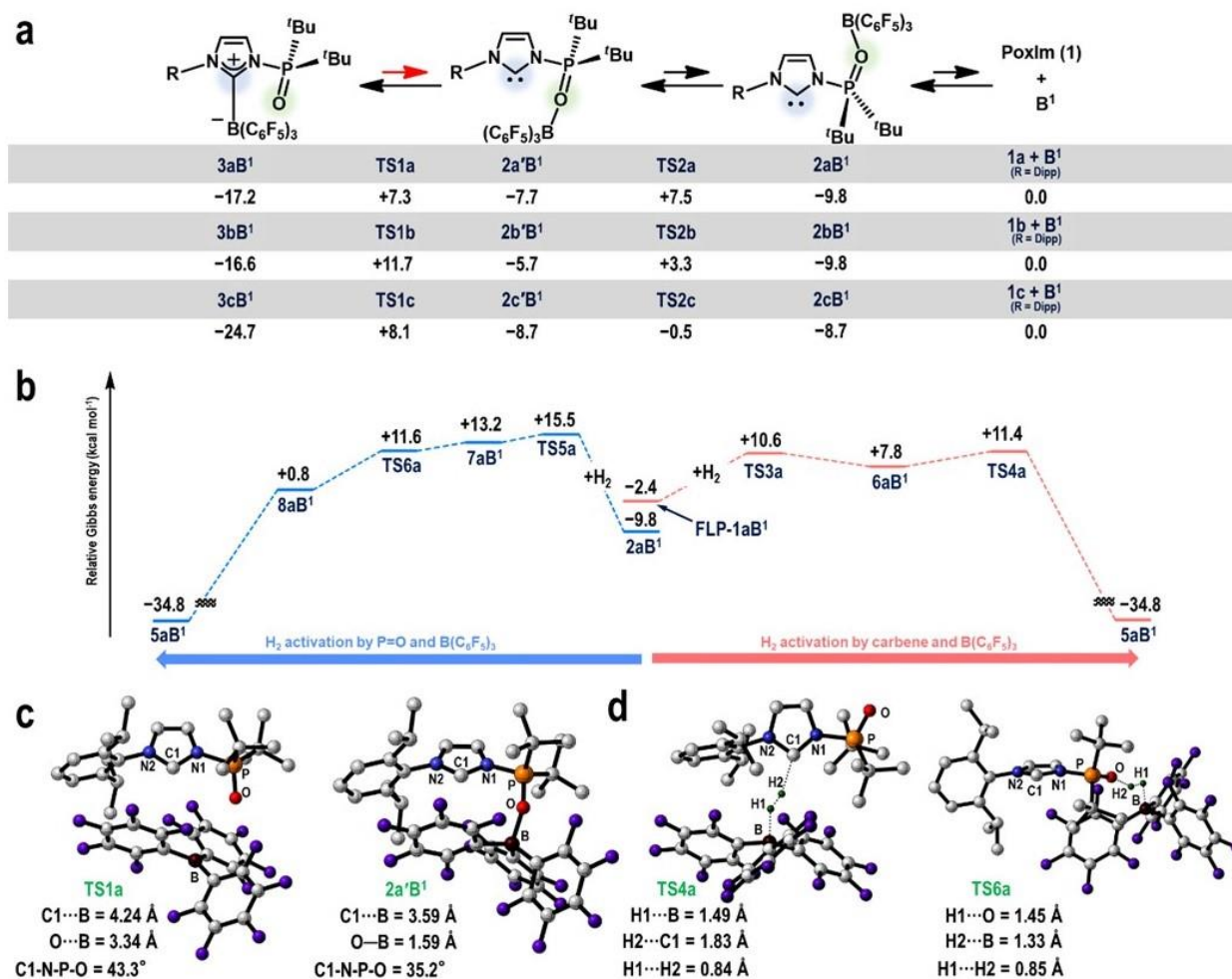


Figure 1.5. Theoretical studies. The relative Gibbs energies [kcal mol^{-1}] are shown with respect to each [**1** + **B**¹], calculated at the $\omega\text{B97X-D}/6\text{-}311\text{G(d,p)}$, PCM (DCE)// $\omega\text{B97X-D}/6\text{-}31\text{G(d,p)}$ (for H_2) and $6\text{-}31\text{G(d)}$ (for all other atoms) level of theory (298.15 K, 1 atm). (a) Proposed mechanism for the regeneration of [**1** + **B**¹] from the carbene–borane complexes **3aB**¹–**3cB**¹. (b) Proposed mechanism for the heterolytic cleavage of H_2 , enabled by the phosphinoyl oxygen and $\text{B}(\text{C}_6\text{F}_5)_3$ moieties (left) or by the carbene and $\text{B}(\text{C}_6\text{F}_5)_3$ moieties (right). (c) DFT-optimized molecular structures for **TS1a** and **2a'B**¹. (d) DFT-optimized molecular structures for **TS4a** and **TS6a**.

the H1–H2 bond ($\text{H1}\cdots\text{H2} = 0.84 \text{ \AA}$) occurs with the partial formation of the H2–C1/H1–B bonds ($\text{H2}\cdots\text{C1} = 1.83 \text{ \AA}$ / $\text{H1}\cdots\text{B} = 1.49 \text{ \AA}$). Based on these results, the overall path from **3aB**¹ to **5aB**¹ via **FLP-1aB**¹ is substantially exothermic ($\Delta G^\circ = -17.6 \text{ kcal}\cdot\text{mol}^{-1}$) and includes an overall activation energy barrier of $+28.6 \text{ kcal}\cdot\text{mol}^{-1}$ required to overcome **TS4a**. In path II, which takes place via **TS5a** (a transition state for the insertion of H_2 into the O–P bond) and **TS6a** (a transition state for the cleavage of H_2 between the O and P atoms), a higher activation energy barrier of $+32.7 \text{ kcal}\cdot\text{mol}^{-1}$ is predicted to yield intermediate **8aB**¹, which contains a $\text{P}=\text{O}-\text{H}^+$ and $\text{B}-\text{H}^-$ species. It should be noted that the potential energy of the optimized **TS6a** (-3633.288355 hartree) is almost identical to that of the optimized **7aB**¹ (-3633.288363 hartree), which causes the reversed Gibbs energy levels as shown in Figure 1.5b after the Gibbs energy correction and implementation of solvent effect. Therefore, the discussion on the activation energy barrier to overcome **TS6a** from **7aB**¹ should be not

essential. The subsequent transfer of H^+ from the *N*-phosphinoyl oxygen atom to the carbene carbon atom furnishes **5aB**¹, although the details of this process remain unclear at this point. The molecular structure of **TS6a** shows that the cleavage of the H1–H2 bond ($\text{H1}\cdots\text{H2} = 0.85 \text{ \AA}$) by the *N*-phosphinoyl oxygen and boron atoms occurs in a cooperative fashion (Figure 1.5d). Given the experimental and theoretical results reported here, I conclude that path I is the more likely one.

The impact of the *N*-aryl substituents on the activation energy barriers for the regeneration of [**1** + **B**¹] was evaluated using calculations on **3bB**¹, which contains an *N*-2,4,6- $\text{Me}_3\text{-C}_6\text{H}_2$ group, as well as **3cB**¹, which contains an *N*-3,5- $\text{tBu}_2\text{-C}_6\text{H}_3$ group. This afforded ΔG^\ddagger values of +28.3 and +32.8 $\text{kcal}\cdot\text{mol}^{-1}$ for **3bB**¹ and **3cB**¹, respectively (Figure 1.5a). These results are consistent with the experimental observations, i.e. that **3aB**¹–**3cB**¹ did not react in the presence or absence of H_2 under ambient conditions under the applied conditions. Furthermore, these results might rationalize the fact that temperature to induce the reaction between these CLAs and H_2 increases in the order **3aB**¹ (60 °C) < **3bB**¹ (80 °C) < **3cB**¹ (120 °C).^{4c}

1.3. Conclusion

In summary, the reaction mechanism for the revival of frustrated carbene–borane pairs from external-stimuli-responsive classical Lewis adducts (CLAs), comprised of *N*-phosphine-oxide-substituted imidazolylidene (PoxIm) and triarylboranes (BAR_3), is reported based on a combination of experimental and theoretical studies. Remarkably, a transfer of the borane moiety from the carbene carbon atom to the *N*-phosphinoyl oxygen atom was identified as a key step in the heterolytic cleavage of H_2 by the regenerated FLP species. The optimized transition-state structure for this borane-transfer process was confirmed to include no bonding interactions between the carbene carbon/phosphinoyl oxygen and boron atoms, albeit that it is stabilized by intermolecular non-covalent interactions between the PoxIm and BAR_3 moieties. The heterolytic cleavage of H_2 takes place via the cooperation of the carbene carbon and the boron atoms and exhibits a lower overall activation energy barrier than that of the path in which a combination of the *N*-phosphinoyl oxygen and boron atom mediates the H_2 cleavage. These results demonstrate the essential role of dynamic conformational isomerization in the regulation of the reactivity of shelf-stable but external-stimuli-responsive Lewis acid-base adducts by multifunctional Lewis bases.

1.4. References and notes

- For recent reviews, see: (a) Stephan, D. W.; Erker, G. *Angew. Chem. Int. Ed.* **2010**, *49*, 46. (b) Paradies, J. *Synlett* **2013**, *24*, 777. (c) Feng, X.; Du, H. *Tetrahedron Lett.* **2014**, *55*, 6959. (d) Stephan, D. W.; Erker, G. *Angew. Chem. Int. Ed.* **2015**, *54*, 6400. (e) Weicker, S. A.; Stephan, D. W. *Bull. Chem. Soc. Jpn.* **2015**, *88*, 1003. (f) Scott, D. J.; Fuchter, M. J.; Ashley, A. E. *Chem. Soc. Rev.* **2017**, *46*, 568900. (g) Fasano, V.; Ingleson, M. J. *Synthesis* **2018**, *50*, 1783. (h) Jupp, A. R.; Stephan, D. W. *Trends Chem.* **2019**, *1*, 35. (i) Hoshimoto, Y.; Ogoshi, S. *ACS Catal.* **2019**, *9*, 5439.
- For recent reviews, see: (a) Pan, T.; Liu, J. *ChemPhysChem* **2016**, *17*, 1752. (b) Cheng, C.; Stoddart, J. F. *ChemPhysChem* **2016**, *17*, 1780. (c) Kassem, S.; Leeuwen, T.; Lubbe, A. S.; Wilson, M. R.; Feringa, B. L.; Leigh, D. A. *Chem. Soc. Rev.* **2017**, *46*, 2592. (d) Findlay, J. A.; Crowley, J. D. *Tetrahedron Lett.* **2018**, *59*, 334.
- Rokob, T. A.; Hamza, A.; Stirling, A.; Pápai, I. *J. Am. Chem. Soc.* **2009**, *131*, 2029.
- For examples on thermal-induced generation of FLPs from their CLAs at the temperature higher than room

- temperature, see: (a) Jiang, C.; Blacque, O.; Fox, T.; Berke, H. *Organometallics* **2011**, *30*, 2117. (b) Herrington, T. J.; Ward, B. J.; Doyle, L. R.; McDermott, J.; White, A. J. P.; Hunt, P. A.; Ashley, A. E. *Chem. Commun.* **2014**, *50*, 12753. (c) Hoshimoto, Y.; Kinoshita, T.; Ohashi, M.; Ogoshi, S. *Angew. Chem. Int. Ed.* **2015**, *54*, 11666. (d) Wu, L.; Chitnis, S. S.; Jiao, H.; Annibale, V. T.; Manners, I. *J. Am. Chem. Soc.* **2017**, *139*, 16780. (e) Han, Y.; Zhang, S.; He, J.; Zhang, Y. *ACS Catal.* **2018**, *8*, 8765. For examples on a system that can generate FLPs from CLAs under ambient conditions, see: (f) Wang, X.; Kehr, G.; Daniliuc, C. G.; Erker, G. *J. Am. Chem. Soc.* **2014**, *136*, 3293. (g) Holtrichter-Rößmann, T.; Rösener, C.; Hellmann, J.; Uhl, W.; Würthwein, E.-U.; Fröhlich, R.; Wibbeling, B. *Organometallics* **2012**, *31*, 3272. (h) Mömming, C. M.; Kehr, G.; Wibbeling, B.; Fröhlich, R.; Erker, G. *Dalton Trans.* **2010**, *39*, 7556. (i) Spies, P.; Kehr, G.; Bergander, K.; Wibbeling, B.; Fröhlich, R.; Erker, G. *Dalton Trans.* **2009**, 1534. (j) Spies, P.; Erker, G.; Kehr, G.; Bergander, K.; Fröhlich, R.; Grimme, S.; Stephan, D. W. *Chem. Commun.* **2007**, 5072. (k) Kolychev, E. L.; Bannenberg, T.; Freytag, M.; Daniliuc, C. G.; Jones, P. G.; Tamm, M. *Chem.-Eur. J.* **2012**, *18*, 16938. (l) Geier, S. J.; Stephan, D. W. *J. Am. Chem. Soc.* **2009**, *131*, 3476.
5. (a) Hazra, S.; Hoshimoto, Y.; Ogoshi, S. *Chem.-Eur. J.* **2017**, *23*, 15238. (b) Hoshimoto, Y.; Ogoshi, S. *Bull. Chem. Soc. Jpn.* **2021**, *94*, 327. (c) Asada, T.; Hoshimoto, Y.; Kawakita, T.; Kinoshita, T.; Ogoshi, S. *J. Org. Chem.* **2020**, *85*, 14333. (d) Asada, T.; Hoshimoto, Y.; Ogoshi, S. *J. Am. Chem. Soc.* **2020**, *142*, 9772.
 6. Fan, L.; Jupp, A. R.; Stephan, D. W. *J. Am. Chem. Soc.* **2018**, *140*, 8119.
 7. Ullrich, M.; Lough, A. J.; Stephan, D. W. *J. Am. Chem. Soc.* **2009**, *131*, 52.
 8. Our group previously has reported that the heterolytic cleavage of H₂ quantitatively proceeded by **3aB**¹ in the presence of excess amounts of H₂ (5 atm, ca. 30–50 equiv) in the autoclave reactor (*V* = 25 mL, see ref. 4c). In this work, I used a pressure-tight NMR tube (*V* = 1.8 mL) that can contain less than 30 equivalents of H₂ after the pressurization at 5 atm.
 9. Anslyn, E. V.; Dougherty, D. A. *Modern Physical Organic Chemistry*, Mill Valley, California: University Science Books (2006).
 10. (a) Bader, R. F. W. Ed. *Atoms in Molecules. A Quantum Theory*; Cambridge University Press: Oxford (1991). (b) Bader, R. F. W.; Stephens, M. E. *J. Am. Chem. Soc.* **1975**, *97*, 7391.
 11. For pioneering reports on the heterolytic cleavage of H₂ by FLPs comprising caebenes and boranes, see: (a) Chase, P. A.; Stephan, D. W. *Angew. Chem. Int. Ed.* **2008**, *47*, 7433. (b) Holschumacher, D.; Bannenberg, T.; Hrib, C. G.; Jones, P. G.; Tamm, M. *Angew. Chem. Int. Ed.* **2008**, *47*, 7428.
 12. Stepen, A. J.; Bursch, M.; Grimme, S.; Stephan, D. W.; Paradies, J. *Angew. Chem. Int. Ed.* **2018**, *57*, 15253.

1.5. Supporting information

1.5.1. General considerations

Unless otherwise noted, all manipulations were conducted under a nitrogen atmosphere using standard Schlenk or dry box techniques. ¹H, ¹¹B, ¹³C, ¹⁹F, and ³¹P NMR spectra were recorded on a Bruker AVANCE III 400 or JEOL JNM-400 spectrometers at 25 °C. The chemical shifts in the ¹H NMR spectra were recorded relative to Me₄Si or residual protonated solvent (CDHCl₂ (δ 5.32) or DCE-*d*₄ (δ 3.75)). The chemical shifts in the ¹¹B NMR spectra were recorded relative to BF₃. The chemical shifts in the ¹³C spectra were recorded relative to Me₄Si or deuterated solvent (CD₂Cl₂ (δ 53.84)). The chemical shifts in the ¹⁹F NMR spectra were recorded relative to α,α,α-trifluorotoluene (δ –65.64). The chemical shifts in the ³¹P NMR spectra were recorded relative to 85% H₃PO₄ as an external standard. Assignment of the resonances in ¹H and ¹³C NMR spectra was based on

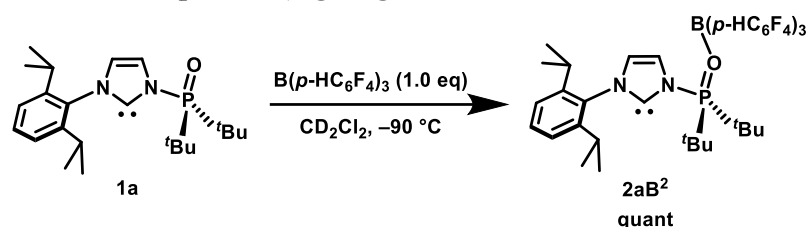
^1H – ^1H COSY, HMQC and HMBC experiments. Elementary analyses were performed at Instrumental Analysis Center, Faculty of Engineering, Osaka University. ESI-MS analyses were performed with a Bruker Daltonics micrOTOF mass spectrometer. X-ray crystal data were collected with Rigaku XtaLAB Synergy equipping with the HyPix-6000HE detector.

1.5.2. Materials

All commercially available reagents were used as received. Unless otherwise noted, toluene, hexane, and mesitylene were distilled from sodium benzophenone ketyl prior to use. CH_2Cl_2 and 1,2-dichloroethane were distilled over CaH_2 prior to use. CD_2Cl_2 and $\text{DCE-}d_4$ were distilled over CaH_2 and stored over molecular sieves (4 Å). PoxIm (**1a**)^{S1} and $\text{B}(p\text{-HC}_6\text{F}_4)_3$ (**B**²)^{S2,S3} were furnished by the known procedure.

Metrical data for the solid state structures are available from Cambridge Crystallographic Data Centre: CCDC2072358 (**3aB**²), 2072359 (**5aB**²), 2072360 (**2aB**²), 2072638 ([**1a-H**][**HO(B**²)₂]).

1.5.4. Reaction between **1a** and $\text{B}(p\text{-HC}_6\text{F}_4)_3$ giving **2aB**²



A solution of **1a** (7.4 mg, 0.02 mmol) and **B**² (9.3 mg, 0.02 mmol) in CD_2Cl_2 (0.5 mL) was prepared at $-30\text{ }^\circ\text{C}$, and then transferred into a J. Young NMR tube. The quantitative formation of **2aB**² was then confirmed at $-90\text{ }^\circ\text{C}$ by ^1H , ^{13}C , ^{19}F , and ^{31}P NMR analyses (Figure 1.S5–8). A single crystal suitable for XRD analysis was prepared by recrystallization from toluene/hexane at $-30\text{ }^\circ\text{C}$.

^1H NMR (400 MHz, CD_2Cl_2 , $-90\text{ }^\circ\text{C}$): δ 7.58–7.33 (m, 3H, Im-*H*, $\text{C}_{\text{Dipp}}\text{-H}$), 7.00–6.97 (m, 4H, Im-*H*, $\text{C}_{\text{Dipp}}\text{-H}$, $\text{C}_{\text{B2}}\text{-H}$), 6.81–6.72 (m, 1H, $\text{C}_{\text{B2}}\text{-H}$), 2.27–2.26 (m, 2H, $\text{CH}(\text{CH}_3)_2$), 1.26–0.97 (m, 30H, tBu-*H*, $\text{CH}(\text{CH}_3)_2$). **^{13}C NMR** (100 MHz, CD_2Cl_2 , $-90\text{ }^\circ\text{C}$): δ 219.5 (d, $^2J_{\text{C,P}} = 32.0\text{ Hz}$, NCN), 147.2 (d, $^1J_{\text{C,F}} = 215\text{ Hz}$), 145.1, 144.8 (dm, $^1J_{\text{C,F}} = 217\text{ Hz}$), 135.5, 129.2, 125.1, 123.5, 123.3, 121.8, 103.1, 38.9 (d, $^1J_{\text{C,P}} = 63.0\text{ Hz}$), 27.7, 25.8, 23.7, 22.7. Resonances of some carbons at the *ipso*, *ortho*, *meta*, and *para* positions in $\text{B}(p\text{-HC}_6\text{F}_4)_3$ could not be identified. **^{19}F NMR** (376 MHz, CD_2Cl_2 , $-90\text{ }^\circ\text{C}$): δ –129.8 (4F), –133.7 (2F), –141.7 (6F). **$^{31}\text{P}\{\text{H}\}$ NMR** (162 MHz, CD_2Cl_2 , $-90\text{ }^\circ\text{C}$): δ 79.3 (s). X-ray data for $\text{C}_{55}\text{H}_{57}\text{BF}_{13}\text{N}_2\text{PO}_{0.25}$ ($M = 1030.85\text{ g/mol}$): monoclinic, space group $\text{P2}_1/\text{c}$ (#14), $a = 16.2735(2)\text{ \AA}$, $b = 15.2296(2)\text{ \AA}$, $c = 20.5604(2)\text{ \AA}$, $\beta = 93.9330(10)^\circ$, $V = 5083.67(10)\text{ \AA}^3$, $Z = 4$, $T = 143.15\text{ K}$, $\mu(\text{Cu K}\alpha) = 1.222\text{ mm}^{-1}$, $D_{\text{calc}} = 1.3467\text{ g/cm}^3$, 65960 reflections measured ($6.7^\circ \leq 2\theta \leq 136.48^\circ$), 9330 unique ($R_{\text{int}} = 0.0346$, $R_{\text{sigma}} = 0.0199$) which were used in all calculations. The final R_1 was 0.0481 ($I \geq 2\sigma(I)$) and wR_2 was 0.1321 (all data).

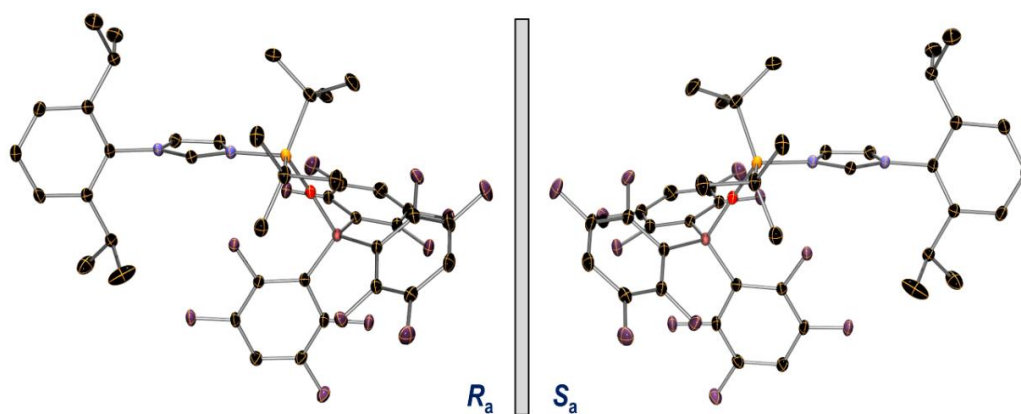


Figure 1.S4. Molecular structure of **2aB²** with ellipsoids set at 30% probability, in which hydrogen atoms and solvated C₇H₈ molecules are omitted for clarity. In this crystalline lattice, (*R_a*)- and (*S_a*)-atropisomers are included.

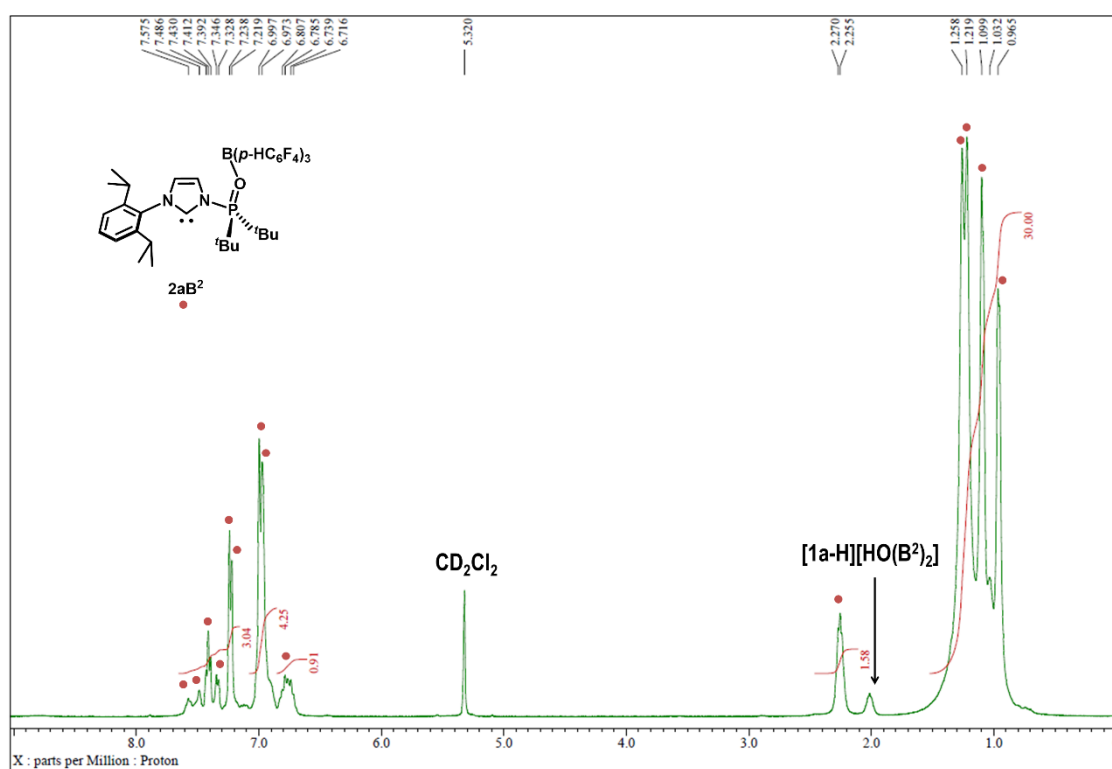


Figure 1.S5. Formation of **2aB²** confirmed at $-90\text{ }^{\circ}\text{C}$ by ^1H NMR.

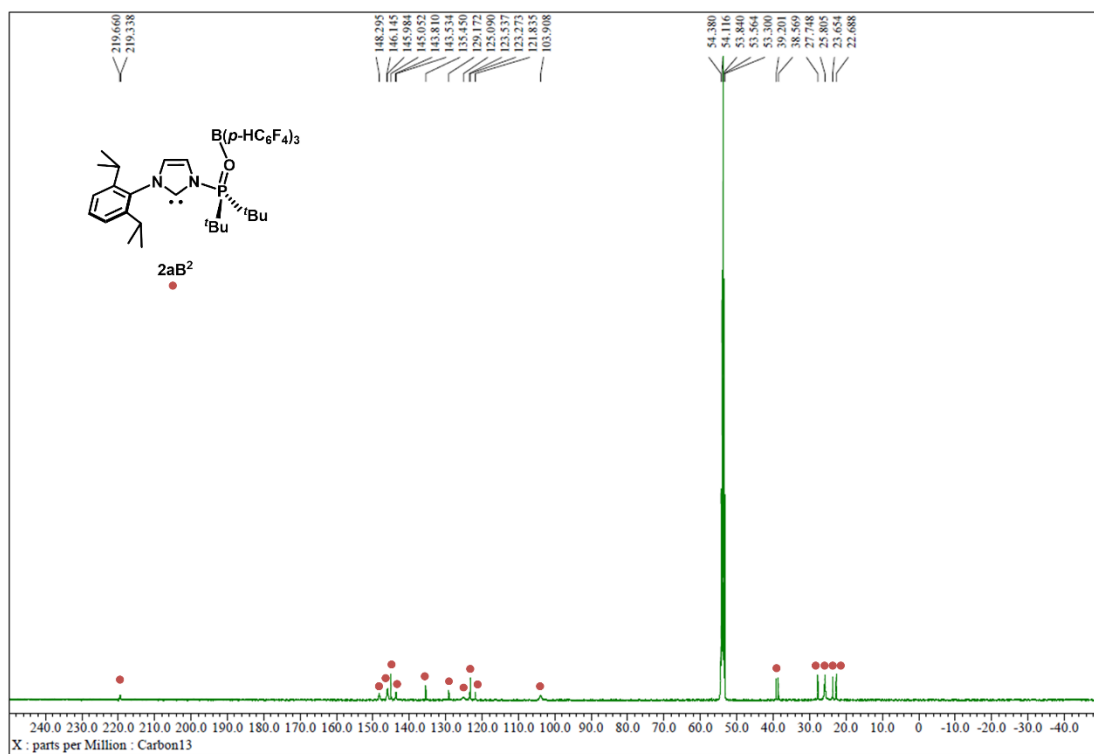


Figure 1.S6. Formation of **2aB²** confirmed at $-90\text{ }^{\circ}\text{C}$ by ^{13}C NMR.

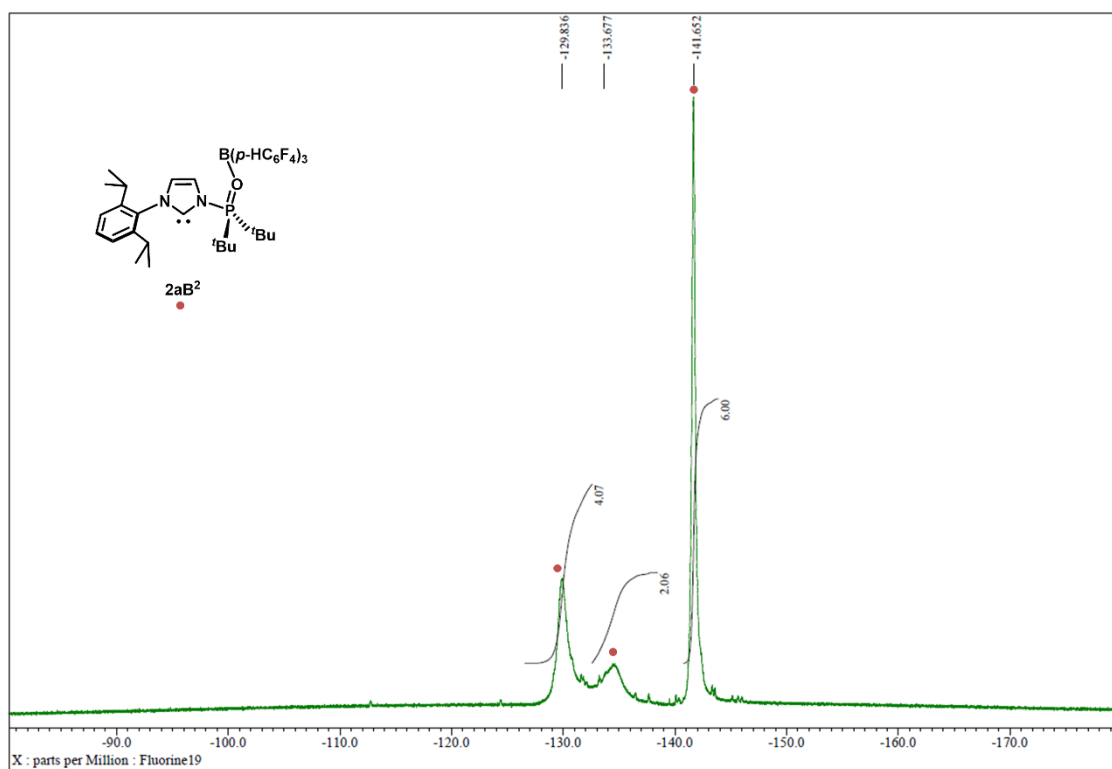


Figure 1.S7. Formation of **2aB²** confirmed at $-90\text{ }^{\circ}\text{C}$ by ^{19}F NMR.

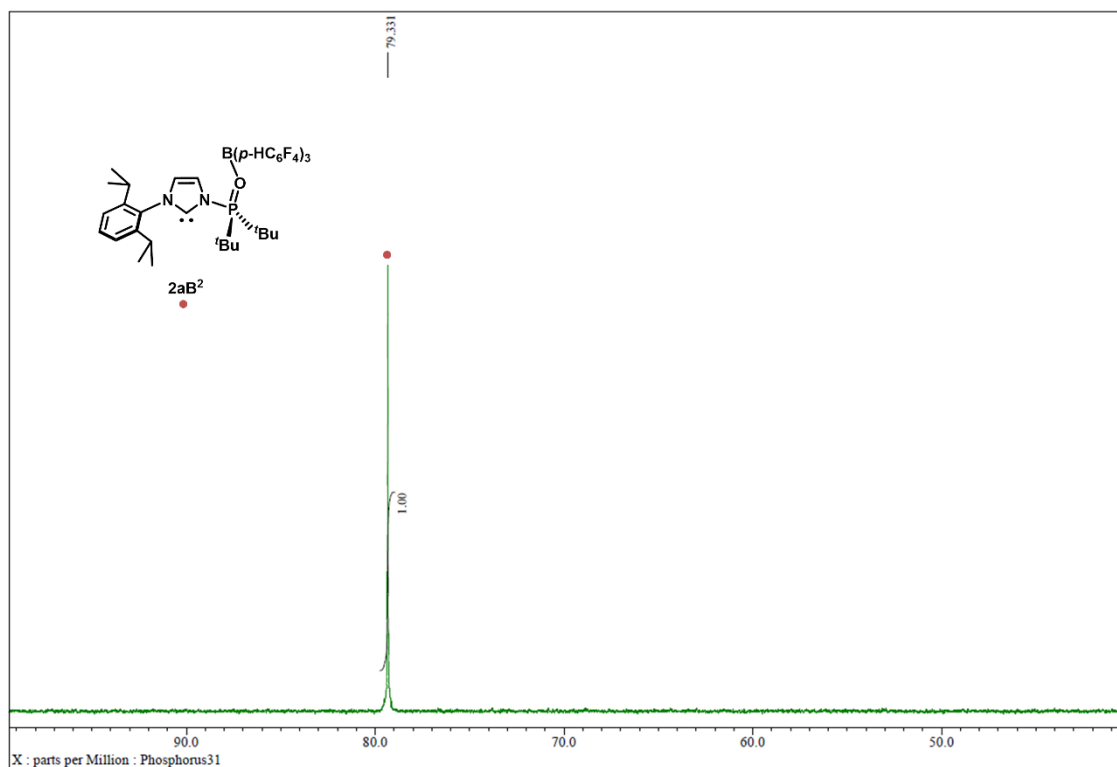
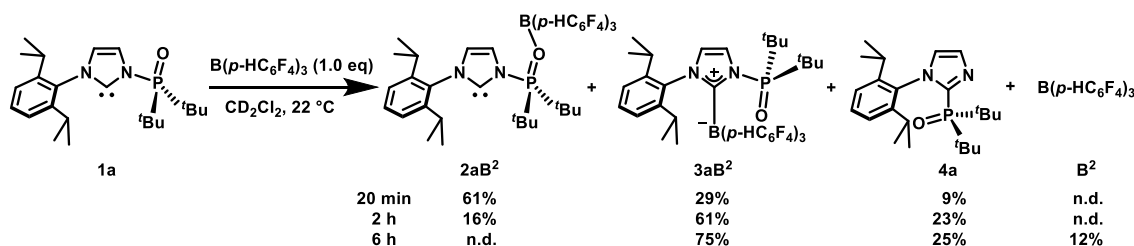


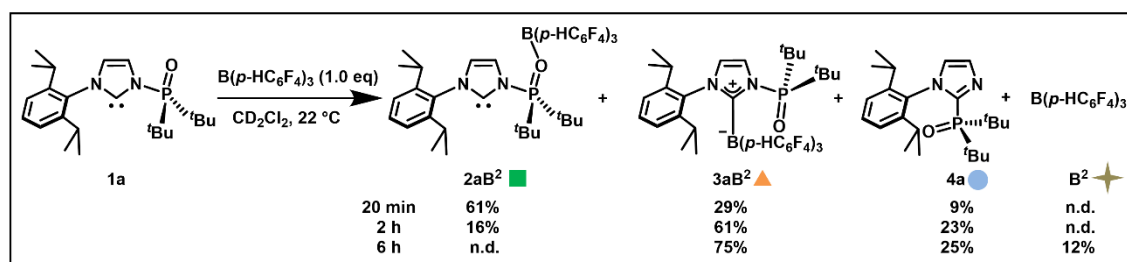
Figure 1.S8. Formation of **2aB²** confirmed at $-90\text{ }^{\circ}\text{C}$ by ^{31}P NMR.

1.5.5. NMR experiments

▪ Reaction between **1a** and **B(p-HC₆F₄)₃** at $22\text{ }^{\circ}\text{C}$



PoxIm **1a** (5.0 mg, 0.01 mmol) and **B²** (5.8 mg, 0.01 mmol) were mixed in CD_2Cl_2 (0.5 mL), and the resultant solution was transferred into a J. Young NMR tube. The reaction was monitored by ^1H , ^{19}F , and ^{31}P NMR analyses conducted at $22\text{ }^{\circ}\text{C}$ (Figure 1.S9–11). Note that the identification of **2aB²** in CD_2Cl_2 at room temperature were independently conducted by ^1H , ^{19}F , and ^{31}P NMR analyses shown in Figure 1.S24–26. Yield of products were estimated by the ^{19}F and ^{31}P NMR analyses.



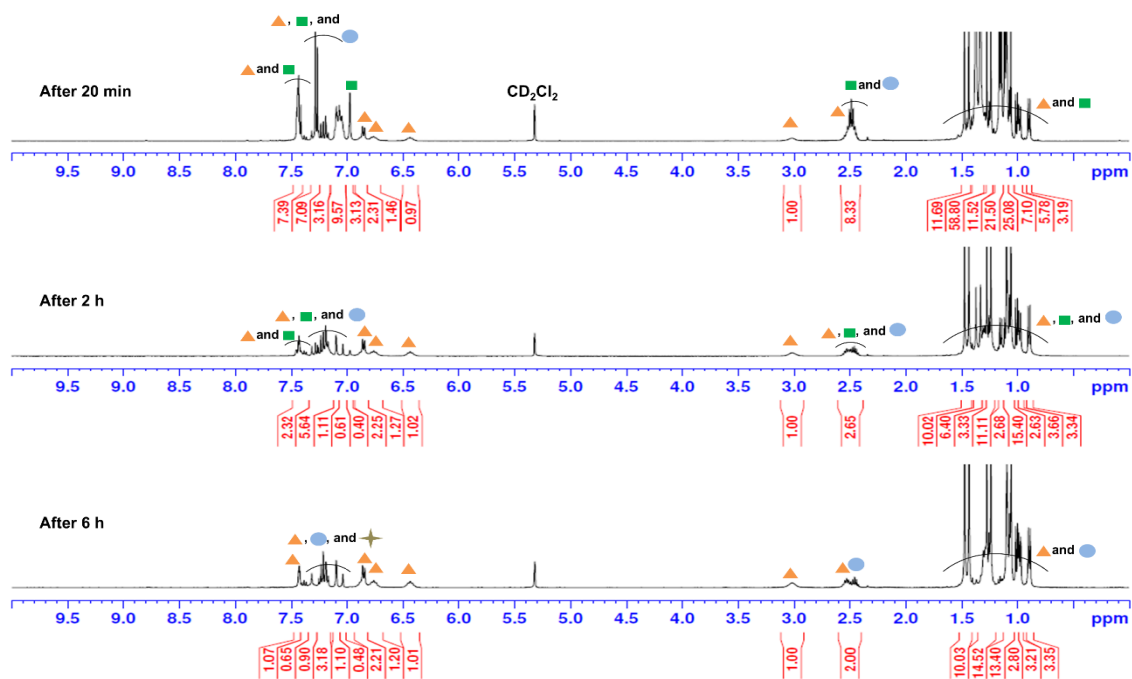


Figure 1.S9. Reaction between **1a** and **B²** at 22 °C monitored by ^1H NMR.

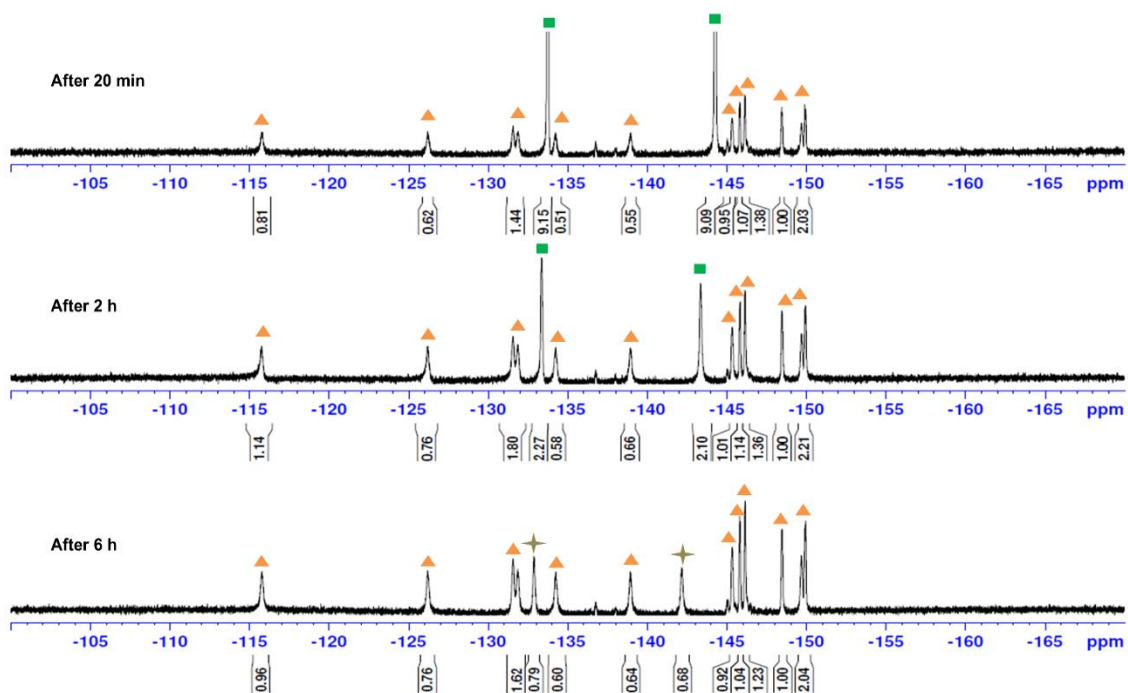


Figure 1.S10. Reaction between **1a** and **B²** at 22 °C monitored by ^{19}F NMR.

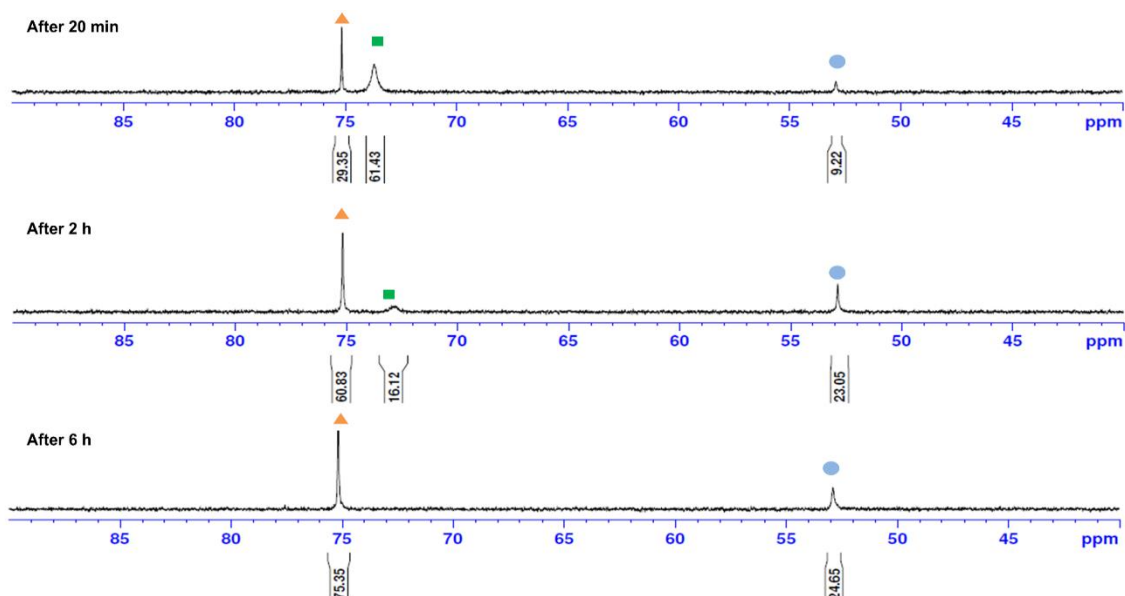
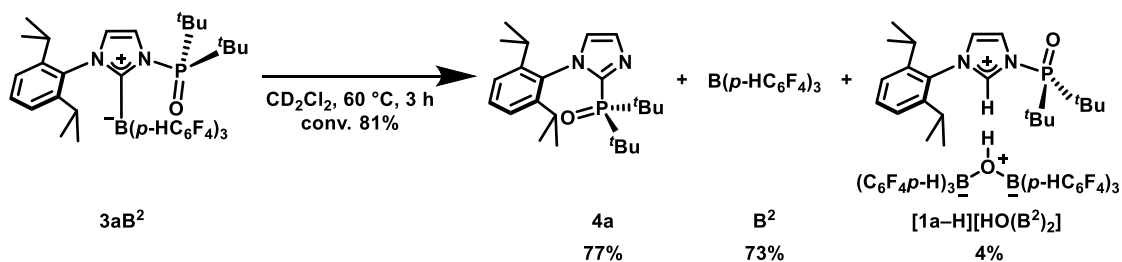
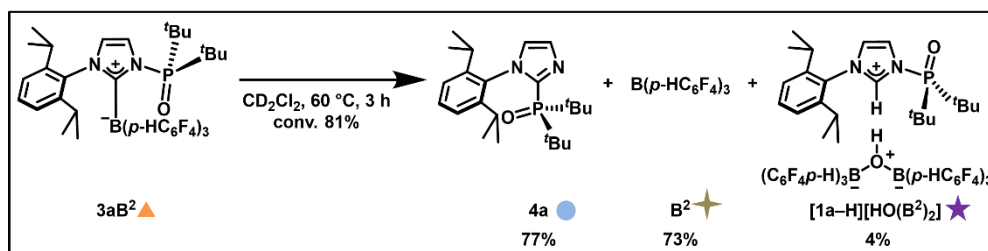


Figure 1.S11. Reaction between **1a** and **B²** at 22 °C monitored by ³¹P NMR.

Thermolysis of **3aB²**



Compound **3aB²** (8.4 mg, 0.01 mmol) and 1,2-dichloroethane (12.5 mg, 0.13 mmol; an internal standard) was dissolved in CD₂Cl₂ (0.5 mL). The resultant mixture was heated at 60 °C for 3 h and NMR analysis was carried out (Figure 1.S12–14), which showed the formation of **4a**, **B²**, and **[1a-H][HO(B²)₂]**.



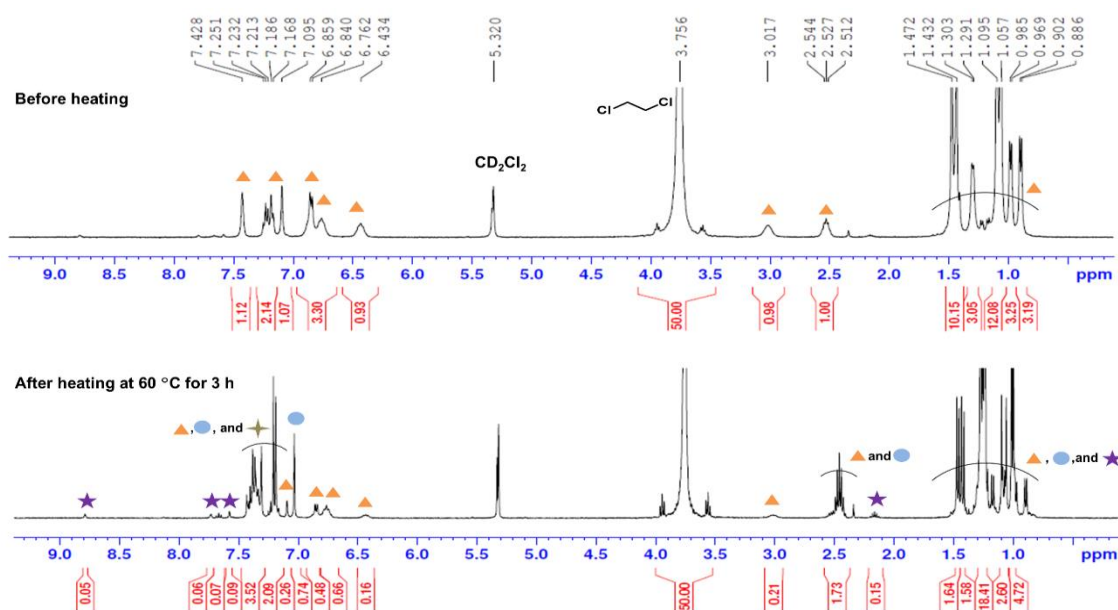


Figure 1.S12. Thermolysis of **3aB²** at 60 °C monitored by ¹H NMR.

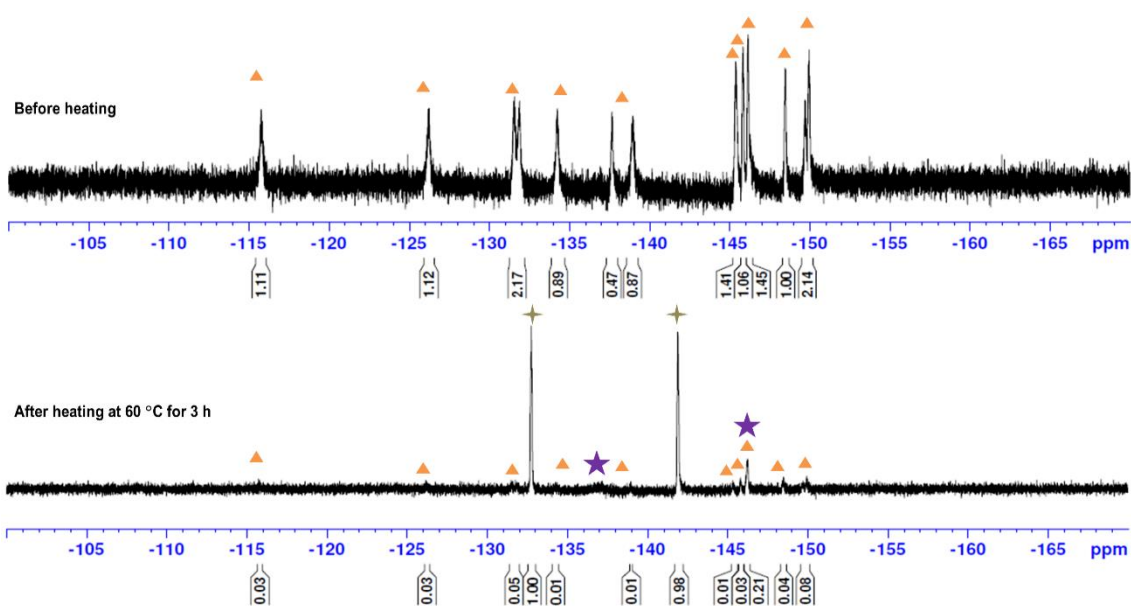


Figure 1.S13. Thermolysis of **3aB²** at 60 °C monitored by ¹⁹F NMR.

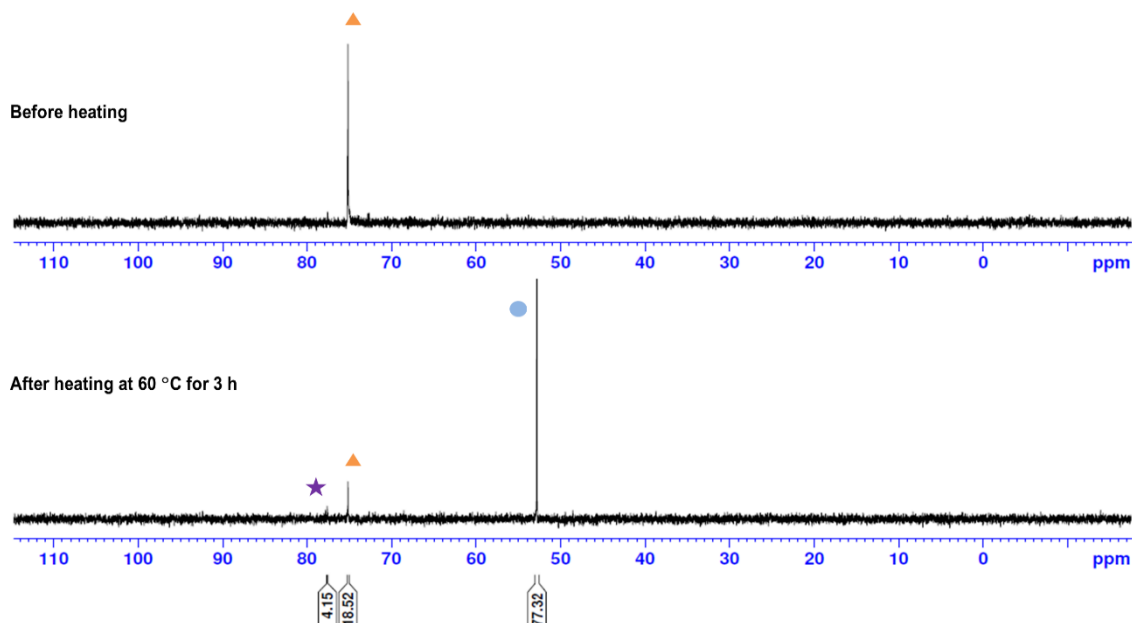
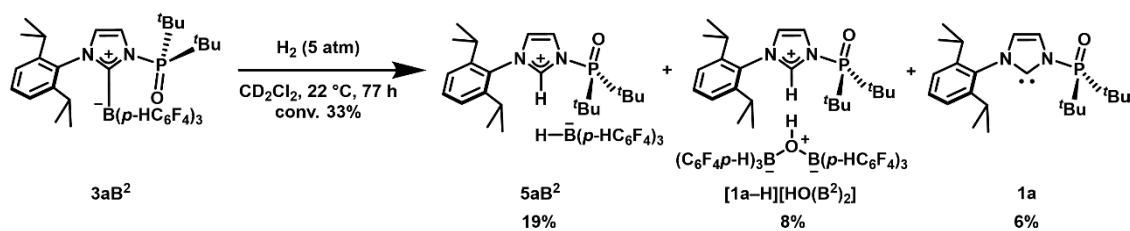
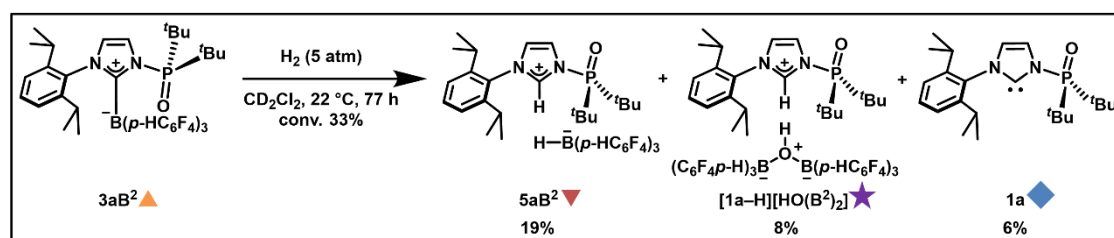


Figure 1.S14. Thermolysis of **3aB²** at 60 °C monitored by ³¹P NMR.

▪ Reaction between **3aB²** and H₂ at 22 °C



A solution of **3aB²** (8.4 mg, 0.01 mmol) in CD₂Cl₂ (0.5 mL) was transferred into a pressure-tight NMR tube. Then, H₂ (5 atm) was pressurized, and the reaction was monitored at room temperature for 77 h by ¹H, ¹⁹F, and ³¹P NMR analyses (Figure 1.S15–17). Yield of products were estimated by the ¹⁹F and ³¹P NMR analyses.



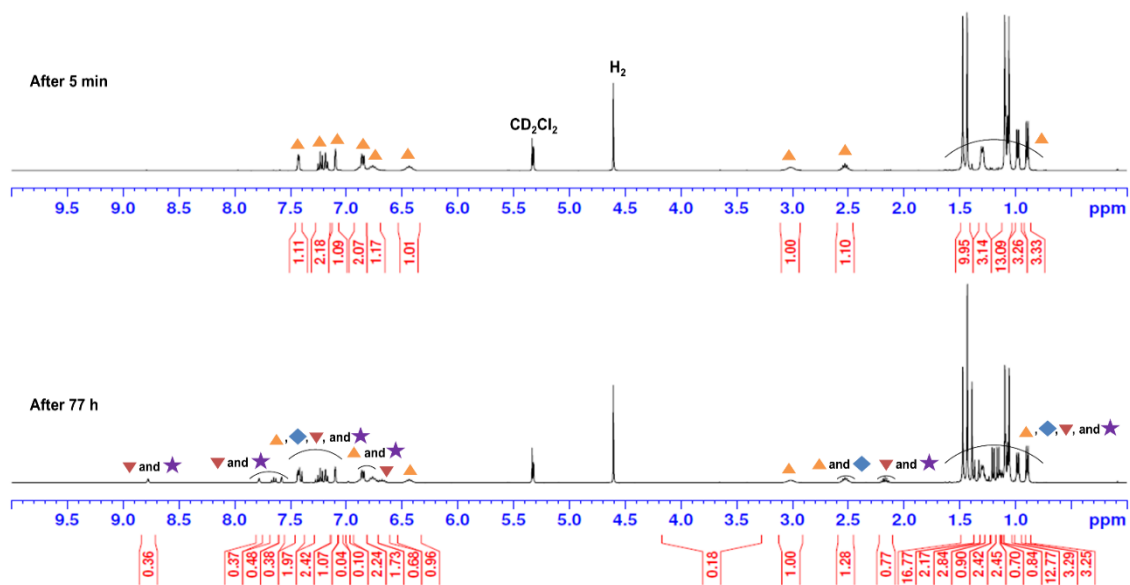


Figure 1.S 15. Reaction between 3aB^2 and H_2 at 22°C monitored by ^1H NMR.

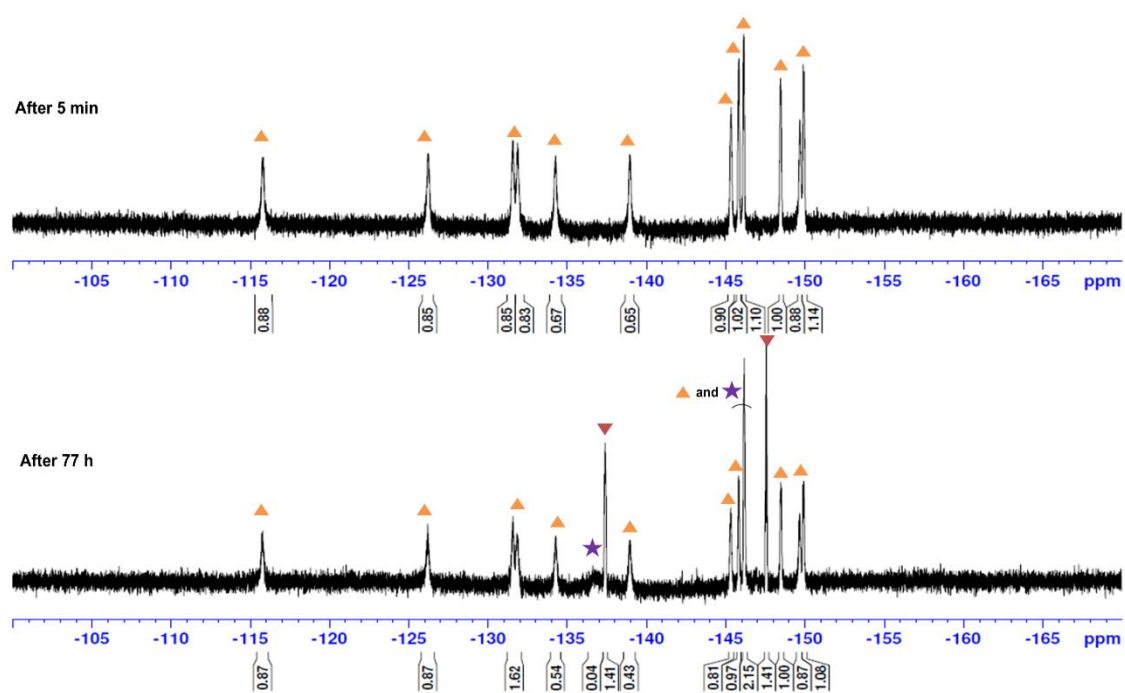


Figure 1.S16. Reaction between 3aB^2 and H_2 at 22°C monitored by ^{19}F NMR.

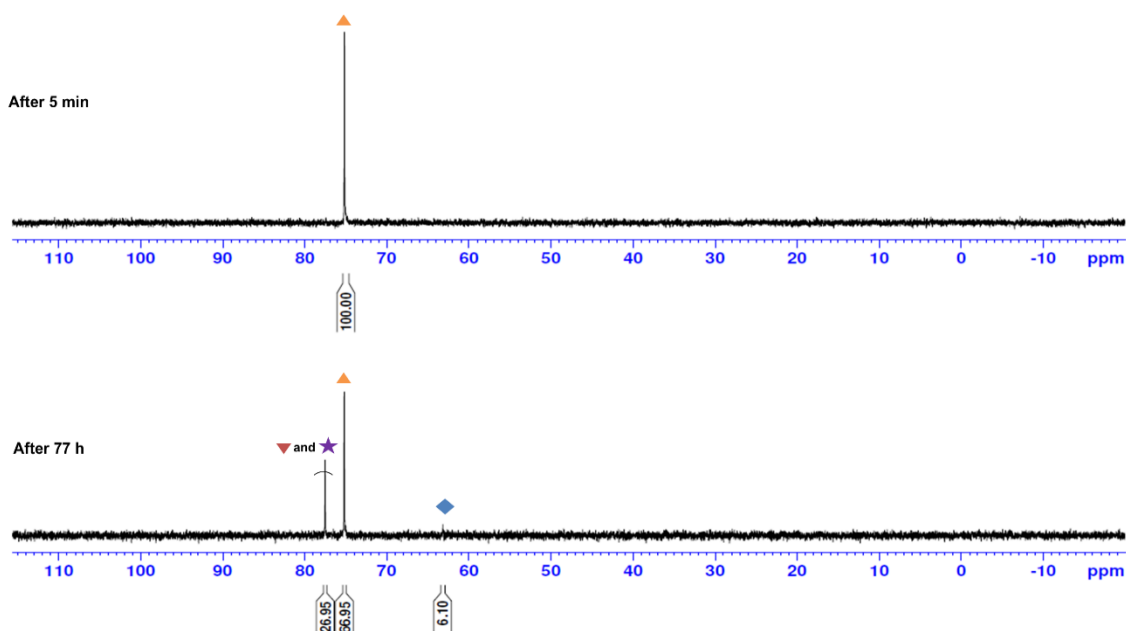
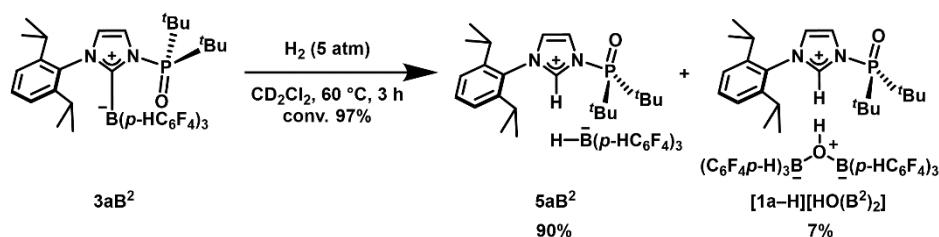
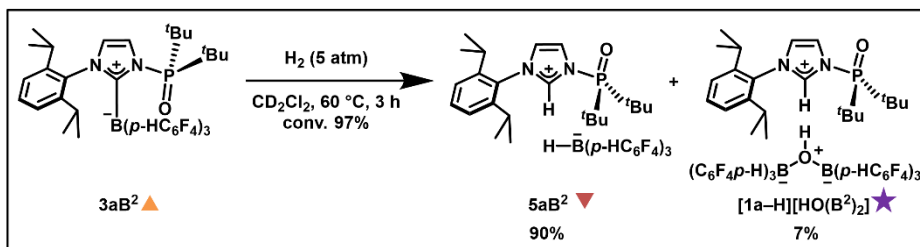


Figure 1.S17. Reaction between **3aB²** and H₂ at 22 °C monitored by ³¹P NMR.

▪ Reaction between **3aB²** and H₂ at 60 °C



A solution of **3aB²** (8.6 mg, 0.01 mmol) in CD₂Cl₂ (0.5 mL) was transferred into a pressure-tight NMR tube. The reaction mixture was heated at 60 °C for 3 h after pressurization of H₂ (5 atm), which was monitored by ¹H, ¹⁹F, and ³¹P NMR analyses (Figure 1.S18–20). Yield of products were estimated by the ¹⁹F and ³¹P NMR analyses.



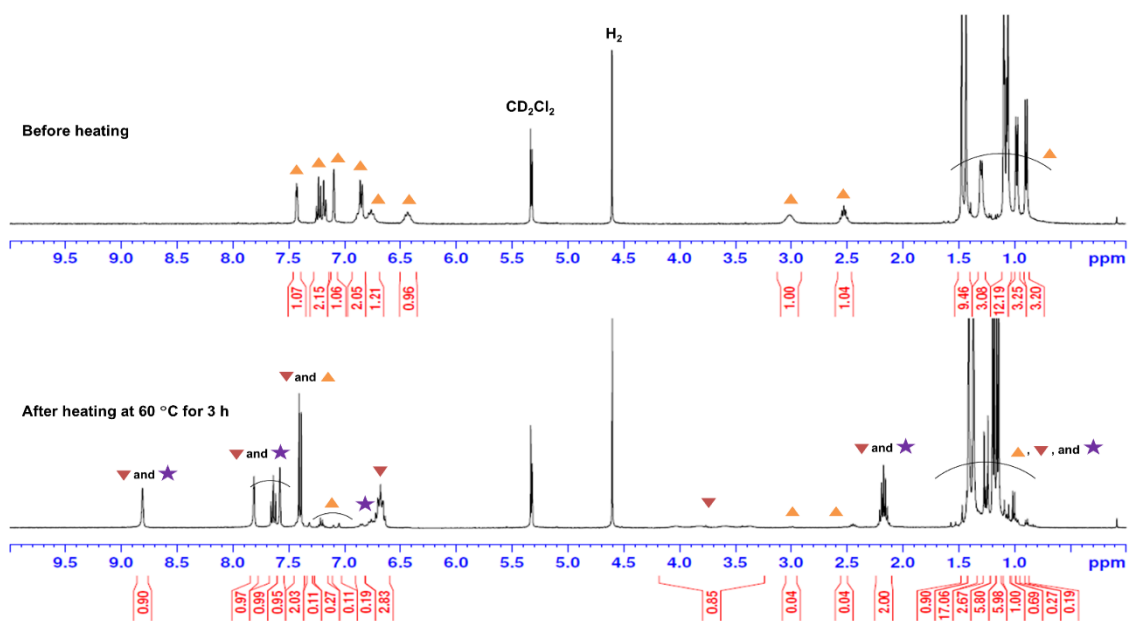


Figure 1.S18. Reaction between 3aB^2 and H_2 at $60\text{ }^\circ\text{C}$ monitored by ^1H NMR.

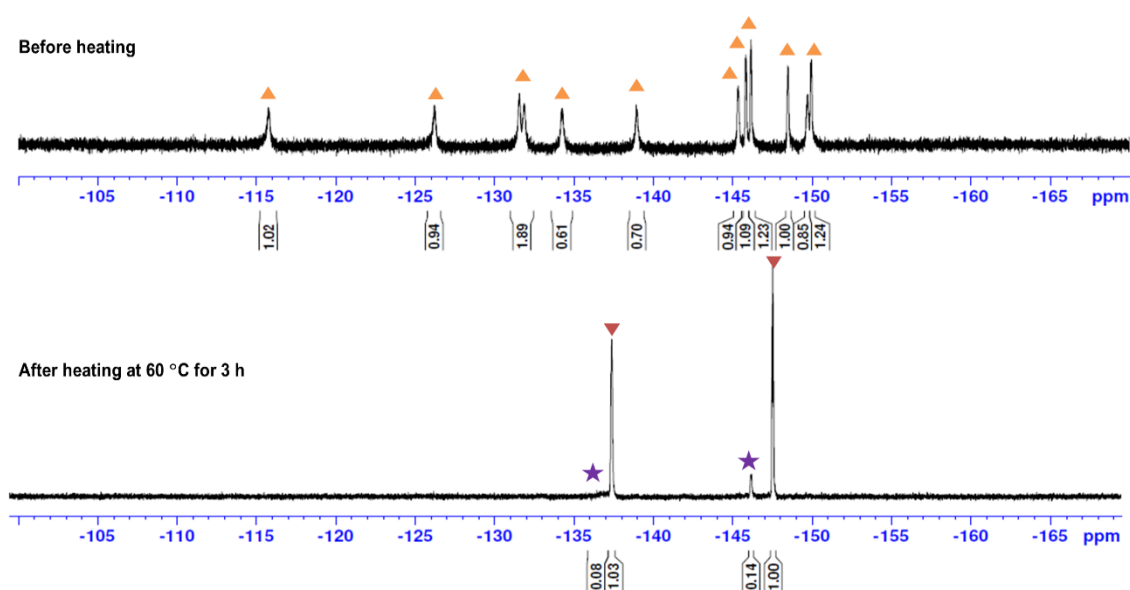


Figure 1.S19. Reaction between 3aB^2 and H_2 at $60\text{ }^\circ\text{C}$ monitored by ^{19}F NMR.

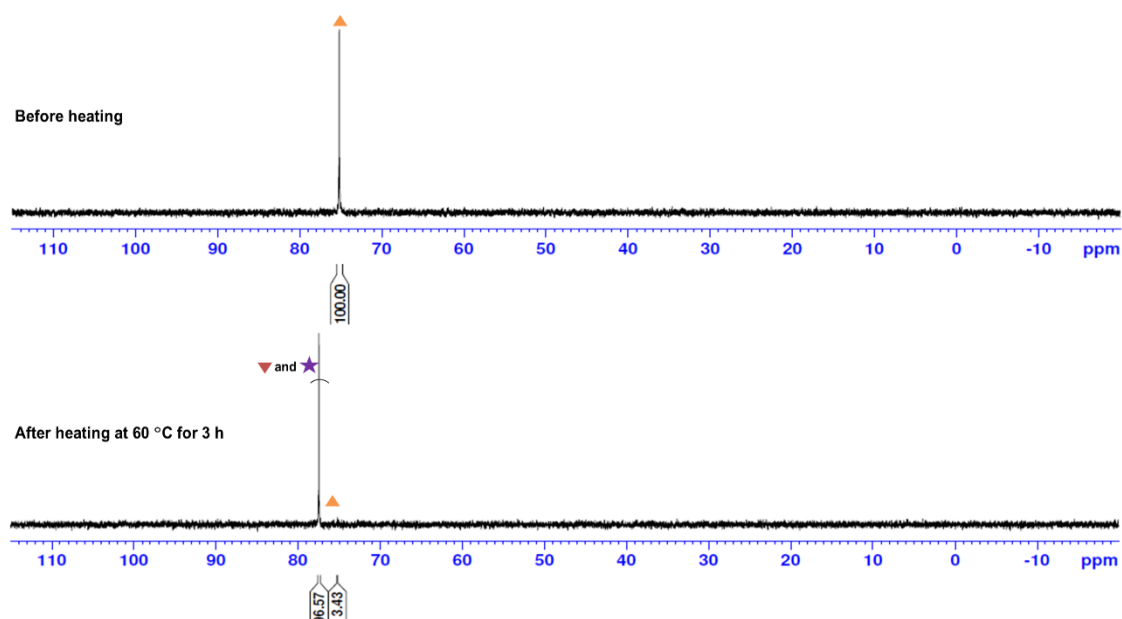
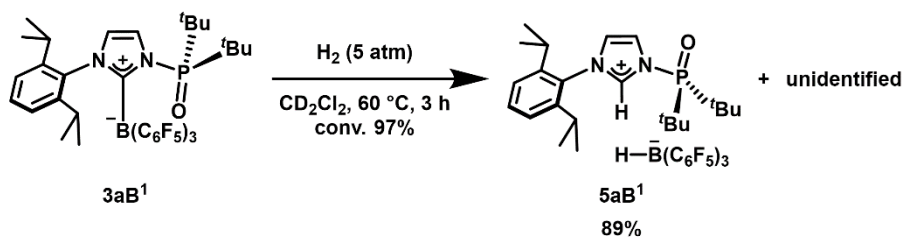
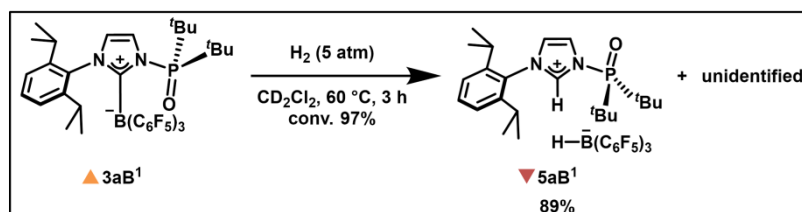


Figure 1.S20. Reaction between **3aB²** and H₂ at 60 °C monitored by ³¹P NMR.

▪ Reaction between **3aB¹** and H₂ at 60 °C



Compound **3aB¹** (9.0 mg, 0.01 mmol) and mesitylene (1.0 mg, 0.01 mmol; an internal standard) was dissolved in CD₂Cl₂ (0.5 mL). After transferring this solution into a pressure-tight NMR tube, H₂ was pressurized at 5 atm. The reaction mixture was then heated at 60 °C for 3 h, monitored by the ¹H, ¹⁹F, and ³¹P NMR analyses (Figure 1.S21–23).



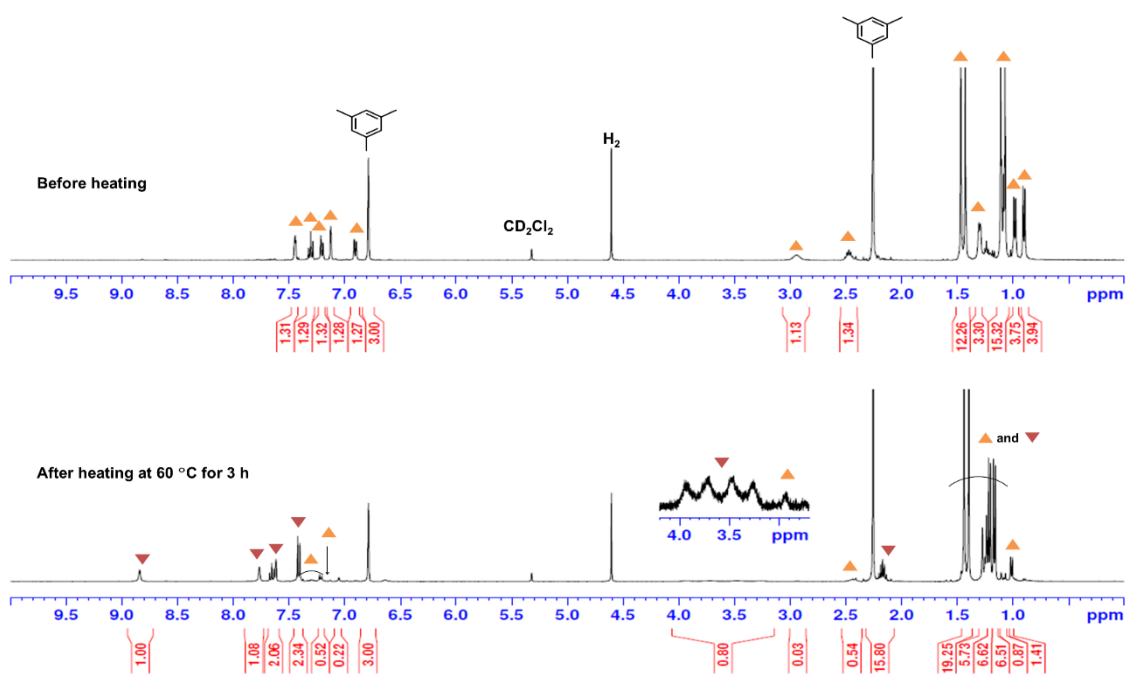


Figure 1.S21. Reaction between **3aB**¹ and H_2 at 60°C monitored by ^1H NMR.

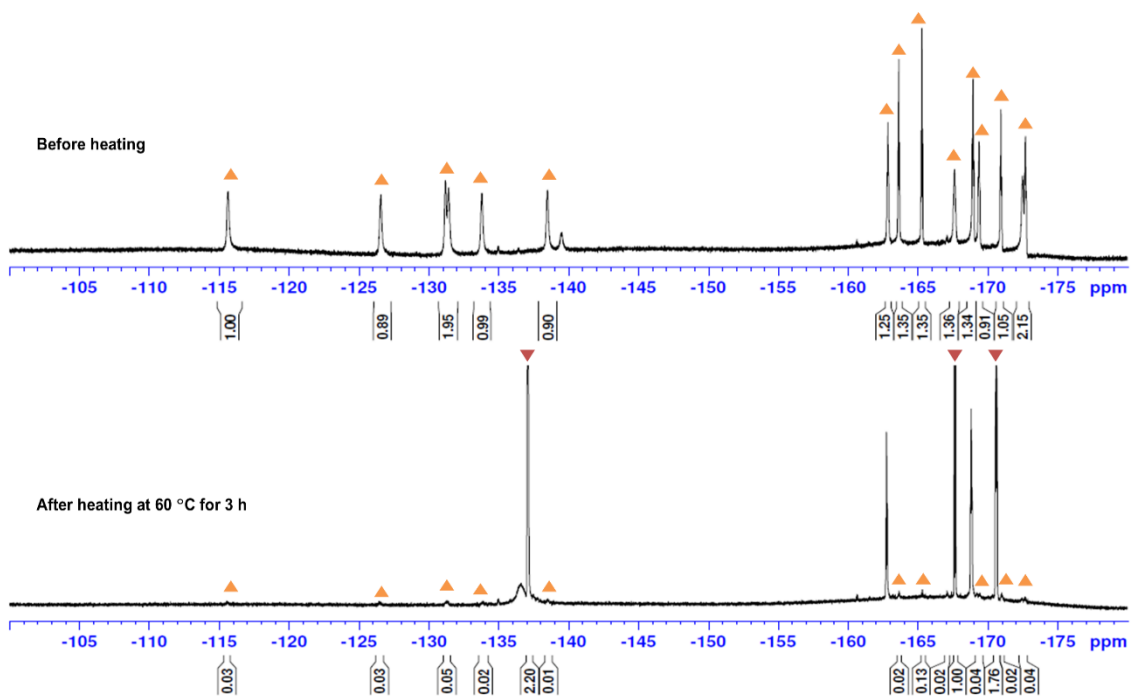


Figure 1.S22. Reaction between **3aB**¹ and H_2 at 60°C monitored by ^{19}F NMR.

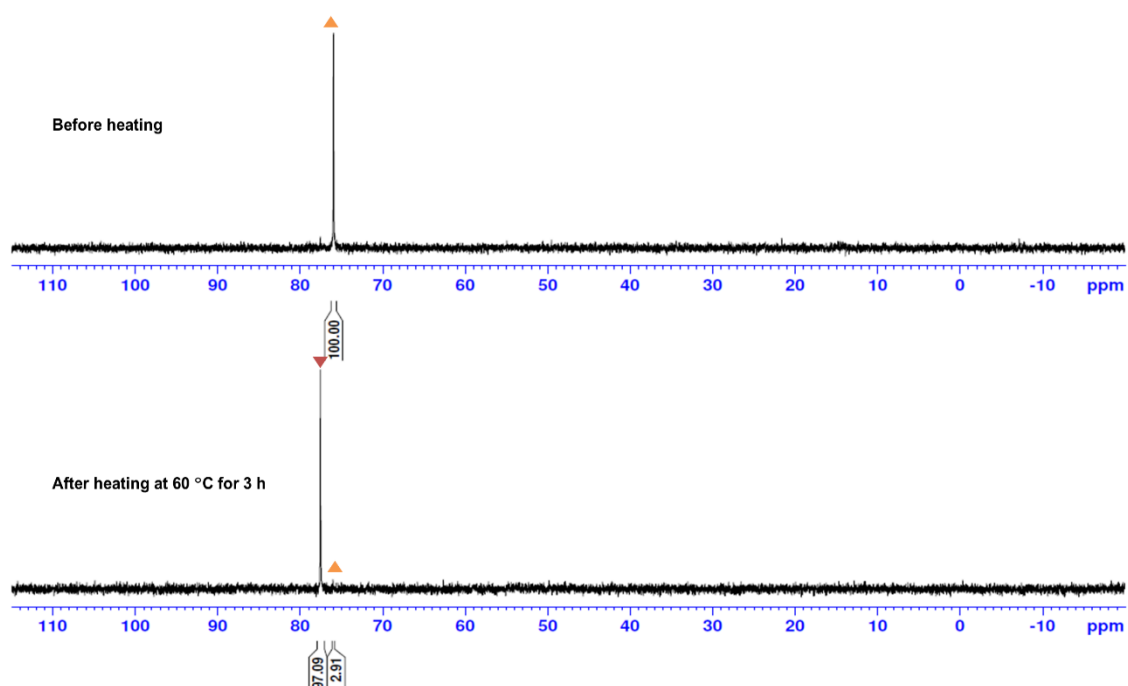
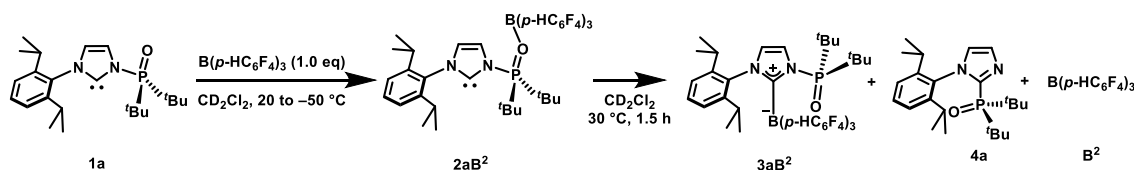


Figure 1.S23. Reaction between **3aB¹** and H₂ at 60 °C monitored by ³¹P NMR.

1.5.6. Variable temperature NMR experiments



A J. Young NMR tube was charged with **1a** (7.6 mg, 0.02 mmol), **B²** (9.4 mg, 0.02 mmol), 1,2-dichloroethane (2.5 mg, 0.03 mmol; an internal standard), and CD_2Cl_2 (0.5 mL). The ¹H, ¹⁹F, and ³¹P NMR analyses were once conducted at 20°C , and then the temperature was changed to -50°C . The NMR measurements were then conducted at every 20°C . Then, the reaction was monitored for 1.5 h after the mixture was allowed to warm to 30°C (Figure 1.S24–26).

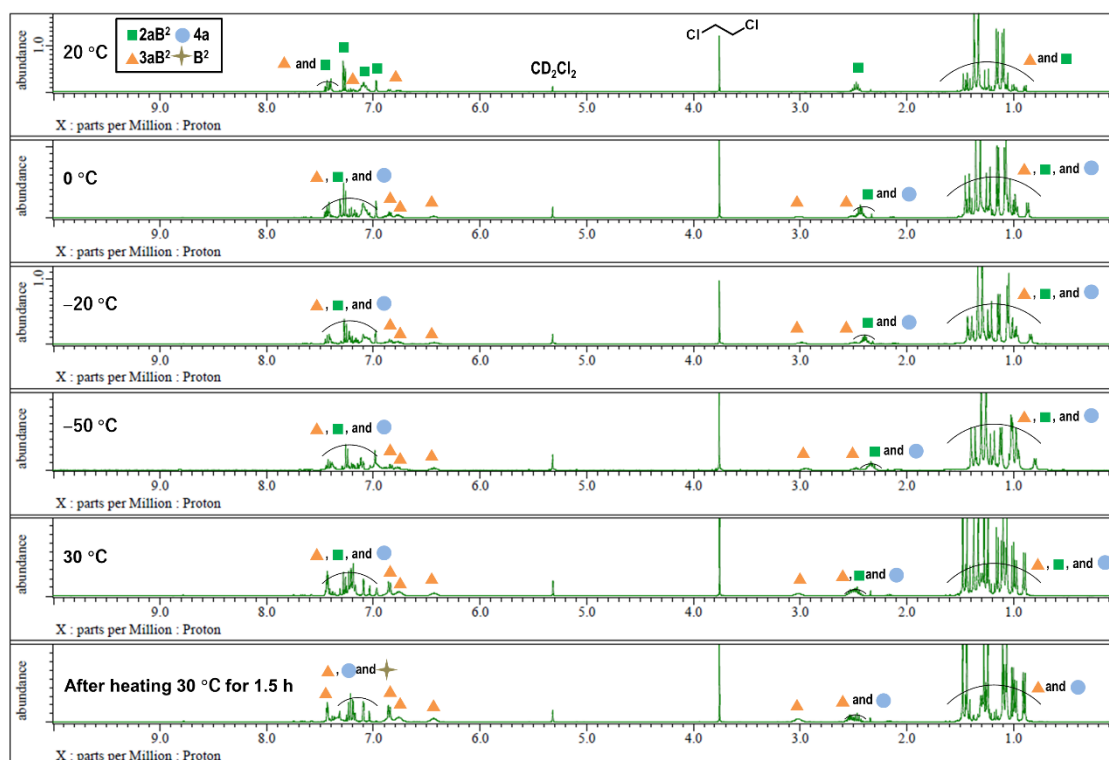


Figure 1.S24. ^1H NMR spectra obtained by the VT-NMR.

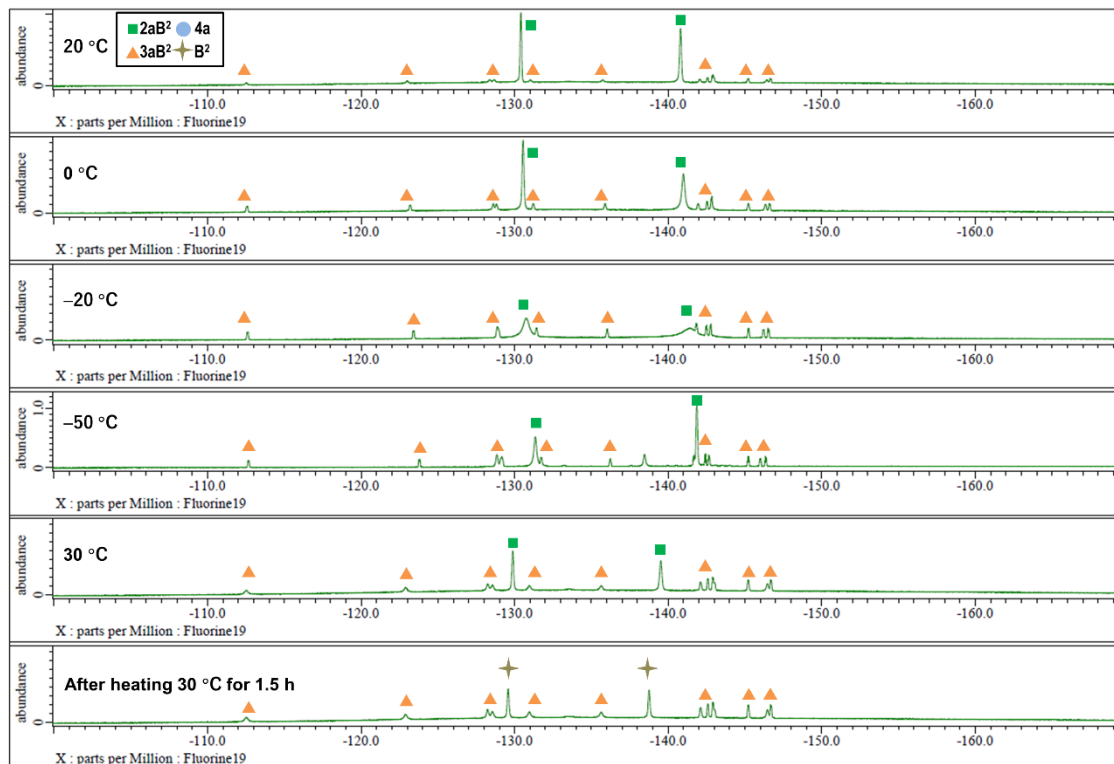


Figure 1.S25. ^{19}F NMR spectra obtained by the VT-NMR.

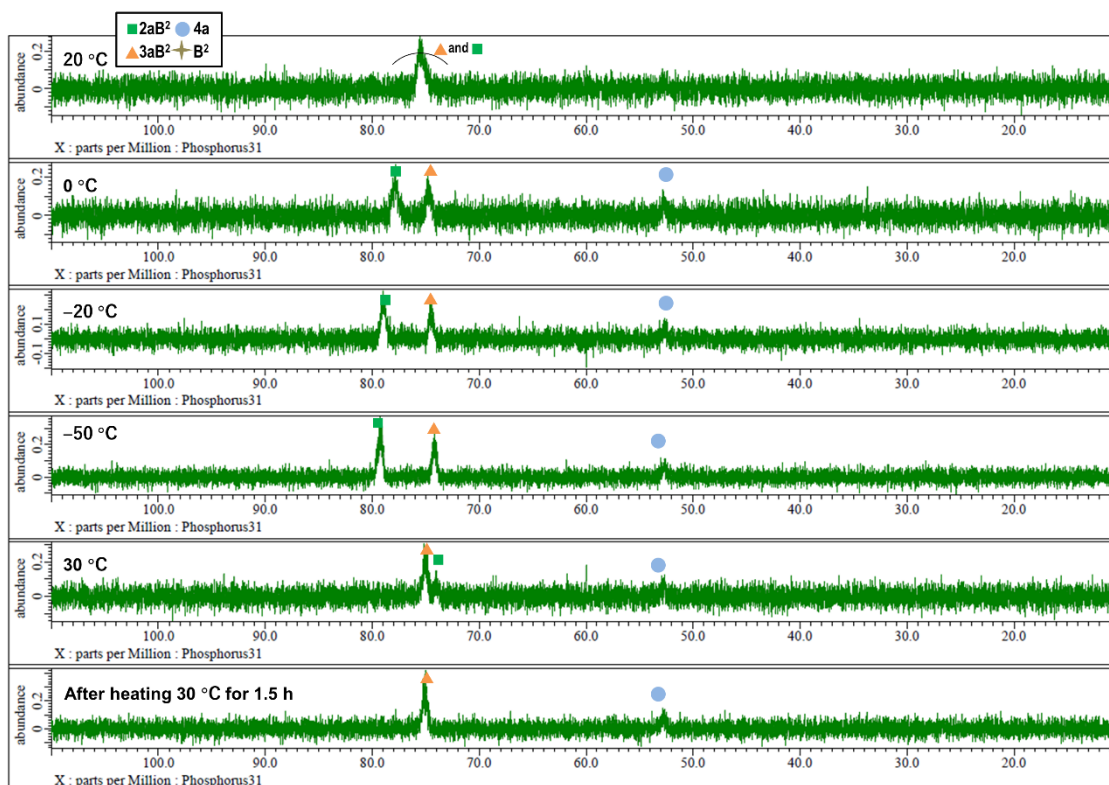
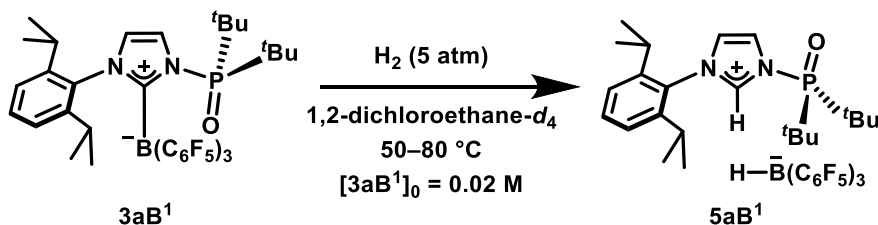


Figure 1.S26. ^{31}P NMR spectra obtained by the VT-NMR.

1.5.7. Kinetics studies

• The Arrhenius plot



A solution of **3aB¹** (9.0 mg, 0.01 mmol) and mesitylene (2.4 mg, 0.02 mmol; an internal standard) in 1,2-dichloroethane- d_4 (0.5 mL) was heated at 60 °C in the presence of H_2 that was pressurized at 5 atm into a pressure-tight NMR tube. The reaction was monitored by ^1H NMR analysis. The rate constant of the production of **5aB¹** was evaluated by least-squares fitting of the time–conversion profiles to a first-order rate equation.

$$d[\mathbf{5aB^1}]/dt = k_{\text{obs}}[\mathbf{3aB^1}]$$

$$k_{\text{obs}} = 11.2(8) (10^{-5} \text{ s}^{-1})$$

The aforementioned procedure was applied for the reaction between H_2 and **3aB¹** conducted at 50, 70, and 80 °C, respectively (Figure 1.S27). All experiments were repeated two times to give k_{obs} (10^{-5} s^{-1}) as an average of values obtained in each experiment (Figure 1.S28). These results were used for the analysis of reaction parameters estimated by the Arrhenius Equation (Eqn. 1).

$$\ln k_{\text{obs}} = -\left(\frac{E_a}{R}\right)\left(\frac{1}{T}\right) + \ln A \quad (1)$$

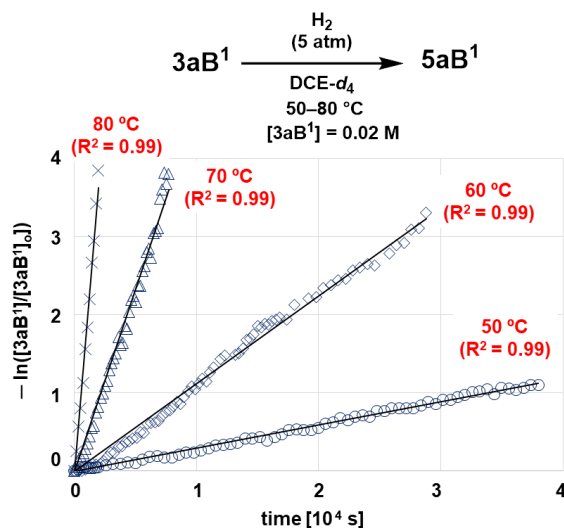
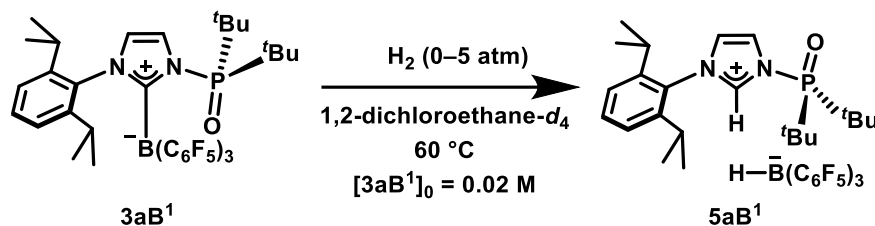


Figure 1.S27. The profiles of time (10^4 s) vs $-\ln([\text{3aB}^1]/[\text{3aB}^1]_0)$ at 50, 60, 70, and 80 °C.

T (°C)	Reaction rate constant, k_{obs} (10^{-5} s^{-1})		
	1 st run	2 nd run	average
50	2.95(2)	2.73(3)	2.84(2)
60	11.2(8)	10.1(14)	10.6(8)
70	46.4(4)	44.0(6)	45.2(4)
80	183(2)	161(2)	172(2)

Figure 1.S28. The list of reaction rate constants, k_{obs} (10^{-5} s^{-1}).

• Order in H_2



A solution of **3aB**¹ (9.0 mg, 0.01 mmol) and mesitylene (internal standard) in 1,2-dichloroethane-*d*₄ (0.5 mL) was heated at 60 °C in the presence of H_2 that was pressurized at 0.5, 1, 2, and 5 atm, respectively, into a pressure-tight NMR tube (Figure 1.S29). The initial reaction rate constants (k_{int} (10^{-5} s^{-1})) for the production of **5aB**¹ were determined based on the results of the ^1H NMR measurements. All experiments were repeated two times to give k_{int} (10^{-5} s^{-1}) as an average of values obtained in each experiment (Figure 1.S30).

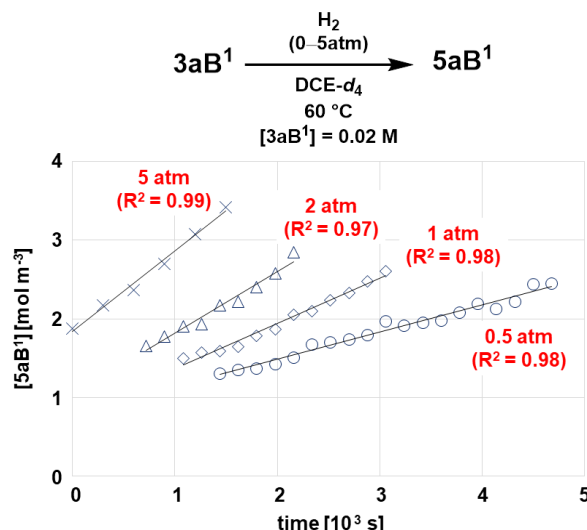


Figure 1.S29. The profiles of time (10^3 s) vs $[5\mathbf{aB}^1]$ (mol m^{-3}) at 0.5, 1, 2, and 5 atm.

	Initial reaction rate constant, k_{int} (10^{-5} s^{-1})		
P (atm)	1 st run	2 nd run	average
0	0	0	0
0.5	1.73(7)	1.72(8)	1.73(5)
1	2.87(13)	2.57(12)	2.72(9)
2	3.92(26)	3.98(13)	3.95(15)
5	5.12(25)	5.13(36)	5.12(22)

Figure 1.S30. The list of initial reaction rate constants, k_{int} (10^{-5} s^{-1}).

1.5.8 Theoretical studies

• Computational details

Geometry optimizations and energy calculations were performed by using the density functional theory (DFT) at the $\omega\text{B97X-D/6-31G(d)}$ ^{S4-S6} level. For the H atoms in H_2 molecule, a p-type polarization function was augmented.^{S6} For the thermal correction, temperature and pressure were set to 298.15 K and 1.0 atm, respectively. At the optimized structures, I performed single-point calculations with the 6-311G(d,p) basis sets with solvation effect. A polarizable continuum model^{S7} was adopted, and the parameters for 1,2-dichloroethane (DCE) were used. The Gaussian 09 package was used for the DFT calculations.^{S8}

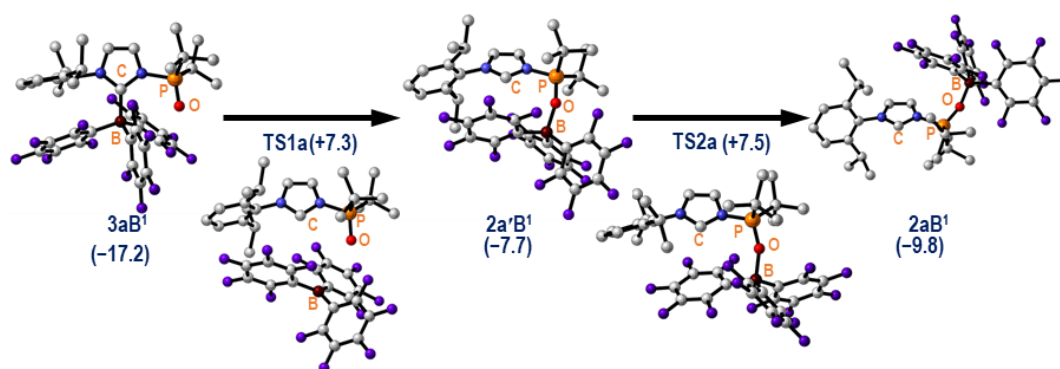
The analyses on the quantum theory of the atoms in molecules were carried out using AIMAll program (Version 19.10.12),^{S9} in which the wave functional wiles were prepared based on the optimized electron density at the $\omega\text{B97X-D/6-31G(d)}$ level of theory.

• Details on proposed mechanism

The relative Gibbs energies shown in Figure 1.S31–33 are shown in kcal mol^{-1} with respect to that of $[1\mathbf{a} + \mathbf{B}^1]$.

Theoretical Calculations for Paths from 3aB¹ to 2aB¹

The relative Gibbs free energies vs [1a + B¹] are given in kcal mol⁻¹.



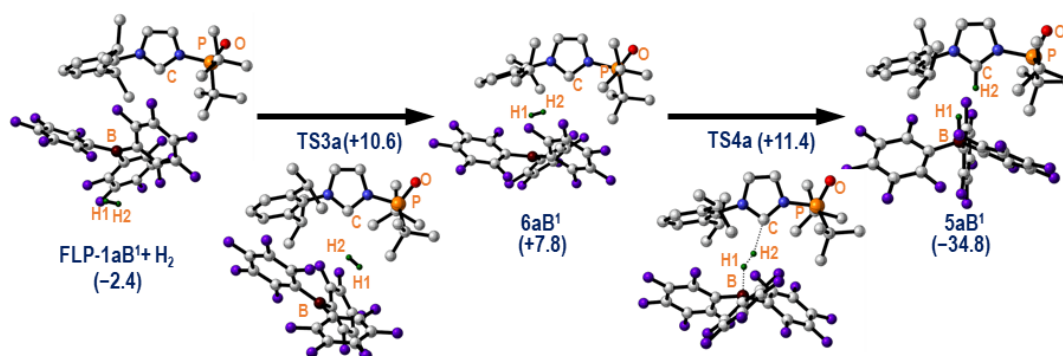
Selected bond lengths/(interatomic distances) (Å) and angles (°)

	3aB ¹	TS1a	2a'B ¹	TS2a	2aB ¹
C-B	1.71	(4.24)	—	—	—
O-B	(3.28)	(3.34)	1.59	1.62	1.58
P-O-B	92.8	141.8	152.7	159.8	150.2
C-N-P-O	3.92	43.3	35.5	60.0	156.0

Figure 1.S31. Theoretical calculations for paths from 3aB¹ to 2aB¹.

Theoretical Calculations for Path-I from FLP to 5aB¹

The relative Gibbs free energies vs [1a + B¹] are given in kcal mol⁻¹.



Selected bond lengths/(interatomic distances) (Å) and angles (°)

	FLP-1aB ¹	TS3a	6aB ¹	TS4a	5aB ¹
H1-H2	0.74	0.74	0.75	0.84	(1.69)
C-H2	—	(3.40)	(2.58)	(1.83)	1.08
B-H1	—	(2.80)	(2.36)	(1.49)	1.22
C-N-P-O	170.5	158.2	169.8	170.0	172.0

Figure 1.S32. Theoretical calculations for path I, affording 5aB¹ from FLP-1aB¹.

Theoretical Calculations for Path-II from 2aB¹ to 5aB¹

The relative Gibbs free energies vs [1a + B¹] are given in kcal mol⁻¹.

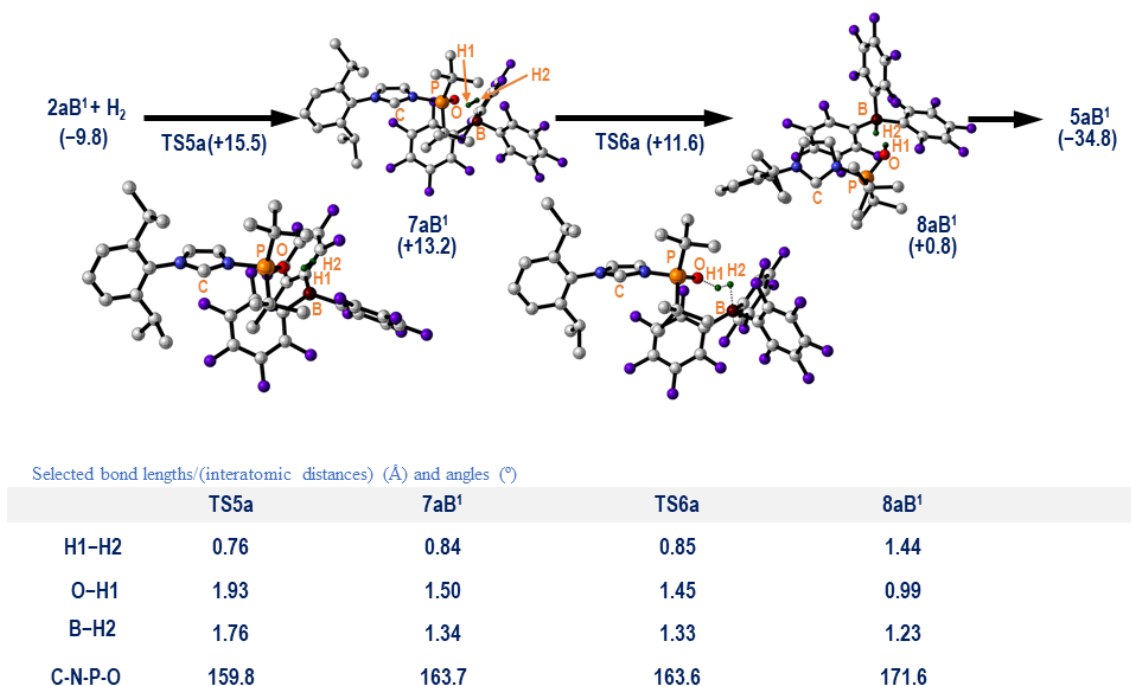


Figure 1.S33. Theoretical calculations for path II, affording **5aB¹** from **2aB¹**.

Discussions for TS1. The potential energy surface around **TS1a** was found to be relatively flat (Figure 1.S34). As ordinary IRC calculations were difficult to apply, I thus performed a relaxed potential energy scan calculation that approximately shows the connection from **2a'B¹** to **3aB¹** via **TS1a**.

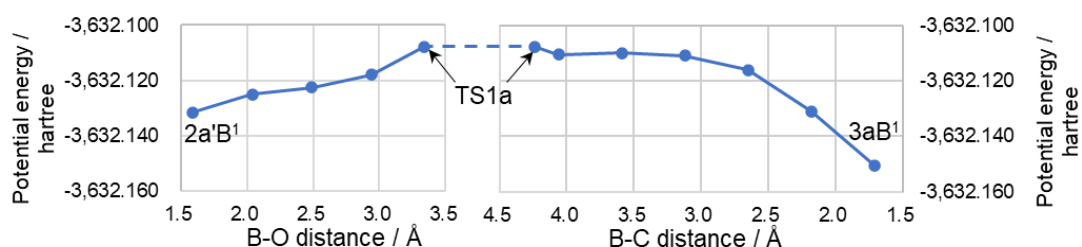


Figure 1.S34. Minimum energy potential pathway from **2a'B¹** to **3aB¹** via **TS1a**, obtained from a relaxed potential energy scan calculation. For the reaction coordinate from **2a'B¹** to **TS1a**, the B–O(P=O) distance was used. For that from **3aB¹** to **TS1a**, the B–C(carbene) distance was used.

Discussions for TS3a. Relative potential energies are shown in Figure 1.S35a for the structures along a minimum energy pathway. To the left of **TS3a**, the result of an IRC calculation is shown. To the right of **TS3a**, the relative potential energy is plotted for structures along the steepest decent pathway that was obtained from a structural optimization with very small increments. This optimization terminated at a metastable minimum which is energetically 0.4 kcal/mol higher than the **6aB¹** state. This metastable point is structurally close to that of the **6aB¹** state (Figure 1.S35b and 35c). Therefore, under thermal fluctuations in the experimental conditions, the system can be expected to reach the **6aB¹** state.

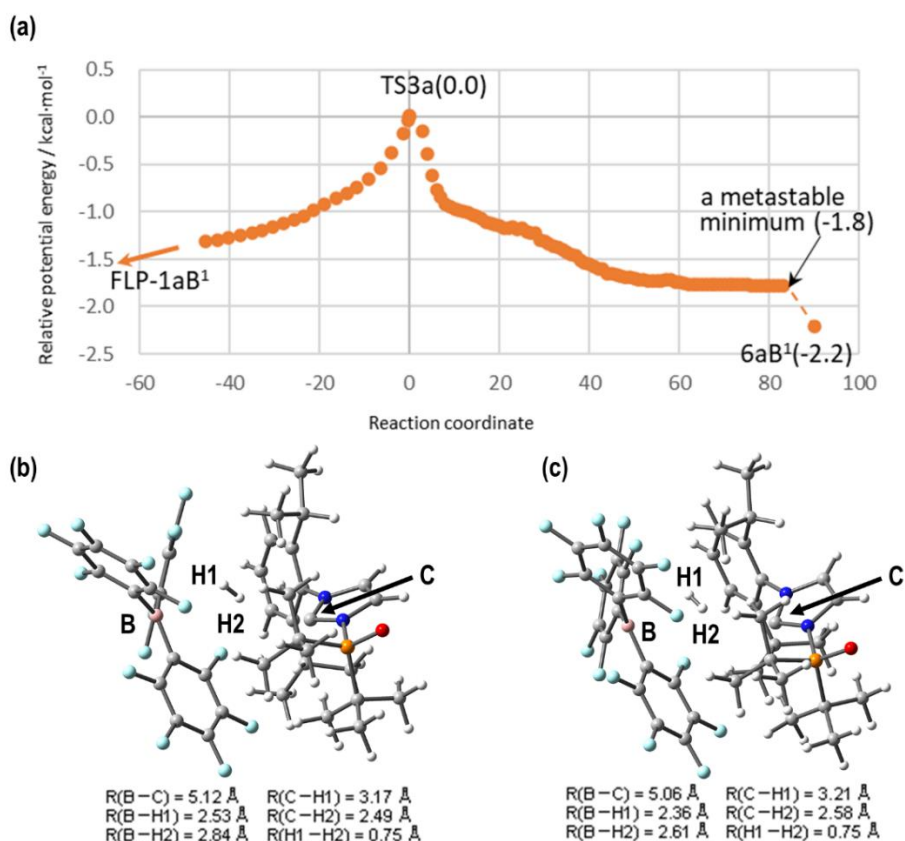


Figure 1.S35. (a) Relative potential energies of structures along a minimum energy pathway via **TS3a**. For the reaction coordinates from 0 (**TS3a**) in negative direction, an IRC is given. Those from 0 in positive direction represent potential energies of structures along the steepest descent direction obtained from a structural optimization with very small increments. For the **6aB¹** state, a reaction coordinate of 90 is given only for representation purposes. The numbers in parentheses are potential energy values relative to that of **TS3a**. Structures of (b) the metastable minimum state and (c) the **6aB¹** state with selected structural parameters.

Discussions for TS5a. Relative potential energies are shown in Figure 1.S36 for the structures along a minimum energy pathway. To the right of **TS5a**, the result of the IRC calculation is given. To the left of **TS5a**, the relative potential energy is plotted for structures along the steepest decent pathway obtained from a structural optimization with very small increments. This optimization terminated at the **7aB¹** state, which shows the connectivity between the two stationary points.

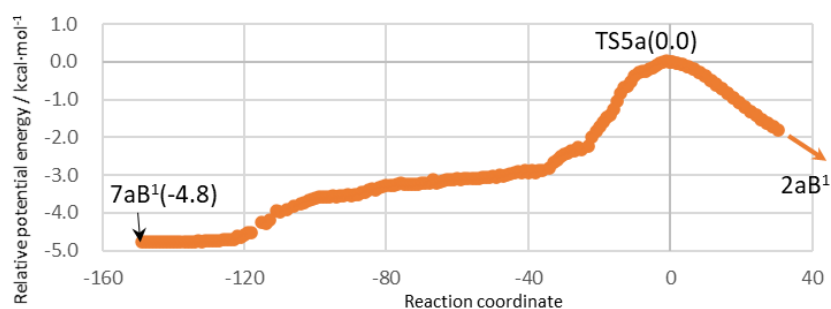


Figure 1.S36. Relative potential energies of structures along a minimum energy pathway via **TS5a**. For reaction coordinates from 0 (**TS5a**) in positive direction, the result of the IRC calculation is given. Those from 0 in negative direction are potential energies of structures along the steepest descent direction given by structural optimization with very small increments. The numbers in parentheses represent potential energy values relative to that of **TS5a**.

Discussions for TS6a. Given the results on the structural optimization, the potential energy of **TS6a** (−3633.288355 hartree) is found to be very close to that of **7aB¹** (−3633.288363 hartree). In general, Gibbs energy correction (ΔG_{Gibbs}) is positive, and ΔG_{Gibbs} to a transition state is smaller than that of an equilibrium state. This causes the reversed energy level between **TS6a** and **7aB¹** found in Figure 1.5b. The energy difference after the Gibbs correction and implementation of solvent effect was 1.5 kcal mol^{−1}, of which 1.4 kcal mol^{−1} arises from ΔG_{Gibbs} .

▪ The AIM analysis of TS1a

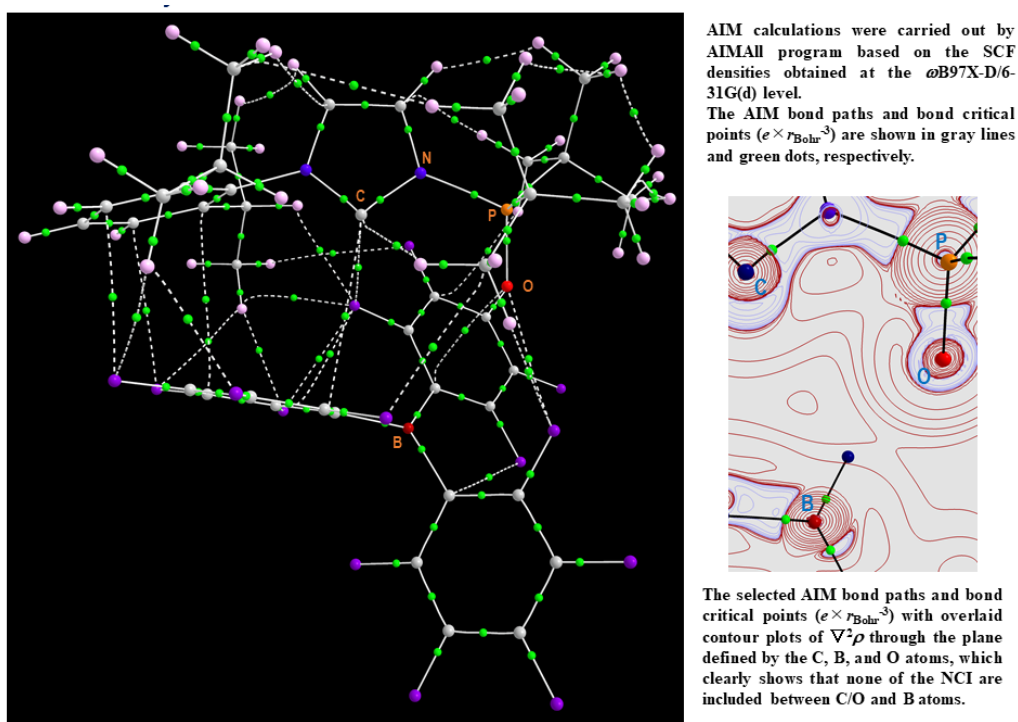


Figure 1.S37. Results of the AIM analysis of **TS1a**.

1.5.9. References for supporting information

- S1. Hoshimoto, Y.; Kinoshita, T.; Ohashi, M.; Ogoshi, S. *Angew. Chem. Int. Ed.* **2015**, *54*, 11666.
- S2. Ullrich, M.; Lough, A. J.; Stephan, D. W. *J. Am. Chem. Soc.* **2009**, *131*, 52.
- S3. Ullrich, M.; Lough, A. J.; Stephan, D. W. *Organometallics* **2010**, *29*, 3647.
- S4. Chai, J.-D.; Head-Gordon, M. *Phys. Chem. Chem. Phys.* **2008**, *10*, 6615.
- S5. Hehre, W. J.; Ditchfield, R.; Pople, J. A. *J. Chem. Phys.* **1972**, *56*, 2257.
- S6. Hariharan, P. C.; Pople, J. A. *The Influence of Polarization Functions on Molecular Orbital Hydrogenation Energies. Theor. Chim. Acta.* **1973**, *28*, 213.

- S7. Tomasi, J.; Mennucci, B.; Cammi, R. *Chem. Rev.* **2005**, *105*, 2999.
- S8. Frisch, M. J.; Trucks, G. W.; Schlegel, H. B.; Scuseria, G. E.; Robb, M. A.; Cheeseman, J. R.; Scalmani, G.; Barone, V.; Mennucci, B.; Petersson, G. A.; Nakatsuji, H.; Caricato, M.; Li, X.; Hratchian, H. P.; Izmaylov, A. F.; Bloino, J.; Zheng, G.; Sonnenberg, J. L.; Hada, M.; Ehara, M.; Toyota, K.; Fukuda, R.; Hasegawa, J.; Ishida, M.; Nakajima, T.; Honda, Y.; Kitao, O.; Nakai, H.; Vreven, T.; Montgomery, J. A.; Peralta, Jr., J. E.; Ogliaro, F.; Bearpark, M.; Heyd, J. J.; Brothers, E.; Kudin, K. N.; Staroverov, R.; Kobayashi, J.; Normand, K.; Raghavachari, A.; Rendell, J. C.; Burant, S. S.; Iyengar, V. N.; Tomasi, J.; Cossi, M.; Rega, N.; Millam, J. M.; Klene, M.; Knox, J. E.; Cross, J. B.; Bakken, V.; Adamo, C.; Jaramillo, J.; Gomperts, R.; Stratmann, R. E.; Yazyev, O.; Austin, A. J.; Cammi, R.; Pomelli, C.; Ochterski, J. W.; Martin, R. L.; Morokuma, K.; Zakrzewski, V. G.; Voth, G. A.; Salvador, P.; Dannenberg, J. J.; Dapprich, S.; Daniels, A. D.; Farkas, Ö.; Foresman, J. B.; Ortiz, J. V.; Cioslowski, J.; Fox, D. J. Gaussian 09, Revision C.02. Gaussian, Inc., Wallingford CT (2009).
- S9. Keith, T. A. TK Gristmill Software, Overland Park KS, USA (2019) (aim.tkgristmill.com).

Chapter 2

Remote Back Strain for Catalytic Hydrogenation of Carbonyl Compounds Using Crude H₂

Abstract: Toward a more efficient use of crude H₂ without its energy-consuming purification, this study employs gaseous mixtures of H₂, CO, CO₂, and CH₄ for the catalytic hydrogenation of aldehydes and ketones in the presence of strategically designed triarylboranes and 4-methyltetrahydropyran as a greener ethereal solvent. The present results emphasize the unexplored utility of less-toxic main-group catalysis for the catalytic hydrogenation using crude H₂ beyond the well-established transition-metal catalysis, which generally requires purified H₂.

2.1. Introduction

Molecular hydrogen (H₂) is commonly used as a reductant in contemporary industries producing indispensable commodities such as fertilizers, fuels, cosmetics, and pharmaceuticals via hydrogenation of unsaturated molecules.¹ In the mid- to long-term future, a large amount of crude H₂, i.e., a gaseous mixture of H₂ and contaminants such as CO, CO₂, and CH₄, is expected to be produced from a variety of hydrocarbon resources (Figure 2.1).² In this context, biomass and hitherto less-explored wastes such as food and livestock wastes include hydrocarbons and can thus be used for the production of H₂ based on the waste-to-hydrogen strategy.³ Industrial off-gases generated in processes such as steel manufacturing, refineries, and contemporary H₂ purification also contain a considerable amount of H₂; however, off-gases have been predominantly used as a fuel for flame stack because efficient H₂-separation strategies remain challenging tasks.^{1,4} In fact, purification processes to remove such contaminants from crude H₂ affect the total energy consumption of the H₂-production process. Accordingly, intense research efforts have been devoted to the optimization/modification of technologies for the efficient and sustainable purification of H₂. Unfortunately, an approach that can fundamentally solve all these challenges remains to be established.

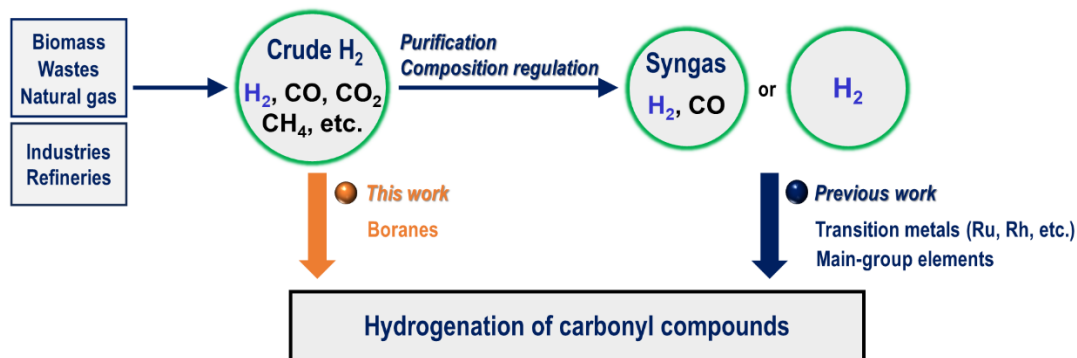


Figure 2.1. Hydrogenation of carbonyl compounds with crude H₂ (this work) or syngas/purified H₂ (previous

work). A simplified scheme of representative contemporary route of syngas/H₂ production from hydrocarbon resources is shown.

Our group has recently demonstrated a strategy to directly use gaseous mixtures of H₂/CO/CO₂/CH₄ (1/1/1/1 molar ratio) or H₂/CO/CO₂ (1/5/1 or 1/1/5 molar ratio) for the catalytic hydrogenation of *N*-heteroaromatics.⁵ In these reactions, frustrated Lewis pairs (FLPs)^{6–8} comprising triarylboranes (BAR₃; note: heteroleptic species including different aryl groups are also represented in this form) and Lewis bases (LBs) such as *N*-heteroaromatics and their reduced derivatives mediate the heterolytic cleavage of H₂ in the copresence of CO and CO₂ even though several undesired quenching paths could potentially occur (Figure 2.2). These results clearly distinguish the BAR₃-based hydrogenation catalysts from transition-metal-based systems that are easily deactivated by CO and/or CO₂, even in the presence of a large excess of H₂.⁹ Subsequently, inspired by pioneering reports demonstrating the catalytic hydrogenation of carbonyl compounds using purified H₂ and FLP species comprising BAR₃ and ethereal solvents,¹⁰ I envisioned the direct use of crude H₂ for the synthesis of alcohols from aldehydes and ketones using BAR₃ catalysts (*cf.* Figure 2.2, wherein X and Y represent C and O). I expected that such FLPs would exhibit a low reactivity toward CO and CO₂,^{8,11} thus preventing the reaction to proceed along undesired paths caused by CO₂ (Figure 2.2; paths II and III), while reversible coordination of CO to BAR₃ could kinetically inhibit the reaction progress (Figure 2.2; path I).^{5,12} Replacing purified H₂ with crude H₂ in the catalytic reduction of carbonyl compounds would contribute to the development of a sustainable synthetic route to alcohols by partially or completely circumventing problematic H₂-purification processes that are generally essential for the transition-metal catalysis (Figure 2.1; previous work). Herein, I report a strategy for the direct catalytic hydrogenation of aldehydes and ketones using newly designed B(2,6-F₂-3,5-R₂-C₆H)₃ (R = Cl, Br) in the copresence of CO, CO₂, CH₄, and a certain amount of H₂O.

It should be noted here that transition-metal carbonyl complexes including Rh and/or Ru have previously been demonstrated to catalyze the hydroformylation/hydrogenation of alkenes with H₂/CO (1/~1 molar ratio), which includes the hydrogenation of *in-situ*-generated aldehydes in the copresence of CO.¹³ Nevertheless, the compatibility of these transition-metal complexes when using crude H₂, which contains CO₂ and/or CH₄, was not explored, as some of the aforementioned Ru and Rh complexes also catalyze the hydrogenation of CO₂.¹⁴

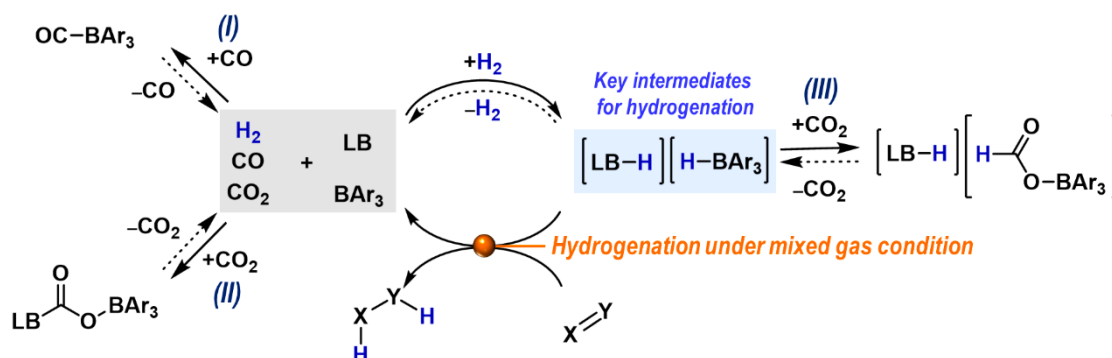


Figure 2.2. Hydrogenation of unsaturated molecules (X=Y) and potential reactions among H₂, CO, CO₂, LB (Lewis base/basic part), and/or BAR₃. Dashed arrows represent backward reactions that do not always occur under the same conditions as the corresponding forward reaction.

2.2. Results and discussion

2.2.1. Catalysts screening

I initially explored the hydrogenation of 1-naphthaldehyde (**9a**) with Shvo's Ru complex (**TM¹**), which is a well-known hydrogenation catalyst, under the model reaction conditions shown in Figure 2.3.^{15,16} Not surprisingly, 1-naphthalenemethanol (**10a**) was obtained in 99% in the presence of purified H₂ (20 atm; conditions B); however, the yield of **10** decreased to 17% when H₂/CO/CO₂ (20 atm each; conditions A) was

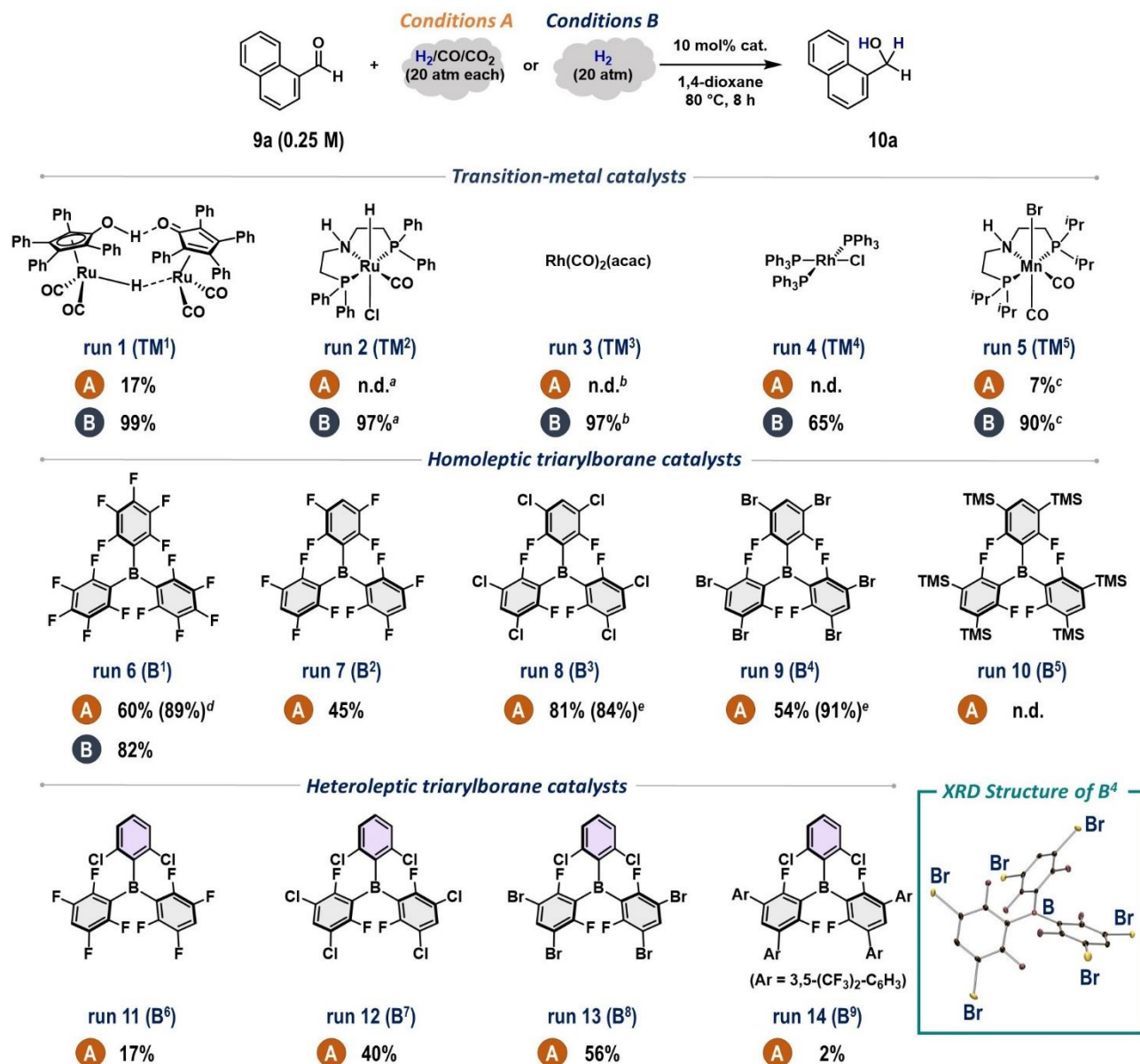


Figure 2.3. Optimization of the catalysts. General conditions: all reactions were conducted in an autoclave (10 mL), wherein **9a** (0.40 mmol, 0.25 M) and the specified catalyst were mixed in 1,4-dioxane, followed by pressurization with H₂/CO/CO₂ (20 atm each, condition A) or H₂ (20 atm, condition B), before heating (80 °C) was applied for 8 h. The product yield was determined by NMR analysis. [a] 0.5 mol% of Ru complex in THF/H₂O (v/v' = 1/2). [b] 0.5 mol% of catalyst with 1.5 mol% of Xantphos in EtOH. [c] Addition of NaO^tBu (30 mol%). [d] 16 h. [e] 12 h with H₂/CO/CO₂ (10 atm each) and 4-methyltetrahydropyran (MTHP) as the solvent. TMS = trimethylsilyl.

used as the feed gas (run 1; Figure 2.3). Similarly, Ru–PNP complex **TM**², Rh–carbonyl complex **TM**³, Wilkinson’s Rh complex **TM**⁴, and Mn–PNP complex **TM**⁵ did not mediate the hydrogenation of **9a** when using mixed-gas conditions, albeit that these complexes exhibit high catalytic activity when using pure H₂ (runs 2–5; Figure 2.3). **TM**¹ and **TM**³ have been reported to catalyze the hydrogenation of aldehydes in the presence of syngas,^{16,17} highlighting the challenging preparation of an active catalyst that can work under mixed-gas conditions, which are akin to crude H₂.

I then turned my attention to the use of BAr₃ (**B**¹–**B**⁹). As elegantly demonstrated by Ashley *et al.* and Stephan *et al.*,^{10a,10b} archetypical B(C₆F₅)₃ (**B**¹) catalyzes the hydrogenation of **9a** in 1,4-dioxane to give **9a** in 82% yield using H₂ (run 6B; Figure 2.3).¹⁸ Moreover, **B**¹ successfully afforded **10a** in 60% yield within 8 h under mixed-gas conditions (run 6A; Figure 2.3), demonstrating the robustness of the FLP toward the applied H₂/CO/CO₂ system. Extending the reaction time to 16 h resulted in the formation of **10a** in 89% yield, suggesting that contaminants induce kinetic inhibition. Decreasing the electrophilicity of the boron atom by substituting the C₆F₅ groups in **B**¹ with 2,3,5,6-F₄-C₆H groups (**B**²)¹⁹ decreased the yield of **10a** to 45% when using H₂/CO/CO₂ (run 7A; Figure 2.3). The yield of **10a** was increasing when the *meta*-substitution was changed from F to Cl, finally to Br in eteroleptic species **B**⁶–**B**⁹, although **10a** was obtained in only moderate yields (runs 11A–14A; Figure 2.3), albeit that these boranes exhibited considerably higher catalytic activity than **B**¹ in the hydrogenation of *N*-heteroaromatics using an identical crude H₂ mixture.⁵

I continued my investigation by optimizing homoleptic BAr₃ derivatives. I then designed *meta*-chlorinated **B**³ and brominated **B**⁴, and theoretically confirmed that these two boranes should show electrophilicity that is nearly identical to that of **B**². In fact, the energy level of the LUMO, which contains the p orbitals on the boron center, was calculated to be –1.16, –1.20, –1.20, and –0.20 eV for **B**², **B**³, **B**⁴, and **B**⁵,²⁰ respectively, using DFT at the DSD-PBEP86-D3BJ/ma-Def2-QZVPP//PBEh-3c/Def2-SVP//gas phase level (Figure 3.1). To be delight, I found that **B**³ and **B**⁴ exhibited excellent catalytic activity (runs 9A and 10A; Figure 2.3). However, **B**⁵, which contains trimethylsilyl groups (TMS), was employed, in that case, **10a** was not obtained due to a drastic decrease in the electrophilicity of the boron atom (run 8A; Figure 2.3). In particular, **10a** was obtained in 91% yield using **B**⁴ after 12 h even when the pressure of the mixed gas was reduced to 10 atm for each fraction of H₂/CO/CO₂. It should also be noted here that the solvent was changed to 4-methyltetrahydropyran (MTHP) due to the poor solubility of **B**⁴ in 1,4-dioxane. When using a combination of **B**³ and MTHP under H₂/CO/CO₂ (10 atm each), **10a** was obtained in 84% yield after 12 h, demonstrating the beneficial effect of using MTHP as a Lewis-basic solvent. After a further exploration of the reaction conditions, I selected MTHP as the optimal solvent (Figure S2.3). Importantly, the catalytic hydrogenation of **9a** did not occur in toluene or CH₂Cl₂, suggesting that the FLPs consisting of BAr₃ and Lewis-basic ethereal compounds mediate the crucial H₂-cleavage process even under the H₂/CO/CO₂ conditions. It is noteworthy that MTHP can be easily separated from water (its solubility in H₂O is ca. 1.5 wt%) and removed *in vacuo* due to its strong hydrophobicity and low heat of vaporization, which renders MTHP a greener ethereal solvent than THF.²¹

2.2.2. Substrate scope

With the optimal conditions (**B**⁴/MTHP) in hands, I subsequently investigated the substrate scope and limitations under the H₂/CO/CO₂ (1/1/1 molar ratio) conditions (Figure 2.4). The hydrogenation of aromatic aldehydes (**9b**–**9n**) and ketones (**9o**–**9q**) was conducted at 80 °C for 12 h using H₂/CO/CO₂ (10 atm each), while higher temperature (120 °C), and H₂/CO/CO₂ pressure (20 atm each) were applied for aliphatic aldehydes (**9r**–

9u). In general, benzaldehyde (**9b**) and its derivatives that contain *para*-electron-withdrawing groups such as halogens (**9c–9f**), CF₃ (**9g**), or an ester (**9i**) afforded the corresponding alcohols in high to excellent yields together with negligible amounts of ether byproducts.¹⁸ Remarkably, no functionalization such as protonation and carbonylation proceeded and the Cl, Br, and I atoms in **9d–9f** thus remained unreacted under the present mixed gas conditions. In contrast, 4-anisaldehyde (**9h**) could not be used efficiently in combination with this mixed gas system (conversion of **9h**: 32%; yield of **10h**: 13%), probably due to the electron-donating nature and Lewis basic reactivity of the methoxy group. The hydrogenation proceeded moderately when **10j**, which contains a *para*-COOH group, and **9m**, which contains a bulky mesityl moiety, were employed. Participation of a Lewis acidic *p*-(pinacolate)boryl group did not affect the progress of the hydrogenation, and **10k** was obtained in 81% yield under the mixed-gas conditions. Again, it is noteworthy that olefinic substituents such as vinyl (**9l**) and hexenyl (**9n**) groups are fully compatible with the present conditions including CO and CO₂, i.e., hydroformylation, hydrogenation, and isomerization did not occur.^{13,17} The gaseous mixture of H₂/CO/CO₂ was also successfully applied to the preparation of secondary alcohols **10o** and **10p** via the hydrogenation of the corresponding ketones (**9o** and **9p**, respectively). Although **B¹** has been reported to catalyze the reductive deoxygenation of **9o** in the presence of molecular sieves and H₂, such a reaction was not observed in this case.^{10d,10e} A substantial decrease in the hydrogenation efficiency was observed for benzophenone (**9q**), which afforded **10q** in only 7% yield (conversion of **9q**: 15%). Although the compatibility of aliphatic aldehydes has been less-explored in the reported BAr₃-catalyzed systems, I found that **9r–9t** were selectively transformed into the corresponding alcohols (**10r–10t**) in the copresence of CO and CO₂. The terminal and internal olefinic moieties remained intact. Alcohol **10s** was obtained in 89% yield under CO-rich H₂/CO (10/20 atm; a model of syngas) conditions. Using 2,6-dimethyl-5-heptenal (**9u**), which contains a trisubstituted olefinic moiety, resulted in the formation of **10u** in 38% yield with concomitant formation of several unidentified byproducts.

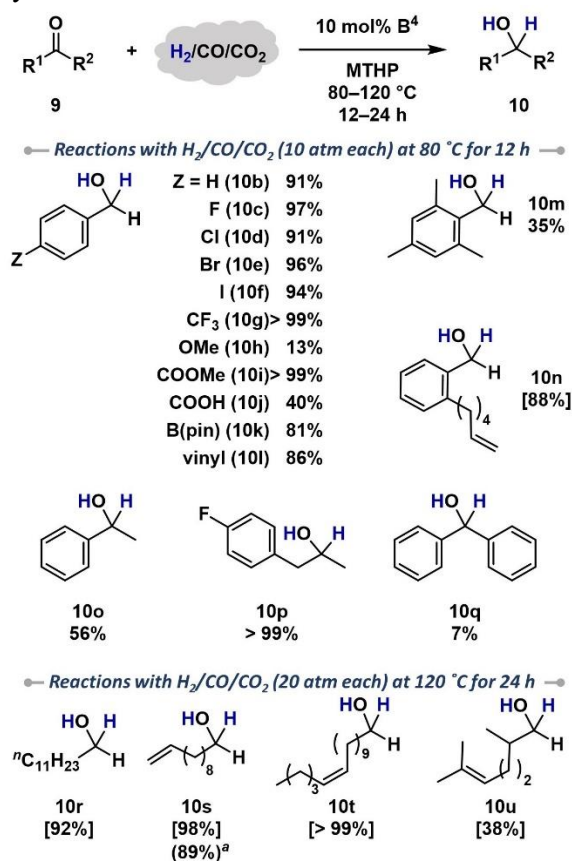


Figure 2.4. Direct use of H₂/CO/CO₂ in the hydrogenation of carbonyl compounds catalyzed by **B**⁴. General conditions: all reactions were conducted in an autoclave (10 mL), wherein **9** (0.40 mmol, 0.25 M) and **B**⁴ (0.04 mmol) were mixed in MTHP followed by pressurization with H₂/CO/CO₂ and heating at 80 °C or 120 °C. The product yield was determined by NMR analysis. Isolated yield is given in the square bracket. [a] Reaction with H₂/CO (10/20 atm).

2.2.3. Deterioration effects of CO and CO₂

To gain insight into the deterioration effects of CO and CO₂, I conducted the hydrogenation of **9a** using **B**¹ (in 1,4-dioxane) or **B**⁴ (in MTHP) in the presence of H₂/N₂ (20/40 atm), H₂/CO/N₂ (20 atm each), H₂/CO₂/N₂ (20 atm each), or H₂/CO/CO₂ (20 atm each) (Figure 2.5). To maintain the total pressure constant during these reactions, the mixtures were pressurized N₂ gas where necessary. As expected, the yields of **10a** were nearly identical in every experiment when using **B**⁴. In contrast, in the case of **B**¹, a slight decrease in the yield of **10a** was confirmed in the presence of CO, probably because the coordination of CO to the boron center kinetically inhibits the generation of the FLP (path I; Figure 2.2). Contamination with CO₂ resulted in a nearly negligible inhibition under the present conditions.

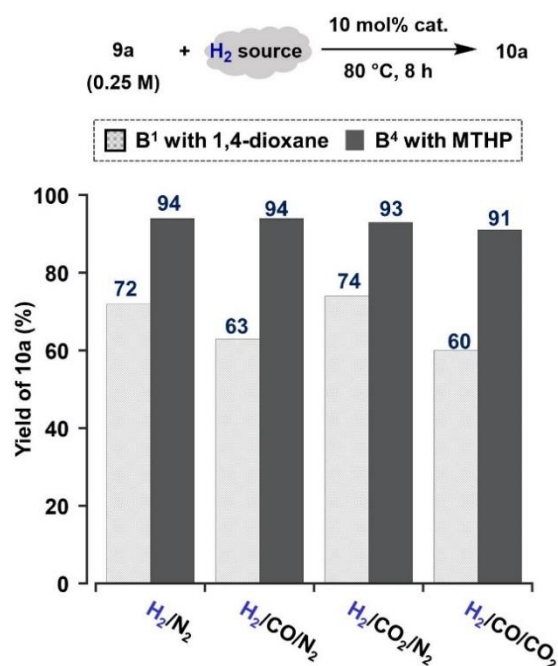


Figure 2.5. Influence of the gas composition on the **B**¹- or **B**⁴-catalyzed hydrogenation of **9a** in the presence of H₂/N₂ (20/40 atm), H₂/CO/N₂ (20 atm each), H₂/CO₂/N₂ (20 atm each), or H₂/CO/CO₂ (20 atm each).

2.2.4. Application for hydrogenation of carbonyl compounds directly using industrial crude H₂

Finally, I applied crude H₂ (H₂/CO/CO₂/CH₄/H₂O 76/0.2/20/3.2/0.6 molar ratio), which was industrially produced from CH₄ via desulfurization, steam reforming, and CO-shift conversion processes, to the **B**⁴-catalyzed synthesis of **10a** and **10s** (Figure 2.6). For that purpose, the crude H₂ was treated with 4 Å MS and then pressurized. Thus, **10a** and **10s** were obtained in 76% and > 99% yield, respectively, via the selective reduction of the formyl groups.

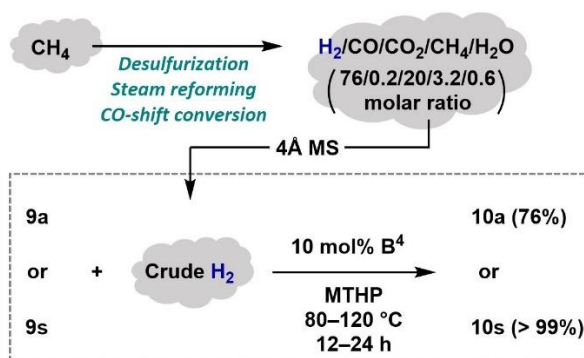


Figure 2.6. Direct use of industrial crude H₂ in the B⁴-catalyzed synthesis of **10a** and **10s**. The reaction using **9** (0.40 mmol, 0.25 M) and B⁴ (0.04 mmol) in MTHP was conducted at 80 °C for 12 h using crude H₂ (~13 atm) for **9a** or at 120 °C for 24 h using crude H₂ (~18 atm) for **9s**. The product yield was determined by NMR analysis.

2.3. Conclusion

In summary, the present work demonstrates the efficiency of main-group catalysis in the catalytic hydrogenation of unsaturated molecules under crude-H₂ conditions, thus circumventing the need for using purified H₂, which is generally required in well-established transition-metal catalysis. I directly used gaseous mixtures that contain H₂, CO, CO₂, and CH₄ in the catalytic hydrogenation of aldehydes and ketones. Key to the construction of effective reaction systems here is using triarylborane catalysts designed to exhibit high compatibility toward the aforementioned contaminants, including a certain amount of H₂O, based on the remote-back-strain strategy. In fact, the combination of B(2,6-F₂-3,5-R₂-C₆H)₃ (R = Cl, Br) with 4-methyltetrahydropyrane (MTHP) generates FLPs that selectively mediate the heterolysis of H₂ under the applied mixed gas conditions. Importantly, the formyl groups in aromatic and aliphatic aldehydes that also contain halogen or olefinic substituents can be selectively hydrogenated under an H₂/CO/CO₂ atmosphere without any functionalization of these substituents (e.g., carbonylation, hydroformylation, and isomerization). Future work will involve the investigation of the applicability of diverse crude H₂ mixtures produced from biomass and wastes toward further improving this waste-to-hydrogen strategy.

2.4. References and notes

- For selected reviews on contemporary strategies for hydrogen production, see: (a) Voldsund, M.; Jordal, K.; Anantharaman, R. *Int. J. Hydrogen Energy* **2016**, *41*, 4969. (b) Abdalla, A. M.; Hossain, S.; Nisfindy, O. B.; Azad, A. T.; Dawood, M.; Azad, A. K. *Energy Convers. Manage.* **2018**, *165*, 602. (c) Dawood, F.; Anda, M.; Shafiullah, G. M. *Int. J. Hydrogen Energy* **2020**, *45*, 3847. (d) Du, Z.; Liu, C.; Zhai, J.; Guo, X.; Xiong, Y.; Su, W.; He, G. *Catalysts* **2021**, *11*, 393. (e) Rahimpour, M. R.; Makarem, M. A.; Meshksar, M. *Advances in Synthesis Gas: Methods, Technologies and Applications, Vol. 3: Syngas Products and Usage*; ELSEVIER, 2023.
- International Energy Agency, Global Hydrogen Review 2021, **2021**, <https://www.iea.org/reports/global-hydrogen-review-2021>.
- For selected reviews, see: (a) Jarunglumlert, T.; Prommuak, C.; Putmai, N.; Pavasant, P. *Int. J. Hydrogen Energy* **2018**, *43*, 634. (b) Lui, J.; Chen, W.-H.; Tsang, D. C. W.; You, S. *Renew. Sustain. Energy Rev.* **2020**, *134*, 110365.

4. Tagliabue, M. Recovering hydrogen and LPG from off-gases in *Petroleum Technology Quarterly Q4*, **2020**, 75–81, <https://www.digitalrefining.com/article/1002557/recovering-hydrogen-and-lpg-from-off-gases>.
5. Hashimoto, T.; Asada, T.; Ogoshi, S.; Hoshimoto, Y. *Sci. Adv.* **2022**, *8*, eade0189.
6. (a) Jupp, A. R.; Stephan, D. W. *Trends Chem.* **2019**, *1*, 35. (b) Fasano, V.; Ingleson, M. J. *Synthesis* **2018**, *50*, 1783. (c) Carden, J. L.; Dasgupta, A.; Melen, R. L. *Chem. Soc. Rev.* **2020**, *49*, 1706. (d) Weicker, S. A.; Stephan, D. W. *Bull. Chem. Soc. Jpn.* **2015**, *88*, 1003. For a selected example using FLPs for separation, see also, (e) D. Voicu, D. W. Stephan, E. Kumacheva, *ChemSusChem* **2015**, *8*, 4202.
7. (a) Stephan, D. W. *J. Am. Chem. Soc.* **2021**, *143*, 20002. (b) Scott, D. J.; Fuchter, M. J.; Ashley, A. E. *Chem. Soc. Rev.* **2017**, *46*, 5689. (c) Paradies, J. *Acc. Chem. Res.* **2023**, *56*, 821. (d) Zhou, R.; Tavandashti, Z. P.; Paradies, J. *SynOpen* **2023**, *7*, 46. (e) Oestreich, M.; Hermeke, J.; Mohr, J. *Chem. Soc. Rev.* **2015**, *44*, 2202. (f) Hoshimoto, Y.; Ogoshi, S. *ACS Catal.* **2019**, *9*, 5439.
8. (a) Stephan, D. W. *Chem. Soc. Rev.* **2023**, *52*, 4632. (b) Stephan, D. W.; Erker, G. *Chem. Sci.* **2014**, *5*, 2625. (c) Stephan, D. W.; Erker, G. *Angew. Chem., Int. Ed.* **2010**, *49*, 46.
9. (a) Braekman-Danheux, C.; Fontana, A.; Laurent, P.; Lolivier, P. *Fuel* **1996**, *75*, 579. (b) Liu, J.; Lucci, F. R.; Yang, M.; Lee, S.; Marcinkowski, M. D.; Therrien, A. J.; Williams, C. T.; Sykes, E. C. H.; Flytzani-Stephanopoulos, M. *J. Am. Chem. Soc.* **2016**, *138*, 6396. (c) Jorschick, H.; Vogl, M.; Preuster, P.; Bösmann, A.; Wasserscheid, P. *Int. J. Hydrogen Energy* **2019**, *44*, 31172. (d) Lin, L.; Yao, S.; Gao, R.; Liang, X.; Yu, Q.; Deng, Y.; Liu, J.; Peng, M.; Jiang, Z.; Li, S.; Li, Y.-W.; Wen, X.-D.; Zhou, W.; Ma, D. *Nat. Nanotechnol.* **2019**, *14*, 354. (e) Wang, K.; Wang, L.; Yao, Z.; Zhang, L.; Zhang, L.; Yang, X.; Li, Y.; Wang, Y.-G.; Li, Y.; Yang, F. *Sci. Adv.* **2022**, *8*, eabo4599. (f) Wang, Z.; Dong, C.; Tang, X.; Qin, X.; Liu, X.; Peng, M.; Xu, Y.; Song, C.; Zhang, J.; Liang, X.; Dai, S.; Ma, D. *Nat. Commun.* **2022**, *13*, 4404. (g) Li, S.; Lin, L.; Wang, Z.; Ma, D. *The Innovation* **2023**, *4*, 100353.
10. (a) Mahdi, T.; Stephan, D. W. *J. Am. Chem. Soc.* **2014**, *136*, 15809. (b) Scott, D. J.; Fuchter, M. J.; Ashley, A. E. *J. Am. Chem. Soc.* **2014**, *136*, 15813. (c) Gyömöre, Á.; Bakos, M.; Földes, T.; Pápai, I.; Domján, A.; Soós, T. *ACS Catal.* **2015**, *5*, 5366. (d) Mahdi, T.; Stephan, D. W. *Angew. Chem., Int. Ed.* **2015**, *54*, 8511. (e) Scott, D. J.; Simmons, T. R.; Lawrence, E. J.; Wildgoose, G. G.; Fuchter, M. J.; Ashley, A. E. *ACS Catal.* **2015**, *5*, 5540. (f) Scott, D. J.; Phillips, N. A.; Sapsford, J. S.; Deacy, A. C.; Fuchter, M. J.; Ashley, A. E. *Angew. Chem., Int. Ed.* **2016**, *55*, 14738. (g) Gao, B.; Feng, X.; Meng, W.; Du, H. *Angew. Chem., Int. Ed.* **2020**, *59*, 4498. (h) Heshmat, M.; Privalov, T. *Chem.-Eur. J.* **2017**, *23*, 1036.
11. (a) Ashley, A. E.; Thompson, A. L.; O'Hare, D. *Angew. Chem., Int. Ed.* **2009**, *48*, 9839. (b) Mömmling, C. M.; Otten, E.; Kehr, G.; Fröhlich, R.; Grimme, S.; Stephan, D. W.; Erker, G. *Angew. Chem., Int. Ed.* **2009**, *48*, 6643. (c) Tran, S. D.; Tronic, T. A.; Kaminsky, W.; Heinekey, D. M.; Mayer, J. M. *Inorg. Chim. Acta* **2011**, *369*, 126. (d) Voss, T.; Mahdi, T.; Otten, E.; Fröhlich, R.; Kehr, G.; Stephan, D. W.; Erker, G. *Organometallics* **2012**, *31*, 2367. (e) Liu, Y.-L.; Kehr, G.; Daniliuc, C. G.; Erker, G. *Chem. Sci.* **2017**, *8*, 1097. (f) Jian, Z.; Kehr, G.; Daniliuc, C. G.; Wibbeling, B.; Erker, G. *Dalton Trans.* **2017**, *46*, 11715. (g) Jie, X.; Sun, Q.; Daniliuc, C. G.; Knitsch, R.; Hansen, M. R.; Eckert, H.; Kehr, G.; Erker, G. *Chem.-Eur. J.* **2020**, *26*, 1269.
12. Finze, M.; Bernhardt, E.; Terheiden, A.; Berkei, M.; Willner, H.; Christen, D.; Oberhammer, H.; Aubke, F. *J. Am. Chem. Soc.* **2002**, *124*, 15385.
13. For selected examples on hydroformylation-hydrogenation of olefines to alcohol, see: (a) Torres, G. M.; Frauenlob, R.; Franke, R.; Börner, A. *Catal. Sci. Technol.* **2015**, *5*, 34. (b) Rodrigues, F. M. S.; Kucmierczyk,

- P. K.; Pineiro, M. Jackstell, R. Franke, R.; Pereira, M. M.; Beller, M. *ChemSusChem* **2018**, *11*, 2310. (c) Becquet, C.; Berche, F.; Bricout, H.; Monflier, E.; Tilloy, S. *ACS Sustainable Chem. Eng.* **2021**, *9*, 9444. (d) Geng, H.-Q.; Meyer, T.; Franke, R.; Wu, X.-F. *Chem. Sci.* **2021**, *12*, 14937. (e) Rösler, T.; Ehmann, K. R.; Köhnke, K.; Leutzsch, M.; Wessel, N.; Vorholt, A. J.; Leitner, W. *J. Catal.* **2021**, *400*, 234. (f) Ternel, J.; Lopes, A.; Sauthier, M.; Buffe, C.; Wiatz, V.; Bricout, H.; Tilloy, S.; Monflier, E. *Molecules* **2021**, *26*, 7322. (g) Tay, D. W. P.; Nobbs, J. D.; Aitipamula, S.; Britovsek, G. J. P.; van Meurs, M. *Organometallics* **2021**, *40*, 1914. (h) Huang, W.; Tian, X.; Jiao, H.; Jackstell, R.; Beller, M. *Chem.-Eur. J.* **2022**, *28*, e202104012. (i) MacNeil, C. S.; Mendelsohn, L. N.; Pabst, T. P.; Hierlmeier, G.; Chirik, P. J. *J. Am. Chem. Soc.* **2022**, *144*, 19219. (j) El Mouat, A.; Becquet, C.; Ternel, J.; Ferreira, M.; Bricout, H.; Monflier, E.; Lahcini, M.; Tilloy, S. *ACS Sustainable Chem. Eng.* **2022**, *10*, 11310. (k) Rösler, T.; Betting, J.; Püschel, S.; Vorholt, A. J.; Leitner, W. *Green Chem.* **2022**, *24*, 6578. (l) Becquet, C.; Ferreira, M.; Bricout, H.; Quienne, B.; Caillol, S.; Monflier, E.; Tilloy, S. *Green Chem.* **2022**, *24*, 7906. (m) Hua, K.; Liu, X.; Chen, J.; Wei, B.; Wang, H.; Sun, Y. *ACS Sustainable Chem. Eng.* **2021**, *9*, 16741.
14. Klankermayer, J.; Wesselbaum, S.; Beydoun, K.; Leitner, W. *Angew. Chem., Int. Ed.* **2016**, *55*, 7296.
 15. Conley, B. L.; Pennington-Boggio, M. K.; Boz, E.; Williams, T. J. *Chem. Rev.* **2010**, *110*, 2294.
 16. (a) Takahashi, K.; Yamashita, M.; Nozaki, K. *J. Am. Chem. Soc.* **2012**, *134*, 18746. (b) Takahashi, K.; Nozaki, K. *Org. Lett.* **2014**, *16*, 5846.
 17. Diab, L.; Šmejkal, T.; Geier, J.; Breit, B. *Angew. Chem., Int. Ed.* **2009**, *48*, 8022.
 18. The formation of 1,1'-(oxybis(methylene))dinaphthalene (~4%) as a byproduct was confirmed in most of the reactions catalyzed by **B**¹–**B**⁹, for details, see: Bakos, M.; Gyömöre, Á.; Domján, A.; Soós, T. *Angew. Chem., Int. Ed.* **2017**, *56*, 5217.
 19. (a) Ullrich, M.; Lough, A. J.; Stephan, D. W. *J. Am. Chem. Soc.* **2009**, *131*, 52. (b) Ullrich, M.; Lough, A. J.; Stephan, D. W. *Organometallics* **2010**, *29*, 3647.
 20. Sakuraba, M.; Morishita, T.; Hashimoto, T.; Ogoshi, S.; Hoshimoto, Y. *Synlett* **2023**, *34*, 2187.
 21. Bijoy, R.; Agarwala, P.; Roy, L.; Thorat, B. N. *Org. Process Res. Dev.* **2022**, *26*, 480.

2.5. Supporting information

2.5.1. General considerations

Unless otherwise noted, all manipulations were conducted under a nitrogen atmosphere using standard Schlenk or dry box techniques. ¹H, ¹¹B, ¹³C, and ¹⁹F NMR spectra were recorded on a Bruker AVANCE III 400 at 25 °C and Bruker AVANCE III 600 spectrometers at 22 °C. The chemical shifts in the ¹H NMR spectra were recorded relative to Me₄Si or residual protonated solvent (C₆D₅H (δ 7.16), CHCl₃ (7.26), CDHCl₂ (δ 5.32), or (CD₂H)₂SO (δ 2.50)). The chemical shifts in the ¹¹B NMR spectra were recorded relative to BF₃. The chemical shifts in the ¹³C spectra were recorded relative to Me₄Si or deuterated solvent (C₆D₆ (δ 128.06), CDCl₃ (77.16), or CD₂Cl₂ (δ 53.84)). The chemical shifts in the ¹¹B NMR spectra were recorded relative to BF₃. The chemical shifts in the ¹⁹F NMR spectra were recorded relative to α,α,α-trifluorotoluene (δ –65.64). Assignment of the resonances in ¹H and ¹³C NMR spectra was based on ¹H–¹H COSY, HMQC, and HMBC experiments if required. Medium-pressure column chromatography was carried out on a Biotage Flash Purification System Isolera, equipped with a 254 nm UV detector. Gel permeation chromatography (GPC) was performed on Japan Analytical Industry LC9225NEXT HPLC system equipped with JAIGEL-1H and JAIGEL-2H. Gas chromatography-mass spectrometry (GC-MS) was carried out on a Shimadzu GCMS-QP2010 SE, equipped

with a flame ionization detector. High resolution mass spectrometry (HRMS) was performed at the Instrumental Analysis Center, Faculty of Engineering, Osaka University. A single-crystal X-ray diffraction analysis was carried out using the Rigaku XtaLAB Synergy equipping with the HyPix-6000HE detector.

2.5.2. Materials

All commercially available reagents including super-dehydrated solvents (toluene, THF, Et₂O, CH₂Cl₂, 1,4-dioxane, EtOH, and DMF) were purchased from Sigma Aldrich, Tokyo Chemical Industry (TCI), and FUJIFILM Wako Pure Chemical Corporation, and used as received. C₆D₆ was distilled from sodium benzophenone ketyl prior to use. CD₂Cl₂ was distilled over CaH₂ and stored over molecular sieves (4 Å). CDCl₃ was stored over molecular sieves (4 Å). 1-Naphtaldehyde (**9a**) was used after distilled over CaH₂. 4-Methyltetrahydropyran (MTHP) was provided from Kuraray Co., Ltd., and used after distillation using sodium benzophenone ketyl. Triaryl boranes (**B**², **B**⁵, **B**⁶, **B**⁷, **B**⁸, and **B**⁹),^{S1–S4} 1,5-dichloro-2,4-difluoro-3-iodobenzene,^{S5} 1,5-dibromo-2,4-difluoro-3-iodobenzene,^{S5} and aldehyde **6l**^{S6} were prepared by following the reported procedures. Gaseous chemicals including H₂, H₂/CO/CO₂ (a 1:1:1 molar ratio), H₂/CO (a 1:1 molar ratio), H₂/CO₂ (a 1:1 molar ratio), CO, and N₂ were purchased from Sumitomo Seika Chemicals Company and used as received. Note that these gases include some impurities as shown in Table 2.S1. Gaseous chemicals including H₂/CO/CO₂/CH₄/H₂O (76/0.2/20/3.2/0.6 molar ratio) (produced by the VHR system from natural gas) were provided from AIR WATER INC. and used after being stored over molecular sieves (4 Å).

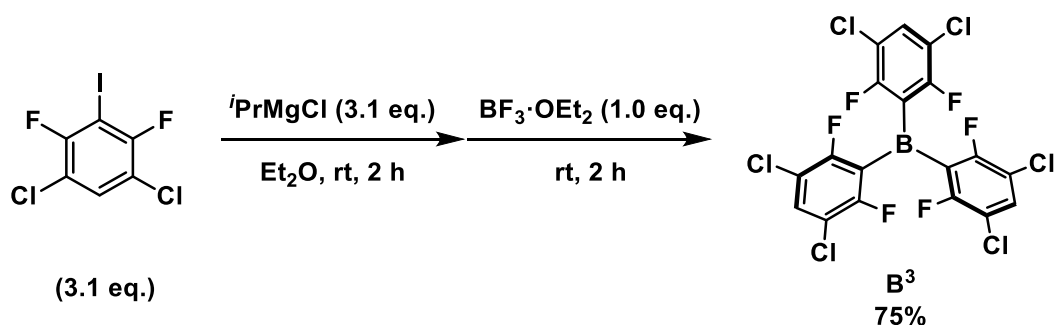
Table 2.S1. Impurities contaminated in H₂, CO, CH₄, and N₂ (shown in ppm).

	Impurity				
	N ₂	O ₂	CO	CO ₂	H ₂
H ₂	<200	<50	<1	<1	-
CO	<500	<100	-	<100	<100
CH ₄	<5000	<500	-	<5000	-
N ₂	-	0.01	0.02	0.02	0.02

Metrical data for the solid-state structures are available from Cambridge Crystallographic Data Centre: CCDC 2297793 (**B**³), 2297792 (**B**⁴), and 2313650 (**8**).

2.5.3. Synthesis of **B**³ and **B**⁴

• Synthesis of **B**³



To a Et₂O (15 mL) solution of 1,5-dichloro-2,4-difluoro-3-iodobenzene (1.4 g, 4.5 mmol, 3.1 eq.),

*i*PrMgCl (4.5 mL of a 1.0 M solution in Et₂O, 4.5 mmol, 3.1 eq.) was slowly added at rt. After stirring the resultant solution for 2 h at rt, BF₃·OEt₂ (204.5 mg, 1.4 mmol, 1.0 eq.) was added quickly to give a yellow solution, and a white precipitate was generated after the period of 1 h. After stirring for 2 h at rt, all volatiles were removed *in vacuo* to give an off-white solid. The resultant solid was extracted with hot hexane (3×30 mL), and filtered through a Celite pad to give **B**³ as a white solid (600.0 mg, 1.1 mmol, 75% yield) after the removal of all volatiles *in vacuo*. A single crystal suitable for the XRD analysis was obtained via crystallization at −30 °C from toluene/hexane solution. ¹H NMR (400 MHz, C₆D₆): δ 6.77 (t, 3H, ⁴J_{H,F} = 7.4 Hz, Ar-*H*). ¹¹B NMR (128 MHz, CD₂Cl₂): Not observed. ¹³C{¹H} NMR (100 MHz, C₆D₆): δ 159.9 (dd, ¹J_{C,F} = 10 Hz, ³J_{C,F} = 253 Hz), 138.0, 120.7 (t, *J* = 25.3 Hz), 119.7 (m). ¹⁹F NMR (376 MHz, C₆D₆): δ −105.2 (s). **Crystal data** for C₁₈H₃BCl₆F₆ (*M* = 556.75): monoclinic, space group *C2/c* (#15), *a* = 14.1339 (2) Å, *b* = 15.9637 (2) Å, *c* = 20.7520 (3) Å, *α* = 90°, *β* = 99.097 (1)°, *γ* = 90°, *V* = 4623.37 (11) Å³, *Z* = 8, *D*_{calcd} = 1.600 g/cm³, *T* = −130 °C, The final *R*_I(*wR*₂) = 0.0340 (0.0970).

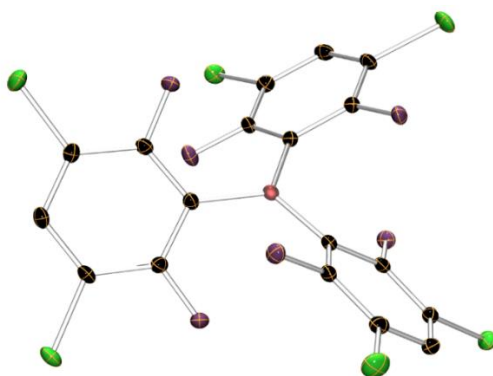
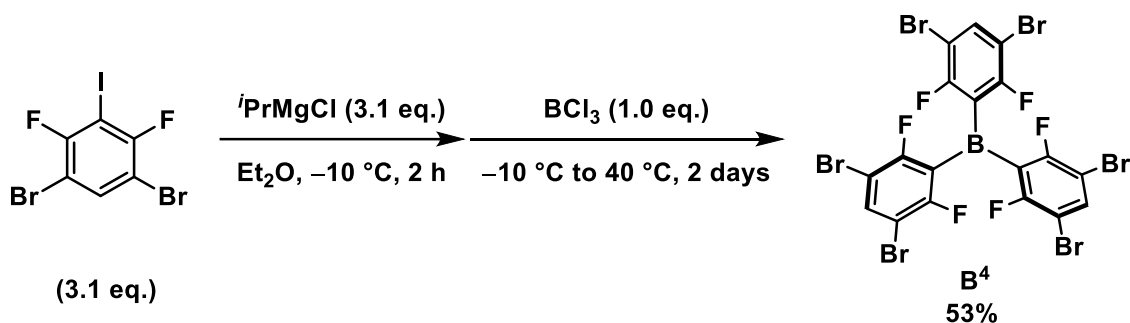


Figure 2.S1. The molecular structure of **B**³ with ellipsoids set at 30% probability; hydrogen atoms are omitted for clarity.

• Synthesis of **B**⁴



To a Et₂O (40 mL) solution of 1,5-dibromo-2,4-difluoro-3-iodobenzene (4.1 g, 10.1 mmol, 3.1 eq.) in a test tube with a screw cap, *i*PrMgCl (10.0 mL of a 1.0 M solution in Et₂O, 10.0 mmol, 3.1 eq.) was slowly added at −10 °C. After stirring the resultant solution for 2 h at −10 °C, a white precipitate was generated after 30 min, and BCl₃ (3.3 mL, of a 1.0 M solution in hexane, 3.3 mmol, 1.0 eq.) was added quickly at −10 °C. After stirring for 2 days at 40 °C in the closed system, all volatiles were removed *in vacuo* to give an off-white solid. The resultant solid was washed with CH₂Cl₂ (cooled to −30 °C prior to use), extracted with toluene (2×30 mL), and filtered through a Celite pad to give **B**⁴ as a white solid (1.4 g, 1.8 mmol, 53% yield) after the removal of all volatiles *in vacuo*. A single crystal suitable for the XRD analysis was obtained via crystallization at −30 °C from toluene/hexane solution. ¹H NMR (400 MHz, CD₂Cl₂): δ 7.98 (t, 3H, ⁴J_{H,F} = 7.0 Hz, Ar-*H*); (400 MHz,

C₆D₆): δ 7.24 (t, 3H, , $^4J_{\text{H,F}} = 7.2$ Hz, Ar-H). ^{11}B NMR (128 MHz, CD₂Cl₂): Not observed. $^{13}\text{C}\{^1\text{H}\}$ NMR (100 MHz, CD₂Cl₂): δ 159.9 (dd, $^1J_{\text{C,F}} = 11$ Hz, $^3J_{\text{C,F}} = 253$ Hz), 140.9, 105.6 (d, $J = 26$ Hz). ^{19}F NMR (376 MHz, CD₂Cl₂): δ -96.7 (s); (376 MHz, C₆D₆): δ -96.2 (s). **Crystal data** for C₁₈H₃BBr₆F₆ ($M = 823.47$ g/mol): triclinic, space group $P\bar{1}$ (#2), $a = 7.2104(1)$ Å, $b = 13.2348(2)$ Å, $c = 13.3494(2)$ Å, $\alpha = 75.258(2)^\circ$, $\beta = 86.732(2)^\circ$, $\gamma = 84.584(2)^\circ$, $V = 1225.75(3)$ Å³, $Z = 2$, $D_{\text{calcd}} = 2.231$ g/cm³, $T = -150$ °C, $R_1(wR_2) = 0.0331$ (0.0906).

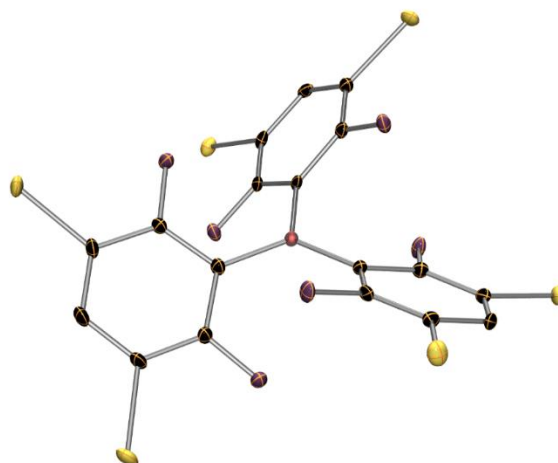
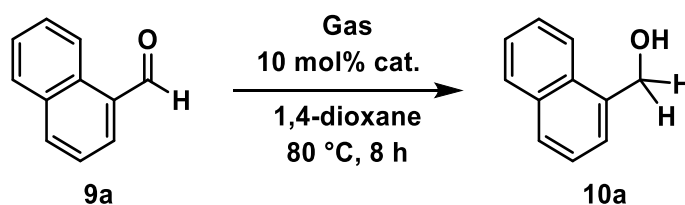


Figure 2.S2. The molecular structure of **B⁴** with ellipsoids set at 30% probability; hydrogen atoms are omitted for clarity.

2.5.4. Screening of catalysts in hydrogenation of **9a**

• Screening of catalysts



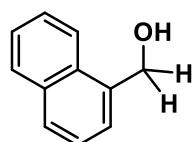
General Procedure: A solution of **9a** (0.4 mmol) and catalyst in 1,4-dioxane (1.6 mL) was transferred to a 10 mL autoclave. Once sealed, the autoclave was pressurized with H₂/CO/CO₂ (20 atm each; Condition A) or H₂ (20 atm; Condition B) at rt and stirred at 80 °C for 8 h. After degassing at rt, the reaction mixture was quenched by MeOH. The resultant mixture was then transferred to a round bottom flask and dried *in vacuo*. Yield of **10a** was determined by ¹H NMR analysis using trimethylphenylsilane as an internal standard in CDCl₃. Noted that 1,1'-(oxybis(methylene))dinaphthalene was obtained in ~4% yield as byproduct in Run 6A–14A.

General Procedure for Run 2: A solution of **9a** (0.4 mmol) and **TM²** (0.002 mmol) in THF/H₂O (1/2 mL) was transferred to a 10 mL autoclave. Once sealed, the autoclave was pressurized with H₂/CO/CO₂ (20 atm each; Condition A) or H₂ (20 atm; Condition B) at rt and stirred at 80 °C for 8 h. After degassing at rt, the reaction mixture was quenched by MeOH. The resultant mixture was then transferred to a round bottom flask and dried *in vacuo*. Yield of **10a** was determined by ¹H NMR analysis using trimethylphenylsilane as an internal standard in CDCl₃.

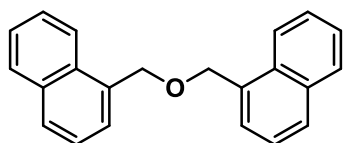
General Procedure for Run 3: A solution of **9a** (0.4 mmol), **TM**³ (0.002 mmol), and Xantphos (0.006 mmol) in EtOH (1.2 mL) was transferred to a 10 mL autoclave. Once sealed, the autoclave was pressurized with H₂/CO/CO₂ (20 atm each; Condition A) or H₂ (20 atm; Condition B) at rt and stirred at 80 °C for 8 h. After degassing at rt, the reaction mixture was quenched by MeOH. The resultant mixture was then transferred to a round bottom flask and dried *in vacuo*. Yield of **10a** was determined by ¹H NMR analysis using trimethylphenylsilane as an internal standard in CDCl₃.

General Procedure for Run 5: A solution of **9a** (0.4 mmol), **TM**⁵, and NaO^tBu (0.1 mmol) in 1,4-dioxane (1.6 mL) was transferred to a 10 mL autoclave. Once sealed, the autoclave was pressurized with H₂/CO/CO₂ (20 atm each; Condition A) or H₂ (20 atm; Condition B) at rt and stirred at 80 °C for 8 h. After degassing at rt, the reaction mixture was quenched by MeOH. The resultant mixture was then transferred to a round bottom flask and dried *in vacuo*. Yield of **10a** was determined by ¹H NMR analysis using trimethylphenylsilane as an internal standard in CDCl₃.

• **Characterization of 10a and 1,1'-[oxybis(methylene)]bis(naphthalene)**

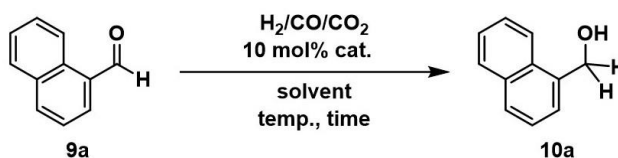


1-Naphthalenemethanol (10a): ¹H NMR (400 MHz, CDCl₃): δ 8.14 (d, *J* = 8.2 Hz, 1H, Ar-*H*), 7.89 (d, *J* = 8.1 Hz, 1H, Ar-*H*), 7.82 (d, *J* = 8.2 Hz, 1H, Ar-*H*), 7.58–7.44 (m, 4H, Ar-*H*), 5.17 (d, *J* = 5.8 Hz, 2H, CH₂OH). A resonance of OH was not observed.



1,1'-(Oxybis(methylene))dinaphthalene: The formation of the product was confirmed from these data; ¹H NMR (400 MHz, CDCl₃): δ 5.07 (s, 4H, CH₂OCH₂). GC-MS (*m/z*): 298.

2.5.5 Screening of reaction conditions in hydrogenation of 9a using B³ or B⁴



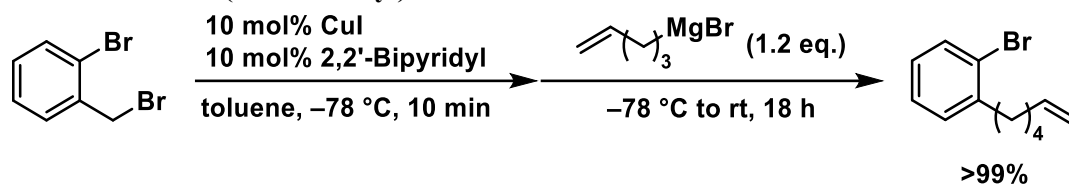
run	cat.	solvent	pressure (atm each)	temp. (°C)	time (h)	yield of 10a (%)
1	B ³	THF	20	80	8	63
2	B ³	Et ₂ O	20	80	8	88
3	B ³	MTHP	20	80	8	88
4	B ³	toluene	20	80	8	4
5	B ³	CH ₂ Cl ₂	20	80	8	4
6	B ⁴	MTHP	20	80	8	91
7	B ⁴	MTHP	10	80	8	75
8	B ⁴	MTHP	10	80	12	91
9	B ³	MTHP	10	80	12	84
10	B ⁴	MTHP	10	60	12	28
11	B ⁴	MTHP	10	100	8	79
12 ^a	B ⁴	MTHP	10	80	12	43

Figure 2.S3. Screening of solvent in hydrogenation of **9a** using **B³** or **B⁴**. [*a*] 5 mol% of catalyst.

General Procedure: A solution of **9a** (0.4 mmol) and catalyst (0.04 mmol) in solvent (1.6 mL) was transferred to a 10 mL autoclave. Once sealed, the autoclave was pressurized with H₂/CO/CO₂ at rt and stirred under heating. After degassing, the reaction mixture was quenched by MeOH. The resultant mixture was transferred to a round bottom flask and dried *in vacuo*. Yield of **10a** was determined by ¹H NMR analysis using trimethylphenylsilane as an internal standard in CDCl₃.

2.5.6. Synthesis of **9n**

• Synthesis of 1-bromo-2-(hex-5-en-1-yl)benzene



A THF (50 mL) solution of 5-bromopent-1-ene (14.9 g, 100.0 mmol) was slowly added to Mg (3.6 g, 150.0 mmol) stirred in THF (30 mL) at 0 °C. After stirring for 2 h at 80 °C, the resultant Grignard solution was cooled to rt. To a toluene (60 mL) solution of 2-bromobenzyl bromide (20.9 g, 83.6 mmol), CuI (1.5 g, 8.0 mmol, 0.1 eq.), and 2,2'-bipyridyl (1.3 g, 8.0 mmol, 0.1 eq.), pent-4-en-1-ylmagnesium bromide (100.0 mL of a 1.0 M solution in THF, 100.0 mmol, 1.2 eq.) was slowly added at -78 °C. After stirring for 2 h at -78 °C, the resultant solution was allowed to warm to rt and then stirred for additional 16 h. The reaction was quenched with sat. NH₄Cl aq. (80 mL), and the organic layer was extracted with Et₂O (3×100 mL), washed with sat. NaHCO₃ aq. (2×40 mL) and brine (3×40 mL) and dried over Na₂SO₄. All volatiles were removed *in vacuo* to give a brown oil (20.3 g, 84.9 mmol, >99%), which was used in the next step after sublimation at 90 °C *in vacuo* (ca. 0.2 mmHg). ¹H NMR (400 MHz, CDCl₃): δ 7.52 (d, *J* = 8.0 Hz, 1H, Ar-*H*), 7.24–7.20 (m, 2H, Ar-*H*), 7.06–7.02 (m, 1H, Ar-*H*), 5.87–5.77 (m, 1H, CH=CH₂), 5.04–4.94 (m, 2H, CH=CH₂), 2.73 (t, *J* = 7.8 Hz, 2H, CH₂), 2.11 (q, *J* = 7.2 Hz, 2H, CH₂), 1.67–1.61 (m, 2H, CH₂), 1.48 (quin, *J* = 7.5 Hz, 2H, CH₂). ¹³C{¹H} NMR (100 MHz, CDCl₃): δ 142.1, 138.9, 132.9, 130.4, 127.5, 127.5, 124.6, 114.6, 36.2, 33.7, 29.5, 28.8. HRMS (EI⁺): *m/z* Calcd for C₁₂H₁₅Br 238.0357, found 238.0355.

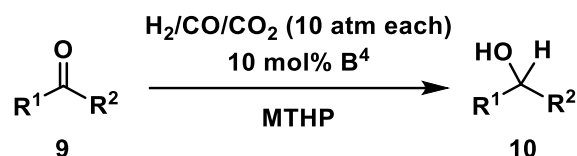
• Synthesis of 2-(hex-5-en-1-yl)benzaldehyde (**9n**)



To a THF (40 mL) solution of 1-bromo-2-(hex-5-en-1-yl)benzene (8.5 g, 35.5 mmol), *n*-BuLi (33.0 mL of a 1.6 M solution in hexane, 53.0 mmol, 1.5 eq.) was slowly added at -78 °C. After stirring for 30 min at -78 °C, a THF (10 mL) solution of DMF (6.8 mL, 88.8 mmol, 2.5 eq.) was slowly added at -78 °C. The resultant solution was allowed to warm to rt and then stirred for an additional 16 h. The reaction was quenched with sat. NH₄Cl aq. (50 mL), and the organic layer was extracted with Et₂O (3×50 mL), washed with sat. NaHCO₃

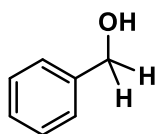
aq.(2×20 mL) and brine(3×20 mL), and dried over Na₂SO₄. All volatiles were removed *in vacuo* and the residue was purified by flash column chromatography on silica gel (EtOAc/hexane = 15/85) to give a pale yellow oil (5.4 g, 28.7 mmol, 81%). ¹H NMR (400 MHz, CDCl₃): δ 10.28 (s, 1H, CHO), 7.83 (d, *J* = 7.6 Hz, 1H, Ar-*H*), 7.50 (t, *J* = 7.2 Hz, 1H, Ar-*H*), 7.36 (t, *J* = 7.6 Hz, 1H, Ar-*H*), 7.27 (d, *J* = 7.2 Hz, 1H, Ar-*H*), 5.85–5.75 (m, 1H, CH=CH₂), 5.03–4.93 (m, 2H, CH=CH₂), 3.03 (t, *J* = 7.6 Hz, 2H, CH₂), 2.12–2.07 (m, 2H, CH₂), 1.67–1.60 (m, 2H, CH₂), 1.53–1.45 (m, 2H, CH₂). ¹³C{¹H} NMR (150 MHz, CDCl₃): δ 192.4, 145.7, 138.8, 133.9, 133.8, 131.7, 131.1, 126.6, 114.7, 33.7, 32.5, 31.9, 28.9. HRMS (EI⁺): *m/z* Calcd for C₁₃H₁₆O 188.1201, found 188.1200.

2.5.7 Substrate scope

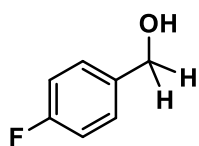


General Procedure (Method A): A solution of **9** (0.4 mmol) and **B**⁴ in MTHP (1.6 mL) was transferred to a 10 mL autoclave. Once sealed, the autoclave was pressurized with H₂/CO/CO₂ (10 atm each) at rt and stirred at 80 °C for 12 h. After degassing at rt, the reaction mixture was transferred to a round bottom flask and dried *in vacuo*. Yields of **10** and ether byproducts were determined by ¹H NMR analysis using trimethylphenylsilane as an internal standard in CDCl₃. The formation of the ether byproducts was confirmed/estimated through the comparison with ¹H NMR spectra of the reported/similar compounds.

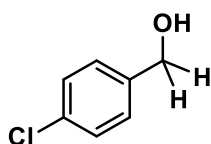
General Procedure (Method B): A solution of **9** (0.4 mmol) and **B**⁴ in MTHP (1.6 mL) was transferred to a 10 mL autoclave. Once sealed, the autoclave was pressurized with H₂/CO/CO₂ (20 atm each) at rt and stirred at 120 °C for 24 h. After degassing at rt, the reaction mixture was transferred to a round bottom flask and dried *in vacuo*. Then, the product was purified by flash column chromatography on silica gel using gradient EtOAc in hexane. Yields of isolated products are given.



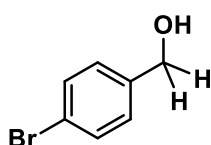
Benzyl alcohol (10b): Followed by the general procedures (Method A) using **9b** (41.5 mg) and **B**⁴ (32.6 mg, 0.04 mmol), giving **10b** in 91% yield confirmed by the NMR analysis using trimethylphenylsilane (9.3 mg, 0.1 mmol). ¹H NMR (400 MHz, CDCl₃): δ 7.37–7.29 (m, 5H, Ar-*H*), 4.70 (s, 2H, CH₂OH). A resonance of OH was not observed. The formation of dibenzyl ether was conformed in 3%, which was calculated using δ 4.56 (s) in ¹H NMR.



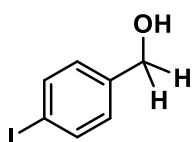
4-Fluorobenzyl alcohol (10c): Followed by the general procedures (Method A) using **9c** (50.5 mg) and **B**⁴ (32.8 mg, 0.04 mmol), giving **10c** in 97% yield confirmed by the NMR analysis using trimethylphenylsilane (15.5 mg, 0.1 mmol). ¹H NMR (400 MHz, CDCl₃): δ 7.35–7.30 (m, 2H, Ar-*H*), 7.04 (t, *J* = 8.6 Hz, 2H, Ar-*H*), 4.64 (s, 2H, CH₂OH), 2.87 (brs, 1H, OH). The formation of 1,1' -(oxybis(methylene))bis(4-fluorobenzene) was conformed in 1%, which was calculated using δ 4.50 (s) in ¹H NMR.



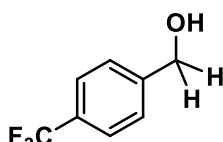
4-Chlorobenzyl alcohol (10d): Followed by the general procedures (Method A) using **9d** (57.0 mg) and **B⁴** (33.0 mg, 0.04 mmol), giving **10d** in 91% yield confirmed by the NMR analysis using trimethylphenylsilane (16.7 mg, 0.1 mmol). ¹H NMR (400 MHz, CDCl₃): δ 7.32–7.28 (m, 4H, Ar-*H*), 4.67 (s, 2H, CH₂OH). A resonance of *OH* was not observed. The formation of 1,1' -(oxybis(methylene))bis(4-chlorobenzene) was confirmed in 4%, which was calculated using δ 4.52 (s) in ¹H NMR.



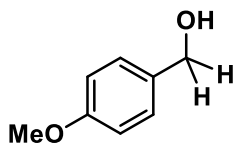
4-Bromobenzyl alcohol (10e): Followed by the general procedures (Method A) using **9e** (74.7 mg) and **B⁴** (33.1 mg, 0.04 mmol), giving **10e** in 96% yield confirmed by the NMR analysis using trimethylphenylsilane (11.9 mg, 0.1 mmol). ¹H NMR (400 MHz, CDCl₃): δ 7.48 (d, *J* = 8.4 Hz, 2H, Ar-*H*), 7.22 (d, *J* = 7.6 Hz, 2H, Ar-*H*), 4.63 (s, 2H, CH₂OH). A resonance of *OH* was not observed. The formation of 1,1' -(oxybis(methylene))bis(4-bromobenzene) was confirmed in 2%, which was calculated using δ 4.50 (s) in ¹H NMR.



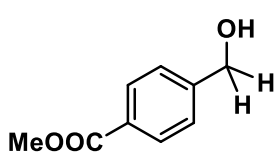
4-Iodobenzyl alcohol (10f): Followed by the general procedures (Method A) using **9f** (92.8 mg) and **B⁴** (33.1 mg, 0.04 mmol), giving **10f** in 94% yield confirmed by the NMR analysis using trimethylphenylsilane (16.0 mg, 0.1 mmol). ¹H NMR (400 MHz, CDCl₃): δ 7.68 (d, *J* = 8.0 Hz, 2H, Ar-*H*), 7.09 (d, *J* = 7.6 Hz, 2H, Ar-*H*), 4.63 (s, 2H, CH₂OH). A resonance of *OH* was not observed. The formation of 1,1' -(oxybis(methylene))bis(4-iodobenzene) was estimated in 1%, which was calculated using δ 4.48 (s) in ¹H NMR.



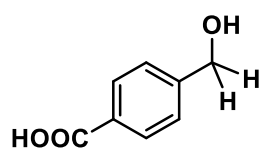
4-(Trifluoromethyl)benzyl alcohol (10g): Followed by the general procedures (Method A) using **9g** (71.2 mg) and **B⁴** (32.4 mg, 0.04 mmol), giving **10g** in > 99% yield confirmed by the NMR analysis using trimethylphenylsilane (10.7 mg, 0.1 mmol). ¹H NMR (400 MHz, CDCl₃): δ 7.62 (d, *J* = 8.0 Hz, 2H, Ar-*H*), 7.47 (d, *J* = 8.0 Hz, 2H, Ar-*H*), 4.77 (s, 2H, CH₂OH), 2.21 (brs, 1H, OH).



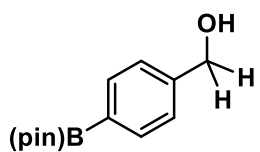
4-Methoxybenzyl alcohol (10h): Followed by the general procedures (Method A) using **9h** (54.9 mg) and **B⁴** (33.2 mg, 0.04 mmol), giving **10h** in 13% yield confirmed by the NMR analysis using trimethylphenylsilane (12.2 mg, 0.1 mmol). ¹H NMR (400 MHz, CDCl₃): δ 7.28 (d, *J* = 8.6 Hz, 2H, Ar-*H*), 6.88 (d, *J* = 8.6 Hz, 2H, Ar-*H*), 4.46 (s, 2H, CH₂OH), 3.81 (s, 3H, OCH₃), 1.89 (brs, 1H, OH). The formation of 1,1' -(oxybis(methylene))bis(4-methoxybenzene) was confirmed in 4%, which was calculated using δ 4.62 (s) in ¹H NMR.



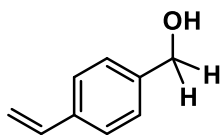
Methyl 4-(hydroxymethyl)benzoate (10i): Followed by the general procedures (Method A) using **9i** (66.2 mg) and **B⁴** (32.4 mg, 0.04 mmol), giving **10i** in > 99% yield, confirmed by the NMR analysis using trimethylphenylsilane (12.4 mg, 0.1 mmol). ¹H NMR (400 MHz, CDCl₃): δ 8.02 (d, *J* = 8.0 Hz, 2H, Ar-*H*), 7.42 (d, *J* = 8.0 Hz, 2H, Ar-*H*), 4.76 (s, 2H, CH₂OH), 2.48 (brs, 1H, OH).



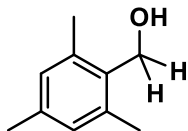
4-(Hydroxymethyl)benzoic acid (10j): Followed by the general procedures (Method A) using **9j** (60.1 mg) and **B⁴** (33.0 mg, 0.04 mmol), giving **10j** in 40% yield confirmed by the NMR analysis using trimethylphenylsilane (10.2 mg, 0.1 mmol). ¹H NMR (400 MHz, DMSO-*d*₆): δ 12.99 (brs, 1H, COOH), 7.90 (d, *J* = 8.0 Hz, 2H, Ar-*H*), 7.43 (d, *J* = 8.0 Hz, 2H, Ar-*H*), 5.38 (brs, 1H, OH), 4.57 (s, 2H, CH₂OH). The formation of 4,4'-(Oxybis(methylene))bisbenzoic acid was estimated in 4%, which was calculated using δ 4.69 (s) in ¹H NMR.



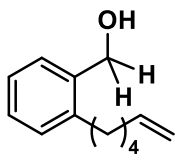
4-(4,4,5,5-Tetramethyl-1,3,2-dioxaborolan-2-yl)benzyl alcohol (10k): Followed by the general procedures (Method A) using **9k** (92.5 mg) and **B⁴** (34.8 mg, 0.04 mmol), giving **10k** in 81% yield confirmed by the NMR analysis using trimethylphenylsilane (10.5 mg, 0.1 mmol). ¹H NMR (400 MHz, CDCl₃): δ 7.81 (d, *J* = 7.6 Hz, 2H, Ar-*H*), 7.36 (d, *J* = 7.4 Hz, 2H, Ar-*H*), 4.70 (s, 2H, CH₂OH), 1.35 (s, 12H, (CH₃)₂CC(CH₃)₂). A resonance of OH was not observed.



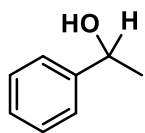
4-Vinylbenzyl alcohol (10l): Followed by the general procedures (Method A) using **9l** (52.5 mg) and **B⁴** (32.9 mg, 0.04 mmol), giving **10l** in 86% yield confirmed by the NMR analysis using trimethylphenylsilane (18.0 mg, 0.12 mmol). ¹H NMR (400 MHz, CDCl₃): δ 7.41 (d, *J* = 8.4 Hz, 2H, Ar-*H*), 7.32 (d, *J* = 8.4 Hz, 2H, Ar-*H*), 6.72 (dd, *J* = 17.6 Hz, 10.8 Hz, 1H, CH=CH₂), 5.76 (dd, *J* = 17.6 Hz, 0.4 Hz, 1H, CH=CH₂), 5.25 (dd, *J* = 10.9 Hz, 0.4 Hz, 1H, CH=CH₂), 4.69 (s, 2H, CH₂OH). A resonance of OH was not observed.



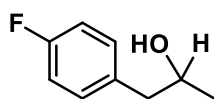
2,4,6-Trimethylbenzyl alcohol (10m): Followed by the general procedures (Method A) using **9m** (59.1 mg) and **B⁴** (33.2 mg, 0.04 mmol), giving **10m** in 35% yield confirmed by the NMR analysis using trimethylphenylsilane (12.8 mg, 0.1 mmol). ¹H NMR (400 MHz, CDCl₃): δ 6.87 (s, 2H, Ar-*H*), 4.72 (s, 2H, CH₂OH), 2.40 (s, 6H, CH₃), 2.27 (s, 3H, CH₃). A resonance of OH was not observed. The formation of 2,2'-(oxybis(methylene))bis(1,3,5-trimethylbenzene) was estimated in 7%, which was calculated using δ 4.55 (s) in ¹H NMR.



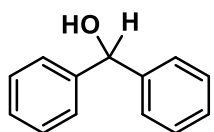
2-(Hex-5-en-1-yl)benzenemethanol (10n): Followed by the general procedures (Method A) using **9k** (75.3 mg) and **B⁴** (31.8 mg, 0.04 mmol), giving **10n** in 89% yield confirmed by the NMR analysis using trimethylphenylsilane (12.4 mg, 0.1 mmol). Analytically pure **10n** was obtained by flash column chromatography on silica gel using gradient EtOAc in hexane, given as a colorless liquid (66.5 mg, 0.35 mmol, 88%). ¹H NMR (400 MHz, CDCl₃): δ 7.37 (d, *J* = 7.6 Hz, 1H, Ar-*H*), 7.27–7.19 (m, 3H, Ar-*H*), 5.87–5.77 (m, 1H, CH=CH₂), 5.04–4.94 (m, 2H, CH=CH₂), 4.72 (s, 2H, CH₂OH), 2.69 (t, *J* = 7.8 Hz, 2H, CH₂), 2.11 (q, *J* = 7.1 Hz, 2H, CH₂), 1.66–1.58 (m, 3H, CH₂ and OH), 1.53–1.46 (m, 2H, CH₂). ¹³C{¹H} NMR (101 MHz, CDCl₃): 140.9, 138.9, 138.3, 129.5, 128.3, 126.2, 114.6, 63.2, 33.8, 32.3, 29.0. HRMS (EI⁺): *m/z* Calcd for C₁₃H₁₈O [M]⁺ 190.1358, found 190.1354. The formation of 2,2'-(oxybis(methylene))bis(hex-5-en-1-ylbenzene) was estimated in 1%, which was calculated using δ 4.58 (s) in ¹H NMR.



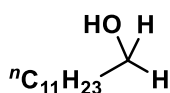
1-Phenylethanol (10o): Followed by the general procedures (Method A) using **9o** (50.8 mg) and **B⁵** (32.2 mg, 0.04 mmol), giving **10o** in 56% yield confirmed by the NMR analysis using trimethylphenylsilane (12.9 mg, 0.1 mmol). ¹H NMR (400 MHz, CDCl₃): δ 7.37–7.33 (m, 5H, Ar-H), 4.90 (q, *J* = 6.4 Hz, 1H, CHOH), 1.50 (d, *J* = 6.4 Hz, 3H, CH₃), 2.27 (s, 3H, CH₃). A resonance of OH was not observed.



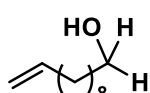
4-Fluoro-α-methylbenzeneethanol (10p): Followed by the general procedures (Method A) using **9p** (72.0 mg) and **B⁴** (32.5 mg, 0.04 mmol), giving **10p** in >99% yield confirmed by the NMR analysis using trimethylphenylsilane (9.0 mg, 0.1 mmol). ¹H NMR (400 MHz, CDCl₃): δ 7.19–7.15 (m, 2H, Ar-H), 7.02–6.98 (m, 2H, Ar-H), 4.03–3.96 (m, 1H, CHOH), 2.78–2.64 (m, 2H, CH₃), 1.24 (d, *J* = 6.4 Hz, 3H, CH₃). A resonance of OH was not observed.



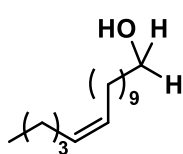
1-Phenylethanol (10q): Followed by the general procedures (Method A) using **9q** (72.8 mg) and **B⁴** (32.7 mg, 0.04 mmol), giving **10q** in 7% yield, confirmed by the NMR analysis using trimethylphenylsilane (11.2 mg, 0.1 mmol).



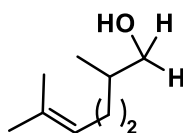
Dodecan-1-ol (10r): Followed by the general procedures (Method B) using **9r** (68.4 mg) and **B⁴** (32.7 mg, 0.04 mmol), giving **10r** as a colorless liquid, which was isolated in 92% yield (63.0 mg, 0.3 mmol). ¹H NMR (400 MHz, CDCl₃): δ 3.64 (t, *J* = 6.6 Hz, 2H, CH₂OH), 1.60–1.53 (m, 2H, CH₂), 1.26 (s, 18H, (CH₂)₉CH₂OH), 0.88 (t, *J* = 6.8 Hz, 3H, CH₃). A resonance of OH was not observed.



Undec-10-en-1-ol (10s): Followed by the general procedures (Method B) using **9s** (66.7 mg) and **B⁴** (33.0 mg, 0.04 mmol), giving **10s** as a colorless liquid, which was isolated in 98% (66.2 mg, 0.4 mmol). ¹H NMR (400 MHz, CDCl₃): δ 5.86–5.76 (m, 1H, CH=CH₂), 5.02–4.91 (m, 2H, CH=CH₂), 3.64 (t, *J* = 6.6 Hz, 2H, CH₂OH), 2.04 (dt, *J* = 6.8 Hz, 7.6 Hz, 2H, CH₂=CHCH₂), 1.60–1.53 (m, 2H, CH₂CH₂OH), 1.29 (s, 13H, (CH₂)₆ and OH).



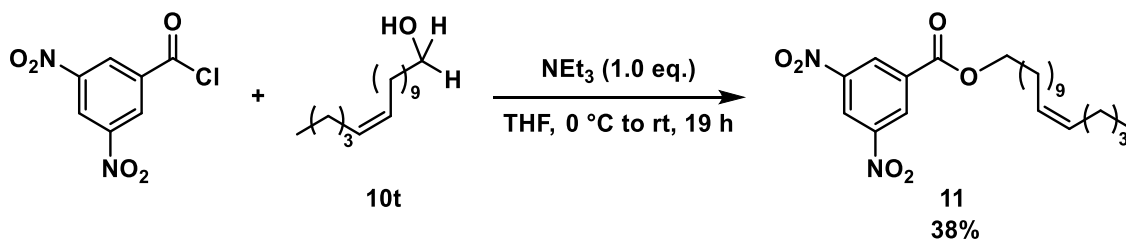
(Z)-Hexadec-11-en-1-ol (10t): Followed by the general procedures (Method B) using **9t** (94.0 mg, >95% purity as received from TCI) and **B⁴** (32.4 mg, 0.04 mmol), giving **10t** as a colorless liquid, which was isolated in > 99% (93.5 mg, 0.4 mmol). Unidentified resonances derived from impurities involved in **9t** are found in ¹H and ¹³C NMR spectra. ¹H NMR (600 MHz, CDCl₃): δ 5.36–5.33 (m, 2H, CH=CH), 3.64 (t, *J* = 6.6 Hz, 2H, CH₂OH), 2.04–2.00 (m, 4H, (CH₂)₂), 1.56 (dt, *J* = 6.9 Hz, 14.4 Hz, 2H, CH₂CH=CH), 1.33–1.28 (m, 19H, (CH₂)₉ and OH), 0.90 (t, *J* = 7.2 Hz, 3H, CH₃). ¹³C{¹H} NMR (100 MHz, CDCl₃): 130.0, 63.3, 33.0, 32.1, 29.9, 29.8, 29.7, 29.7, 29.6, 29.4, 27.3, 27.1, 25.9, 22.5, 14.2.



2,6-Dimethylhept-5-en-1-ol (10u): Followed by the general procedures (Method B) using **9u** (55.3 mg) and **B⁴** (32.2 mg, 0.04 mmol), giving **10u** as a colorless liquid, which was isolated in 38% (21.3 mg, 0.2 mmol). ¹H NMR (400 MHz, CDCl₃): δ 5.12–5.09 (m, 2H, C=CH), 3.54–3.40 (m, 2H, CH₂OH), 2.09–1.92 (m, 2H, CH₂), 1.68 (s, 3H, CH₃), 1.66–1.62

(m, 1H, *CH*), 1.61 (s, 3H, *CH*₃), 1.48–1.39 (m, 1H, *C(H)H*), 1.20–1.10 (m, 1H, *C(H)H*), 0.93 (d, *J* = 6.4 Hz, 3H, *CH*₃). A resonance of *OH* was not observed.

2.5.8. Synthesis of (*Z*)-pentadec-10-en-1-yl 3,5-dinitrobenzoate (**11**) to determine the molecular structure of **10t**



To a THF (1 mL) solution of **10t** (413.2 mg, 1.2 mmol) and NEt₃ (166.0 μ L, 1.2 mmol, 1.0 eq.), 3,5-dinitrobenzoyl chloride (2.5 mL of a 0.5 M solution in THF, 1.2 mmol, 1.0 eq.) was slowly added at 0 °C. After stirring for 1 h at 0 °C, the resultant solution was allowed to warm to rt and then stirred for additional 18 h. All volatiles were removed *in vacuo* to give yellow liquid. The resultant liquid was purified by GPC to give **11** as colorless liquid (196.2 mg, 0.5 mmol, 38% yield) after the removal of all volatiles *in vacuo*. A single crystal suitable for the XRD analysis was obtained via crystallization at 5 °C from EtOH/H₂O solution. ¹H NMR (400 MHz, CD₂Cl₂): δ 9.23 (t, 1H, *J* = 2.2, Ar-*H*), 9.16 (d, 2H, *J* = 2.0 Hz, Ar-*H*), 5.36–5.33 (m, 2H, *CH=CH*), 4.45 (t, *J* = 6.8 Hz, 2H, COOCH₂), 2.02–1.99 (m, 4H, (CH₂)₂), 1.83 (dt, *J* = 6.8 Hz, 14.8 Hz, 2H, CH₂CH=CH), 1.48–1.29 (m, 18H, (CH₂)₉), 0.89 (t, *J* = 7.0 Hz, 3H, CH₃). ¹³C{¹H}NMR (100 MHz, CD₂Cl₂): δ 162.7, 148.8, 134.3, 130.0, 130.0, 129.6, 122.4, 67.3, 32.7, 32.4, 32.1, 29.9, 29.7, 29.4, 29.4, 28.7, 27.3, 27.1, 26.0, 22.5, 14.1. HRMS (EI⁺): *m/z* Calcd for C₂₃H₃₄N₂O₆ 434.2417, found 434.2421. **Crystal data** for C₂₃H₃₄N₂O₆ (*M* = 434.24 g/mol): monoclinic, space group *P*2₁/*c* (#14), *a* = 10.1763(12) Å, *b* = 5.4945(7) Å, *c* = 43.514(7) Å, α = 90°, β = 94.966(13)°, γ = 90°, *V* = 2423.9(6) Å³, *Z* = 4, *D*_{calcd} = 1.191 g/cm³, *T* = –30 °C, *R*₁(*wR*₂) = 0.0708 (0.2104).

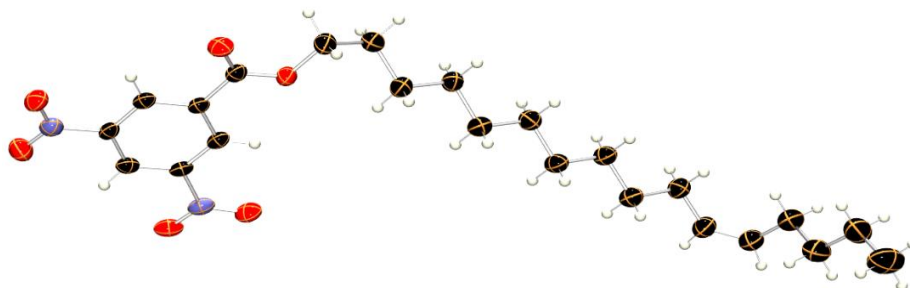
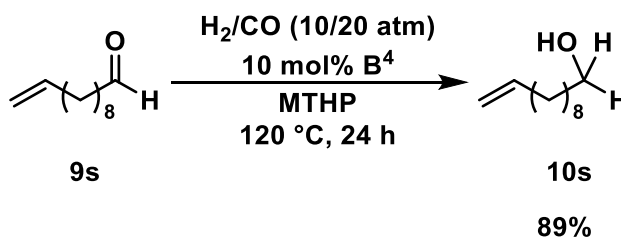


Figure 2.S4. The molecular structure of **11** with ellipsoids set at 30% probability.

2.5.9. Hydrogenation of **9s** using H₂/CO (10/20 atm)



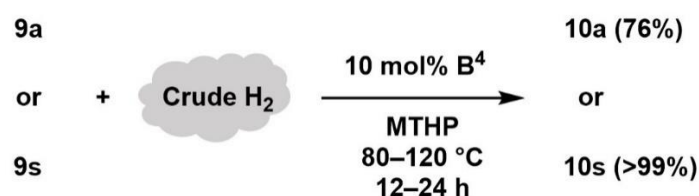
A solution of **9s** (67.5 mg, 0.4 mmol) and **B⁴** (32.7 mg, 0.04 mmol) in MTHP (1.6 mL) was transferred to a 10 mL autoclave. Once sealed, the autoclave was pressurized with CO (20 atm) and H₂ (10 atm) at rt and stirred at 120 °C for 24 h. After degassing at rt, the reaction mixture was transferred to a round bottom flask and dried *in vacuo*, giving **10s** in 89% yield confirmed by the NMR analysis using trimethylphenylsilane (13.0 mg, 0.1 mmol).

2.5.10. Influence of contaminants

General Procedure using B¹: A solution of **9a** (62.5 mg, 0.4 mmol) and **B¹** (20.5 mg, 0.04 mmol) in 1,4-dioxane (1.6 mL) was transferred to a 10 mL autoclave. Once sealed, the autoclave was pressurized with H₂ (20 atm) and N₂ (40 atm), H₂/CO (20 atm each) and N₂ (20 atm), H₂/CO₂ (20 atm each) and N₂ (20 atm), or H₂/CO/CO₂ (20 atm each) at rt and stirred at 80 °C for 8 h. After degassing at rt, the reaction mixture was transferred to a round bottom flask and dried *in vacuo*. Yield of **10a** was determined by ¹H NMR analysis using trimethylphenylsilane as an internal standard in CDCl₃.

General Procedure using B⁴: A solution of **9a** (62.5 mg, 0.4 mmol) and **B⁴** (32.9 mg, 0.04 mmol) in MTHP (1.6 mL) was transferred to a 10 mL autoclave. Once sealed, the autoclave was pressurized with H₂ (20 atm) and N₂ (40 atm), H₂/CO (20 atm each) and N₂ (20 atm), H₂/CO₂ (20 atm each) and N₂ (20 atm), or H₂/CO/CO₂ (20 atm each) at rt and stirred at 80 °C for 8 h. After degassing at rt, the reaction mixture was transferred to a round bottom flask and dried *in vacuo*. Yield of **10a** was determined by ¹H NMR analysis using trimethylphenylsilane as an internal standard in CDCl₃.

2.5.11. Hydrogenation of 9a or 9s using an industrial crude H₂



Procedure using 9a: A solution of **9a** (62.8 mg, 0.4 mmol) and **B⁴** (33.0 mg, 0.04 mmol) in MTHP (1.6 mL) was transferred to a 10 mL autoclave. Once sealed, the autoclave was pressurized with H₂/CO/CO₂/CH₄/H₂O (total ca. 13 atm; partial pressure of H₂ is ca. 10 atm) at rt and stirred at 80 °C for 12 h. After degassing at rt, the reaction mixture was transferred to a round bottom flask and dried *in vacuo*, giving **10a** and 1,1'-(oxybis(methylene))dinaphthalene in 76% and 3% yield, respectively, confirmed by the NMR analysis using trimethylphenylsilane (9.2 mg, 0.1 mmol).

Procedure using 9s: A solution of **9s** (67.5 mg, 0.4 mmol) and **B⁴** (32.7 mg, 0.04 mmol) in MTHP (1.6 mL) was transferred to a 10 mL autoclave. Once sealed, the autoclave was pressurized with H₂/CO/CO₂/CH₄/H₂O (total ca. 18 atm; partial pressure of H₂ is ca. 14 atm) at rt and stirred at 120 °C for 24 h. After degassing at rt, the reaction mixture was transferred to a round bottom flask and evaporated *in vacuo*, giving **10s** in >99% yield confirmed by the NMR analysis using trimethylphenylsilane (9.8 mg, 0.1 mmol).

2.5.12. Titration of H₂O contaminated in an industrial crude H₂

A pressure-tight NMR tube (Wilmad-LabGlass 542-PV-7; $V = 1.8$ mL) was charged with 1,3-dimethoxybenzene (13.8 mg, 0.1 mmol; an internal standard) and C₆D₆ (500 μ L). Once sealed, the NMR tube was pressurized with a gaseous mixture of H₂/CO/CO₂/CH₄/H₂O (received by AIR WATER INC.) stored over 4 Å MS overnight. The contaminated H₂O was quantified by ¹H NMR analysis (Table 2.S2).

Table 2.S2. Titration of H₂O (ppm).

Run	After dehydrated by 4 Å MS
1	300
2	450
average	375

2.5.13. References for Supporting Information

- S1. (a) Ullrich, M.; Lough, A. J.; Stephan, D. W. *J. Am. Chem. Soc.* **2009**, *131*, 52. (b) Ullrich, M.; Lough, A. J.; Stephan, D. W. *Organometallics* **2010**, *29*, 3647.
- S2. Sakuraba, M.; Morishita, T.; Hashimoto, T.; Ogoshi, S.; Hoshimoto, Y. *Synlett* **2023**, *34*, 2187
- S3. Hashimoto, T.; Asada, T.; Ogoshi, S.; Hoshimoto, Y. *Sci. Adv.* **2022**, *8*, eade0189.
- S4. Gyömöre, Á.; Bakos, M.; Földes, T.; Pápai, I.; Domján, A.; Soós, T. *ACS Catal.* **2015**, *5*, 5366.
- S5. Manka, J. T.; Kaszynski, P. *J. Fluor. Chem.* **2003**, *124*, 39.
- S6. Yamaguchi, T.; Takashima, T.; Kaneko, H.; Nakagawa, Y.; Hosaka, N. Patent JP2016011265A (2016) <https://patents.google.com/patent/JP2016011265A/ja?q=JP2016011265>.
- S7. Neese, F.; Wennmohs, F.; Becker, U.; Riplinger, C. *J. Chem. Phys.* **2020**, *152*, 224108.

Chapter 3

Studies on Details of Remote Back Strain

Abstract: A strategy for modulating the Lewis acidity of triarylboranes is proposed based on the concept of ‘remote’ back strain. I studied the details on remote back strain using $B(2,6-F_2-3,5-R_2-C_6H)_3$ ($R = F, Cl, \text{ and } Br$) and $B(2,6-F_2-3,5-R_2-C_6H)_3$ ($R = TMS, \text{ allyl, and } H$). Steric repulsion and non-covalent interactions, both generated between the aryl *meta* substituents of triarylboranes, are found to be critical for determining the strength of the remote back strain. It should be noted that I synthesized $B(2,6-F_2-3,5-TMS_2-C_6H)_3$ and the liquid $B(2,6-F_2-3,5-allyl_2-C_6H)_3$ designed based on the concept of remote back strain and demonstrated their superior catalytic activity for the hydrogenation of quinoline relative to $B(C_6F_5)_3$ and $B(2,6-F_2-C_6H_3)_3$. Moreover, I established the first example of the catalytic hydrogenation of quinoline using $B(2,6-F_2-3,5-allyl_2-C_6H)_3$ in the presence of a gaseous mixture of $H_2/CO/CO_2$ (1/1/1 molar ratio).

3.1. Introduction

Our group has recently investigated the hydrogenation of 2-methylquinoline using a gaseous mixture of $H_2/CO/CO_2$ and demonstrated that the catalyst turnover number (TON) increases significantly when the *meta* substituent R in $B(2,6-Cl_2C_6H_3)(2,6-F_2-3,5-R_2-C_6H)_2$ was changed from F (1000) to Cl (1400) and finally to Br (1520).¹ I have also reported the hydrogenation of carbonyl compounds using a gaseous mixture of $H_2/CO/CO_2$ and demonstrated reaction efficiency was increased from F to Cl and to Br in Chapter 2. Given their nearly identical LUMO(+1) levels, I speculated that the size and shape of the *meta* substituents (R in Figure 3.1) could have a substantial impact on the Lewis acidity and reactivity of BAr_3 (or BAr_2Ar') via control of the ‘remote’ back strain.

Herein, I report evaluation of the remote back strain through the comparison with $B(2,6-F_2-3,5-R_2-C_6H)_3$ (**B²**: $X = F$, **B³**: $X = Cl$, and **B⁴**: $X = Br$) (Figure 3.1, Group A). I also report the synthesis of novel homoleptic boranes $B(2,6-F_2-3,5-R_2-C_6H)_3$ (**B⁵**: $R = \text{trimethylsilyl, TMS}$; **B¹⁰**: $R = \text{allyl}$) to evaluate the impact of the remote back strain on global and effective Lewis acidity through the comparison with **B¹¹** ($R = H$) (Figure 3.1, Group B). I discuss the degree of the remote back strain based on the changes in the relative Gibbs energies (ΔG°) for the adduct formation with selected LBs such as $Et_3P=O$, H_2O , CO , THF , and NMe_3 . In addition, I calculated deformation energies (E_{DEF})^{2a,c,3} for the evaluation of an energetic penalty paying for the geometrical rearrangement around the boron from trigonal planar to tetrahedral through the adduct formation. Application of **B⁵**, **B¹⁰**, and **B¹¹** to the catalytic hydrogenation of quinoline using H_2 or $H_2/CO/CO_2$ are also reported.

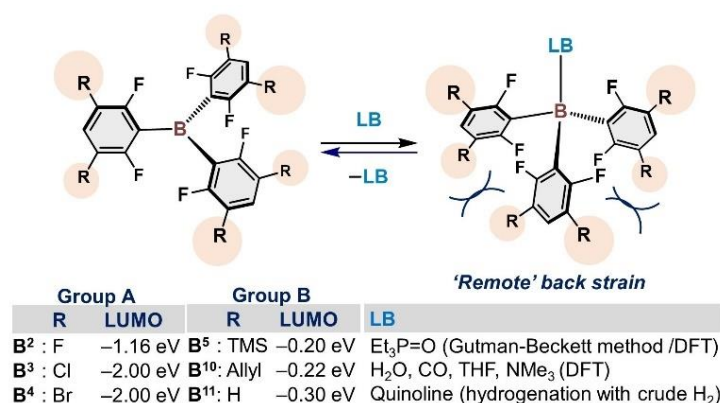


Figure 3.1 Triarylboranes **B²–B⁵**, **B¹⁰**, and **B¹¹** used in this work. The energy levels of the LUMOs (eV), calculated at the RI-DSD-PBEP86-D3BJ/ma-Def2-QZVPP//PBEh-3c/Def2-SVP level (gas phase), are also shown. [*a*] LUMO+1.

3.2. Results and discussion

3.2.1. Comparison between **B²–B⁴**

First, to evaluate the remote back strain, I calculated $\tau_8(B)$ for the evaluation of the degree of geometrical deviation from the ideal tetrahedral geometry around the boron center,^{4,5} where $\tau_8(B) = \{360 - (\alpha + \beta)/141 \times \beta/\alpha\}$ (α and β are the largest and second largest C–B–C angles). When the boron center adopts ideal tetrahedral geometry, the value of $\tau_8(B)$ provide 1.0 as their maximum, and smaller values thus suggest the more distorted tetrahedral geometry. The values of $\tau_8(B)$ are summarized in Figure 3.2. I compared $\tau_8(B)$, then it was clarified that the geometries around each boron center in THF–**Bⁿ** adducts are nearly identical, regardless of differences in the *meta* substituents. Next, to evaluate the relative degree of the remote-back-strain for **B²–B⁴**, I compared the deformation energies (E_{DEF} in kcal mol⁻¹)² when forming the LB–**Bⁿ** adducts ($n = 2–4$; LB = THF). As summarized in Figure 3.2., the introduction of larger atoms (*meta*-F < Cl < Br) results in an increase in the E_{DEF} values, i.e., **B²** (+25.3 kcal mol⁻¹) < **B³** (+25.6 kcal mol⁻¹) < **B⁴** (+25.7 kcal mol⁻¹), and a destabilization of the adducts, i.e., THF–**B²** (–9.5 kcal mol⁻¹) < **B³** (–9.3 kcal mol⁻¹) < **B⁴** (–8.9 kcal mol⁻¹), where relative energies are given with respect to [THF + **Bⁿ**] (+0.0 kcal mol⁻¹). Although these energy differences are not sufficient to exclude calculation errors, it suggested that FLP was generated efficiently from MTHP–**Bⁿ** adduct ($n = 3$ and 4) by remote back strain generated in *meta*-Cl/Br, thus, the hydrogenation of carbonyl compounds in Chapter 2 was proceeded efficiently when using **B³** and **B⁴**.

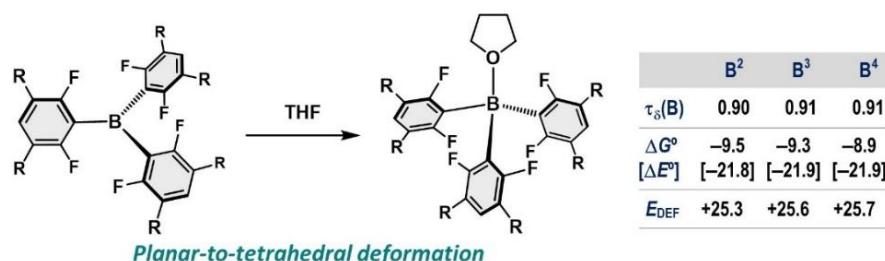


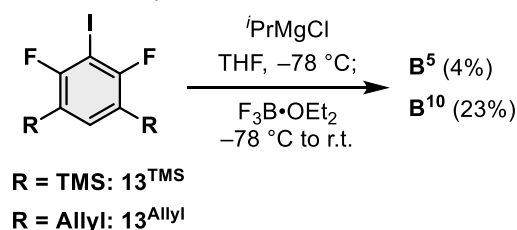
Figure 3.2. Comparison of the LUMO (eV), E_{DEF} (kcal mol⁻¹), and relative Gibbs energy levels of THF–**Bⁿ** adducts ($n = 2–4$) with respect to [THF + **Bⁿ**] (+0.0 kcal mol⁻¹).

3.2.2. Strategy to design **B⁵** and **B¹⁰**

To explore a relationship between the remote back strain and Lewis acidity, model molecules should be appropriately designed. In this context, I synthesized **B**⁵ and **B**¹⁰ through the introduction of *meta*-TMS and allyl group, respectively, for comparison with *meta*-protonated **B**¹¹. A preliminary computation revealed that their intrinsic Lewis acidity would be nearly comparable (Figure 3.1). In fact, the difference in the energy level of LUMO (eV) is negligible between **B**⁵ (−0.20) and **B**¹⁰ (−0.22), albeit the differences compared to **B**¹¹ (−0.30) might be carefully considered. BAr₃ compounds bearing electron withdrawing substituents at the *meta* positions should be inappropriate due to the significant difference in their LUMO levels, as exemplified by B(2,3,4,5-F₄-C₆H)₃ (−1.16 eV, calculated at the identical conditions shown in Figure 3.1). In addition, the comparison of the percent buried volume (%*V*_{Bur})⁶ revealed that *meta*-TMS groups occupy larger area (Δ%*V*_{Bur} +2.6~4.7%) around the *B*-aryl groups than *meta*-allyl groups, simulated using H₂B(2,6-F₂-R₂-C₆H) (R = TMS or allyl) as model molecules (Figure 3.S7). I also confirmed that an influence of the Buttrressing effect⁷ caused by *meta*-TMS and allyl groups should be negligible under the presented conditions (Figure 3.S8).

3.2.2. Synthesis of **B**⁵ and **B**¹⁰

The preparation of **B**⁵ followed the procedures shown in Scheme 3.1. A stepwise introduction of two TMS groups was achieved with 1,5-Br₂-2,4-F₂-C₆H₂ (**12**) and TMSOTf by a silver-catalyzed transmetalation.⁸ Then, subsequent iodination of the product afforded **13**^{TMS} which was converted into **B**⁵ by treatment with ⁱPrMgCl in THF followed by the addition of BF₃·OEt₂. Eventually, **B**⁵ was isolated as a colorless crystal in 35% yield from a hot hexane solution, and analytically pure **B**⁵ was isolated in 4% yield after repeated recrystallization. The molecular structure of **B**⁵ was unambiguously confirmed by multinuclear NMR and single-crystal X-ray diffraction (SC-XRD) analyses (Scheme 3.S1). I also synthesized **B**¹⁰ in 23% yield from **13**^{Allyl}, which was prepared by a catalyst-free one-pot reaction between allyl bromide and a Grignard reagent generated from **12**. Interestingly, **B**¹⁰ is a liquid under ambient conditions and was thus identified by multinuclear NMR analysis. The introduction of the allyl groups onto the ortho-fluorinated triarylborane motif was further confirmed by SC-XRD analysis of the CH₃CN–**B**¹⁰ adduct (Scheme 3.S2). The CH₃CN–**B**¹⁰ adduct can be stored under ambient conditions (22 °C, ~30% humidity) for at least seven days without apparent decomposition. The coordinated CH₃CN moiety can be removed in vacuo after dissolving the adduct in toluene.

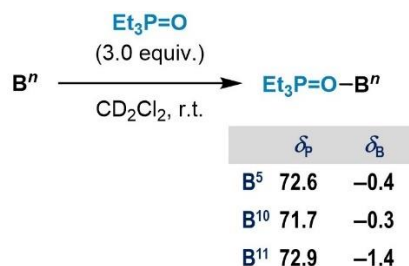


Scheme 3.1 Synthesis of **B**⁵ and **B**¹⁰. Yield of isolated products is shown.

3.2.3. Evaluation of the effective Lewis acidity

I then evaluated the effective Lewis acidity of **B**⁵, **B**¹⁰, and **B**¹¹ by using the Gutmann-Beckett method,⁹ i.e. by comparing the deviation in chemical shifts (Δδ_P) upon the formation of Et₃P=O–**B**^{*n*} (*n* = 5, 10, and 11) relative to free Et₃P=O (δ_P = 51.4 in CD₂Cl₂). A larger value of Δδ_P is expected for triarylboranes that exhibit higher Lewis acidity toward Et₃P=O. As shown in Scheme 3.2, the value of Δδ_P follows the order of **B**¹⁰ (Δδ_P = +20.3) < **B**⁵ (Δδ_P = +21.2) ≈ **B**¹¹ (Δδ_P = +21.5), showing that the LUMO(+1) levels alone cannot be used to

rationalize the relative Lewis acidities of **B**⁵, **B**¹⁰, and **B**¹¹. The formation of Et₃P=O–**B**^{*n*} was also confirmed by ¹¹B NMR spectroscopy, and resonances that indicate the generation of four-coordinate boron species were observed at $\delta_B = -0.4$ (**B**⁵), -0.3 (**B**¹⁰), and -1.4 (**B**¹¹), respectively. Cooling of a 1:1 mixture of **B**⁵ and Et₃P=O to -30 °C afforded colorless crystals, which were suitable for the SC-XRD analysis. The molecular structure of Et₃P=O–**B**⁵ are shown in Scheme 3.S3. A 1:1 mixture of Et₃P=O and **B**¹⁰ remained a liquid.



Scheme 3.2. (A) Reaction between **B**^{*n*} (*n* = 5, 10, and 11) and Et₃P=O (3 equiv.) in CD₂Cl₂.

3.2.4. Evaluation of τ_8 , ΔG° (ΔE°), and E_{DEF}

I then reproduced the geometrical parameters obtained for Et₃P=O–**B**⁵ from SC-XRD analysis by using DFT calculations at the PBEh-3c/Def2-mSVP level (gas phase).^{2a} The final single-point energy was calculated at the RI-DSD-PBEP86-D3BJ/ma-Def2-QZVPP, CPCMC(CH₂Cl₂) level and combined with the thermal corrections from the PBEh-3c calculations. Similarly, structural optimizations and single point energy calculations were conducted for the corresponding adducts containing **B**¹⁰ and **B**¹¹ based on the optimized geometry of Et₃P=O–**B**⁵. In addition, the theoretical calculations were carried out for the reaction between **B**^{*n*} (*n* = 5, 10, and 11) and a variety of LBs, including H₂O, CO, THF, and NMe₃. From these geometrical parameters, I calculated $\tau_8(\text{B})$ for the evaluation of the degree of geometrical deviation from the ideal tetrahedral geometry around the boron center.^{4,5} The values of $\tau_8(\text{B})$ and energies (kcal mol^{–1}) such as ΔG° (ΔE°) with respect to [**B**^{*n*} + LB] (+0.0 kcal mol^{–1}) and E_{DEF} are summarized in Figure 3.3.

(A) LB: Et ₃ P=O				(B) LB: H ₂ O				(C) LB: CO			
	B ⁵	B ¹⁰	B ¹¹		B ⁵	B ¹⁰	B ¹¹		B ⁵	B ¹⁰	B ¹¹
$\tau_8(\text{B})$	0.90	0.90	0.94	$\tau_8(\text{B})$	0.90	0.91	0.91	$\tau_8(\text{B})$	0.88	0.92	0.90
ΔG°	–8.0	–6.0	–6.8	ΔG°	+1.2	+1.7	–0.2	ΔG°	+3.0	+3.8	+2.6
$[\Delta E^\circ]$	[–23.2]	[–21.2]	[–21.2]	$[\Delta E^\circ]$	[–10.2]	[–8.6]	[–11.7]	$[\Delta E^\circ]$	[–8.1]	[–5.9]	[–8.4]
E_{DEF}	+27.3	+27.9	+22.8	E_{DEF}	+17.3	+19.4	+17.1	E_{DEF}	+17.7	+18.3	+15.9

(D) LB: THF				(E) LB: NMe ₃			
	B ⁵	B ¹⁰	B ¹¹		B ⁵	B ¹⁰	B ¹¹
$\tau_8(\text{B})$	0.90	0.90	0.90	$\tau_8(\text{B})$	0.95	0.95	0.95
ΔG°	–4.2	–3.8	–4.9	ΔG°	+2.9	+4.7	+1.7
$[\Delta E^\circ]$	[–17.5]	[–16.5]	[–17.0]	$[\Delta E^\circ]$	[–13.1]	[–9.7]	[–13.5]
E_{DEF}	+24.4	+26.1	+24.0	E_{DEF}	+30.4	+31.8	+29.3

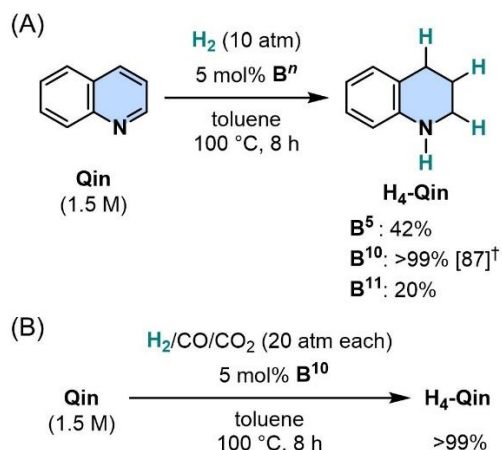
Figure 3.3. The relative Gibbs energies (kcal mol^{–1}), $\Delta G^\circ/\Delta E^\circ$ with respect to [**B**^{*n*} + LB], and the deformation energies, E_{DEF} , calculated for the formation of LB–**B**^{*n*} at the RI-DSDPBEP86-D3BJ/ma-Def2-QZVPP//PBEh-3c/Def2-mSVP level of theory (gas-phase). Final single point energy was carried out with CPCMC(CH₂Cl₂) implementation for the corresponding results in (A).

The $\tau_8(\text{B})$ values show that the geometries around each boron center in LB–**B**^{*n*} adducts, when the same

LB is used, are nearly identical, regardless of differences in the *meta* substituents. Moreover, the formation of $\text{Et}_3\text{P}=\text{O}-\mathbf{B}^5$ ($\Delta G^\circ = -8.0 \text{ kcal mol}^{-1}$) is energetically more favorable compared to both cases of $\text{Et}_3\text{P}=\text{O}-\mathbf{B}^{11}$ ($\Delta G^\circ = -6.8 \text{ kcal mol}^{-1}$) and $\text{Et}_3\text{P}=\text{O}-\mathbf{B}^{10}$ ($\Delta G^\circ = -6.0 \text{ kcal mol}^{-1}$) (Figure 3.3A). Considering the relative energies of their LUMO(+1) levels (Figure 3.1) and that TMS is sterically more demanding than the H and allyl substituents (Figure 3.S7), I attribute the stabilization of $\text{Et}_3\text{P}=\text{O}-\mathbf{B}^5$ to non-covalent interactions (NCIs) arising from the TMS groups.¹⁰ In fact, I found that several NCIs exist between *P*-Et groups and *meta*-R groups in $\text{Et}_3\text{P}=\text{O}-\mathbf{B}^n$ ($n = 5, \text{R} = \text{TMS}; n = 10, \text{R} = \text{allyl}$), although the corresponding NCI is not confirmed in $\text{Et}_3\text{P}=\text{O}-\mathbf{B}^{11}$ (Figure 3.S15–17). Furthermore, in the case of $\text{Et}_3\text{P}=\text{O}-\mathbf{B}^5$, NCIs also exist between the individual *meta*-TMS groups. These multiple NCIs that exist in $\text{Et}_3\text{P}=\text{O}-\mathbf{B}^5$ would render its formation more exothermic than that of \mathbf{B}^{11} . The NCIs between the individual *meta*-TMS groups probably play a critical role for the enhancement of global and effective Lewis acidity of \mathbf{B}^5 with respect to \mathbf{B}^{10} . When LB in the $\text{LB}-\mathbf{B}^n$ adducts is H_2O , CO , THF , and NMe_3 (Figure 3.3B–E), the values of ΔG° increase in the order of $\text{LB}-\mathbf{B}^{11} (m\text{-H}) < \text{LB}-\mathbf{B}^5 (m\text{-TMS}) < \text{LB}-\mathbf{B}^{10} (m\text{-allyl})$. These results show good consistency with the results obtained by the Gutmann-Beckett method (Scheme 3.2A). NCIs that exist between such small LBs and the *meta*-substituents are not expected to play a significant role in stabilizing $\text{LB}-\mathbf{B}^n$. Instead, NCIs that exist between the individual *meta*-TMS groups should play a key role in making the formation of $\text{LB}-\mathbf{B}^5$ a more-exothermic process than the case of $\text{LB}-\mathbf{B}^{10}$. These results are also consistent with the calculated E_{DEF} values. For the $\text{LB}-\mathbf{B}^n$ adducts explored in this work, E_{DEF} increases in the order $\mathbf{B}^{11} (m\text{-H}) < \mathbf{B}^5 (m\text{-TMS}) < \mathbf{B}^{10} (m\text{-allyl})$. Thus, E_{DEF} can be used as an indicator to compare the relative strength of remote back strain when the front strain is comparable.

3.2.5. Hydrogenation of quinoline

Subsequently, I examined the catalytic activity of \mathbf{B}^5 , \mathbf{B}^{10} , and \mathbf{B}^{11} in the hydrogenation of quinoline (**Qin**) to give 1,2,3,4-tetrahydroquinoline (**H₄-Qin**) (Scheme 3.3). The catalytic hydrogenation of 2-substituted and/or 8-substituted derivatives of **Qin** has been developed by using H_2 and triarylboranes, such as $\text{B}(\text{C}_6\text{F}_5)_3$. The reaction proceeds through the generation of an FLP species in situ from boranes and the quinoline derivative (or a produced cyclic amine).¹¹ However, the hydrogenation of **Qin** itself remains challenging as it tends to form stable classical Lewis adducts with triarylboranes¹² and, consequently, the generation of an FLP species becomes unfavorable after the removal of the 2-and/or 8-substituents. In fact, it has been reported that $\text{B}(\text{C}_6\text{F}_5)_3$ is an ineffective catalyst for the hydrogenation of **Qin** ($\text{TON} = 0$).¹³ In this context, modulation of the front strain based on the size-exclusion design has been demonstrated as an effective solution, and the heteroleptic catalyst $\text{B}(2,3,5,6\text{-F}_4\text{C}_6\text{H})_2(\text{Mes})$ exhibits a TON of ~ 20 for the formation of **H₄-Qin**.¹³ The \mathbf{B}^{11} -catalyzed hydrogenation of **Qin** initially furnished **H₄-Qin** in 20% yield after eight hours at 100 °C (Scheme 3.3A). This result shows that lowering the intrinsic Lewis acidity of the catalyst is a key to promoting the reaction, as \mathbf{B}^{11} has the virtually same front strain as $\text{B}(\text{C}_6\text{F}_5)_3$. The hydrogenation of **Qin** was significantly accelerated by using catalysts with *meta*-TMS or *meta*-allyl groups, which furnished **H₄-Qin** in yields of 42% and >99%, respectively. The TON reached 87 after 24 hours when 2 mol% of \mathbf{B}^{10} was employed, clearly demonstrating the benefits of modulating the remote back strain. Finally, I applied \mathbf{B}^{10} to the catalytic hydrogenation of **Qin** by using a 1:1:1 molar gaseous mixture of H_2 , CO , and CO_2 , a model of the crude H_2 that is produced from a variety of carbon-based resources such as natural gas or biomass (Scheme 3.3B).^{1,14} **H₄-Qin** was obtained in >99% yield, demonstrating that **Qin** can be potentially used as an organic material that simultaneously separates and stores H_2 directly from crude H_2 .



Scheme 3.3. (A) Catalytic hydrogenation of quinoline (**Qin**) in the presence of 5 mol% **Bⁿ**. Yield of 1,2,3,4-tetrahydroquinoline (**H₄-Qin**) was determined by GC analysis. [†]Catalyst turnover number after 24 h using 2 mol% **B¹⁰**. (B) **B¹⁰**-catalyzed hydrogenation of **Qin** using H₂/CO/CO₂ (20 atm each) as a model of crude H₂.

3.3. Conclusion

This study proposes a strategy of modulating the remote back strain of triarylboranes to finely tune their Lewis acidity by varying the size and shape of their aryl *meta*-substituents. A comparison of the effective and global Lewis acidities of B(2,6-F₂-3,5-R₂-C₆H)₃ (**B²**, R = F; **B³**, R = Cl; **B⁴**, R = Br; **B⁵**, R = TMS; **B¹⁰**, R = allyl; **B¹¹**, R = H) revealed that consideration of both the steric repulsion and noncovalent interactions generated between R groups is essential for successfully modulating the remote back strain. In this context, the deformation energy serves as an informative indicator for comparing the strength of the remote back strain between such triarylboranes. The triarylboranes studied here were also used as catalysts for the hydrogenation of quinoline, and a large improvement in the catalytic activity was observed when the catalyst was changed from **B¹¹** (*meta*-H) to **B⁵** (*meta*-TMS) or **B¹⁰** (*meta*-allyl). Subsequently, the **B¹⁰**-catalyzed hydrogenation of quinoline using a 1:1:1 molar gaseous mixture H₂, CO, and CO₂ was achieved for the first time. These results can be expected to pave the way for further progress in advanced main-group catalytic processes and molecular-based H₂ purification technologies.

3.4. References and notes

1. Hashimoto, T.; Asada, T.; Ogoshi, S.; Hoshimoto, Y. *Sci. Adv.* **2022**, *8*, eade0189.
2. Recently, Greb et al. proposed the classification of Lewis acidity as global, effective, and intrinsic ones, which concerns the thermodynamic energy change through the adduct formation ($\Delta E/\Delta G$), spectroscopic changes on a probe Lewis base (e.g. the Gutmann-Beckett method), and intrinsic properties of free BAr₃ (e.g. the energy level of the empty p-orbitals and electron affinity), respectively. For details, see: (a) Erdmann, P.; Greb, L. *Angew. Chem. Int. Ed.* **2022**, *61*, e202114550. (b) Greb, L. *Chem. Eur. J.* **2018**, *24*, 17881. See also, (c) Rodrigues Silva, D.; de Azevedo Santos, L.; P. Freitas, M.; Fonseca Guerra, C.; Hamlin, T. A. *Chem. Asian J.* **2020**, *15*, 4043. (d) Muller, P. *Pure Appl. Chem.* **1994**, *66*, 1077.
3. Timoshkin, A. Y.; Davydova, E. I. Sevastianova, T. N. Suvorov, A. V.; Schaefer, H. F. *Int. J. Quantum Chem.* **2002**, *88*, 436.
4. Reineke, M. H.; Sampson, M. D.; Rheingold, A. L.; Kubiak, C. P. *Inorg. Chem.* **2015**, *54*, 3211.

5. I also calculated a tetrahedral character of each boron center and obtained the identical to the $\tau_8(\text{B})$ values; for details, see Figure 3.S10–14.
6. (a) Poater, A.; Cosenza, B.; Correa, A.; Giudice, S.; Ragone, F.; Scarano, V.; Cavallo, L. *Eur. J. Inorg. Chem.* **2009**, 1759. (b) Falivene, L.; Cao, Z.; Petta, A.; Serra, L.; Poater, A.; Oliva, R.; Scarano, V.; Cavallo, L. *Nat. Chem.* **2019**, *11*, 872. (c) Zapf, M.; Riethmann, M.; Föhrenbacher, S. A.; Finze, M.; Radius, U. *Chem. Sci.* **2023**, *14*, 2275.
7. (a) Adams, R.; yuan, H. C. *Chem. Rev.* **1933**, *12*, 261. (b) Patton, A.; Dirks, J. W.; Gust, D. J. *Org. Chem.* **1979**, *44*, 4749. For example including trialkylsilyl groups, see: (c) Gorecha, J.; Heiss, C.; Scopelliti, R.; Schlosser, M. *Org. Lett.* **2004**, *6*, 4591.
8. Murakami, K.; Hirano, K.; Yorimitsu, H.; Oshima, K. *Angew. Chem. Int. Ed.* **2008**, *47*, 5833.
9. Sivaev, I. B.; Bregadze, V. I. *Coord. Chem. Rev.* **2014**, 270–271, 75.
10. Holtrop, F.; Helling, C.; Lutz, M.; van Leest, N. P.; de Bruin, B.; Slootweg, J. C. *Synlett* **2023**, *34*, 1122.
11. For selected examples, see: (a) Geier, S. J.; Chase, P. A.; Stephan, D. W. *Chem. Commun.* **2010**, *46*, 4884. (b) Scott, D. J.; Fuchter, M. J.; Ashley, A. E. *Angew. Chem. Int. Ed.* **2014**, *53*, 1021. (c) Zhang, Z.; Du, H. *Org. Lett.* **2015**, *17*, 6266. (d) Han, C.; Zhang, E.; Feng, X.; Wang, S.; Du, H. *Tetrahedron Lett.* **2018**, *59*, 1400.
12. Mahdi, T.; del Castillo, J. N.; Stephan, D. W. *Organometallics* **2013**, *32*, 1971.
13. Erős, G.; Nagy, K.; Mehdi, H.; Pápai, I.; Nagy, P.; Király, P.; Tárkányi, G.; Soós, T. *Chem. Eur. J.* **2012**, *18*, 574.
14. (a) Jorschick, H.; Vogal, M.; Preuster, P.; Bosmann, A.; Wasserscheid, P. *Int. J. Hydrog. Energy* **2019**, *44*, 31172. (b) Li, S.; Lin, L.; Wang, Z.; Ma, D. *The Innovation*, **2023**, *4*, 100353.

3.5. Supporting information

3.5.1. General considerations

All manipulations were conducted under a nitrogen atmosphere by using standard Schlenk or grove box techniques unless otherwise noted. Molecular sieves (4 Å) were activated by heating with a heat gun *in vacuo* (ca. 0.2 mmHg). ^1H , ^{11}B , ^{13}C , ^{19}F , and ^{31}P NMR spectra were recorded on a Bruker AVANCE III 400 at 25 °C unless otherwise noted. The chemical shifts in the ^1H NMR spectra were recorded relative to Me_4Si or residual protonated solvent ($\text{C}_6\text{D}_5\text{H}$ (δ 7.16), CHCl_3 (δ 7.26), or CD_2HCN (δ 1.94)). The chemical shifts in the ^{13}C spectra were recorded relative to Me_4Si or deuterated solvent (C_6D_6 (δ 128.06), CDCl_3 (δ 77.16), or CD_3CN (δ 118.26, 1.32)). The chemical shifts in the ^{11}B NMR spectra were recorded relative to BF_3 . The chemical shifts in the ^{19}F NMR spectra were recorded relative to α,α,α -trifluorotoluene (δ 65.64). The chemical shifts in the ^{31}P NMR spectra were recorded relative to 85% H_3PO_4 as an internal standard. Assignment of the resonances in ^1H and ^{13}C NMR spectra was based on ^1H – ^1H COSY, HMQC and/or HMBC experiments if required. High resolution mass spectrometry (HRMS) was performed at the Instrumental Analytical Center, Faculty of Engineering, Osaka University. A single-crystal X-ray diffraction analysis was carried out using the Rigaku XtaLAB Synergy equipping with the HyPix-6000HE detector.

3.5.2. Materials

All commercially available reagents including super dehydrated solvents (THF and Et₂O) were employed as received. Benzene-*d*₆ was distilled from sodium benzophenone ketyl prior to use. Compound **B**¹¹ was prepared by following the reported procedure.^{S1}

Gaseous chemicals including H₂ and H₂/CO/CO₂ (a 1:1:1 molar ratio) were purchased from Sumitomo Seika Chemicals Company and used as received. Note that these gases include some impurities as shown in Table 3.S1.

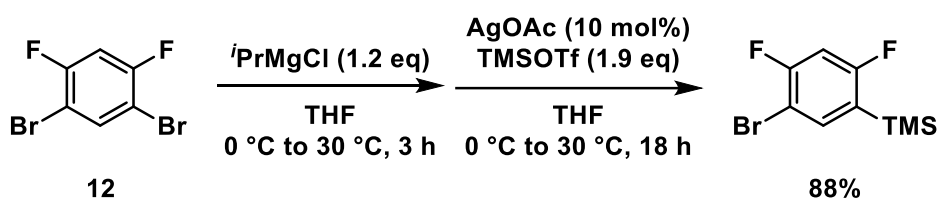
Table 3.S1. Impurities contaminated in H₂ and CO (shown in ppm).

	Impurity				
	N ₂	O ₂	CO	CO ₂	H ₂
H ₂	<200	<50	<1	<1	-
CO	<500	<100	-	<100	<100

Metrical data for the solid-state structures are available from Cambridge Crystallographic Data Centre CCDC2265357 (**B**⁵), 2265358 (CH₃CN-**B**¹⁰), 2265359 (Et₃P=O-**B**⁵).

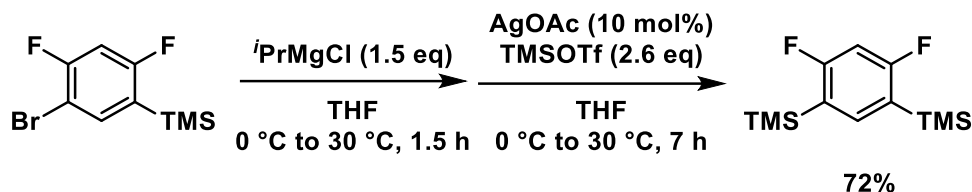
3.5.3. Synthesis of Tris(2,6-difluoro-3,5-bis(trimethylsilyl)phenyl)borane (**B**⁵)

• Synthesis of (5-bromo-2,4-difluorophenyl)trimethylsilane^{S2}



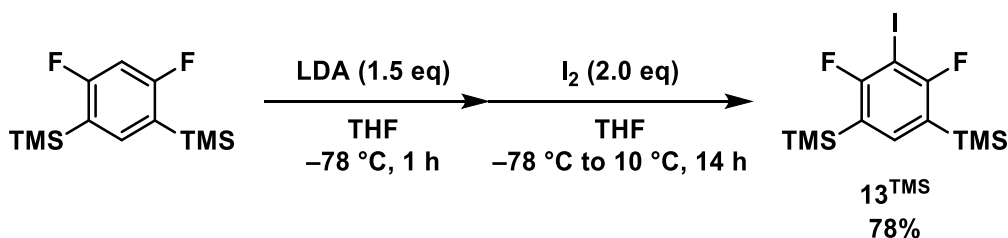
An Et₂O solution of *i*PrMgCl (1.0 M, 96.0 mL, 96.0 mmol) was slowly added to a THF solution of 1,5-dibromo-2,4-difluorobenzene (1.3 M, 21.8 g, 80.0 mmol) at 0 °C. After stirring for 3 h at 30 °C, the resultant solution was transferred to another flask where trimethylsilyl trifluoromethanesulfonate (27.3 mL, 151.3 mmol) and AgOAc (1.3 g, 8.0 mmol) were mixed in THF (280.0 mL) at 0 °C. After stirring 18 h at 30 °C, saturated NH₄Cl aq. (20.0 mL) was added to the resultant solution. The reaction mixture was concentrated *in vacuo*, then the organic layer was extracted with hexane (100.0 mL × 3), washed with water (20.0 mL × 3) and brine (20.0 mL × 3), and dried over Na₂SO₄. After filtration, the combined organic layer was concentrated *in vacuo* to afford (5-bromo-2,4-difluorophenyl)trimethylsilane as a yellow liquid (18.6 g, 70.2 mmol, 88%), which was used in the following step without further purification after dehydration over 4 Å MS. Characterization data of ¹H^{S3} and ¹⁹F^{S3} NMR analyses was consistent with literature values. ¹H NMR (400 MHz, CDCl₃): δ 7.49 (dd, ⁴J_{H,F} = 5.6 Hz, 8.4 Hz 1H, Ar-*H*), 6.82 (t, ³J_{H,F} = 8.4 Hz, 1H, Ar-*H*), 0.31 (d, *J* = 0.8 Hz, 18H, Si(CH₃)₃). ¹⁹F NMR (376 MHz, CDCl₃): δ -101.8 (m, 1F), -105.2 (dd, *J* = 8.8 Hz, 1F).

• Synthesis of (4,6-difluoro-1,3-phenylene)bis(trimethylsilane)^{S2}



An Et₂O solution of *i*PrMgCl (1.0 M, 60.0 mL, 60.0 mmol) was slowly added to a THF solution of (5-bromo-2,4-difluorophenyl)trimethylsilane (1.3 M, 10.6 g, 40.0 mmol) at 0 °C. After stirring for 1.5 h at 30 °C, the resultant solution was transferred to another flask where trimethylsilyl trifluoromethanesulfonate (19.0 mL, 105.2 mmol) and AgOAc (0.7 g, 4.0 mmol) were mixed in THF (150.0 mL) at 0 °C. After stirring 7 h at 30 °C, saturated NH₄Cl aq. (10.0 mL) was added to the resultant solution. The reaction mixture was concentrated *in vacuo*, and then the organic layer was extracted with hexane (100.0 mL × 3), washed with water (20.0 mL × 3) and brine (20.0 mL × 3), and dried over Na₂SO₄. After filtration, the combined organic layer was concentrated *in vacuo* and the residue was purified by the chromatography on a silica gel, eluted with hexane, to afford (4,6-difluoro-1,3-phenylene)bis(trimethylsilane) as a colorless liquid (7.4 g, 28.8 mmol, 72%). This product was used in the following step without further purification after dehydration over 4 Å MS. ¹H NMR (400 MHz, CDCl₃): δ 7.38 (t, ⁴J_{H,F} = 7.2 Hz, 1H, Ar-*H*), 6.66 (t, ³J_{H,F} = 9.0 Hz, 1H, Ar-*H*), 0.31 (s, 18H, Si(CH₃)₃). ¹³C{¹H} NMR (101 MHz, CDCl₃): δ 169.2 (dd, ¹J_{C,F} = 246.4 Hz, ³J_{C,F} = 12.1 Hz), 141.5 (t, ³J_{C,F} = 13.1 Hz), 121.4 (m), 102.6 (dt, *J* = 28.8 Hz, *J* = 5.1 Hz), −0.89. ¹⁹F NMR (376 MHz, CDCl₃): δ −99.8 (t, *J* = 7.5 Hz, 2F). HRMS (EI⁺): *m/z* Calcd for C₁₂H₂₀F₂Si₂ 258.1072, found 258.1075.

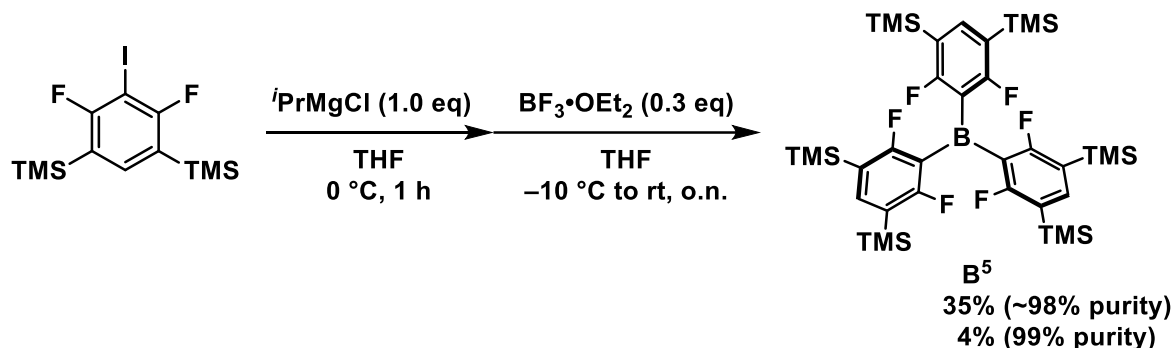
• **Synthesis of (4,6-difluoro-5-iodo-1,3-phenylene)bis(trimethylsilane) (13^{TMS})**



To a THF solution of diisopropylamine (0.3 M, 4.5 mL, 32.0 mmol) was slowly added a hexane solution of ⁿBuLi (1.2 M, 26.7 mL, 32.0 mmol) at −60 °C. After stirring at −60 °C for 1 h, the resultant solution was slowly added to a THF solution of (4,6-difluoro-1,3-phenylene)bis(trimethylsilane) (0.2 M, 5.5 g, 21.3 mmol) at −78 °C. After stirring at −78 °C for 1 h followed by addition of a THF solution of I₂ (1.1 M, 10.8 g, 42.6 mmol), the resultant mixture was allowed to warm to room temperature and then stirred for additional 14 h. After diluted with saturated Na₂S₂O₃ aq. (50.0 mL), the mixture was poured into water (100.0 mL). The organic layer was extracted with hexane (200.0 mL × 2) and Et₂O (100.0 mL × 1), washed with brine (50.0 mL × 3), and dried over Na₂SO₄. The combined organic layer was concentrated *in vacuo* and the residue was purified by the chromatography on a silica gel, eluted with hexane. After removal of all volatiles *in vacuo*, the residue was washed with EtOH to afford (4,6-difluoro-5-iodo-1,3-phenylene)bis(trimethylsilane) as a colorless crystal (6.4 g, 16.6 mmol, 78%) which was used in the next step after sublimation at 100 °C *in vacuo* (ca. 0.2 mmHg). ¹H NMR (400 MHz, C₆D₆): δ 7.36 (t, ⁴J_{H,F} = 6.8 Hz, 1H, Ar-*H*), 0.22 (s, 18H, Si(CH₃)₃). ¹³C{¹H} NMR (101 MHz, C₆D₆): δ 168.4 (dd, ¹J_{C,F} = 244.4 Hz, ³J_{C,F} = 6.1 Hz), 141.5 (t, ³J_{C,F} = 13.1 Hz), 122.5 (d, *J* =

35.4 Hz), 72.1, -1.2. ^{19}F NMR (376 MHz, C_6D_6): δ -81.7 (d, $^4J_{\text{H,F}} = 7.5$ Hz, 2F). HRMS (EI $^+$): m/z Calcd for $\text{C}_{12}\text{H}_9\text{F}_2\text{Si}_2\text{I}$ 384.0038, found 384.0043.

• Synthesis of tris(2,6-difluoro-3,5-bis(trimethylsilyl)phenyl)borane (**B**⁵)



A THF solution of (4,6-difluoro-5-iodo-1,3-phenylene)bis(trimethylsilane) (0.2 M, 3.2 g, 8.3 mmol) was slowly added to a THF solution of $i\text{PrMgCl}$ (2.0 M, 4.1 mL, 8.3 mmol) at 0 °C. The reaction mixture was stirred at 0 °C for 1 h, and then $\text{BF}_3 \cdot \text{OEt}_2$ (0.3 mL, 2.6 mmol) was added quickly at -10 °C. After stirring at room temperature overnight, the reaction mixture was concentrated *in vacuo*. The residue was extracted with hexane through a Celite pad and the extracted hexane solution was concentrated *in vacuo*. Recrystallization at 15–20 °C from a saturated hot hexane to afford **B**⁵ of 95–98% purity as a colorless crystal (717.8 mg, 0.92 mmol, 35%). Analytically pure **B**⁵ was obtained by repeating the recrystallization in 4% yield, when another reaction was carried out by following the aforementioned procedure using (4,6-difluoro-5-iodo-1,3-phenylene)bis(trimethylsilane) (1.0 mmol). The crystal obtained by these recrystallization processes was suitable for the SC-XRD analysis. ^1H NMR (400 MHz, C_6D_6): δ 7.78 (t, $^4J_{\text{H,F}} = 7.0$ Hz, 3H, Ar-*H*), 0.26 (s, 54H, $\text{Si}(\text{CH}_3)_3$). ^{11}B NMR (128 MHz, C_6D_6): Not observed. $^{13}\text{C}\{^1\text{H}\}$ NMR (101 MHz, C_6D_6): δ 172.2 (dd, $^1J_{\text{C,F}} = 248.5$ Hz, $^3J_{\text{C,F}} = 12.1$ Hz), 146.6 (dt, $J = 15.2$ Hz, $J = 3.0$ Hz), 121.3 (m), 118.7 (t, $J = 28.3$ Hz), -1.0. ^{19}F NMR (376 MHz, C_6D_6): δ -86.7 (d, $^4J_{\text{H,F}} = 7.5$ Hz, 6F). **Crystal data** for $\text{C}_{39}\text{H}_{64}\text{BF}_6\text{Si}_6$ ($M = 826.25$): triclinic, space group $P\bar{1}$ (#2), $a = 10.5151(1)$ Å, $b = 11.0701(1)$ Å, $c = 21.2591(2)$ Å, $\alpha = 97.628(1)^\circ$, $\beta = 91.037(1)^\circ$, $\gamma = 90.654(1)^\circ$, $V = 2452.09(4)$ Å³, $Z = 2$, $T = -150$ °C, $\mu(\text{Cu K}\alpha) = 1.990$ mm⁻¹, $D_{\text{calcd}} = 1.119$ g/cm³, 32168 reflections measured ($8.058^\circ \leq 2\theta \leq 136.502^\circ$), 8960 unique ($R_{\text{int}} = 0.0304$, $R_{\text{sigma}} = 0.0226$) which were used in all calculations. The final R_I was 0.0385 ($I \geq 2\sigma(I)$) and wR_2 was 0.1021 (all data).

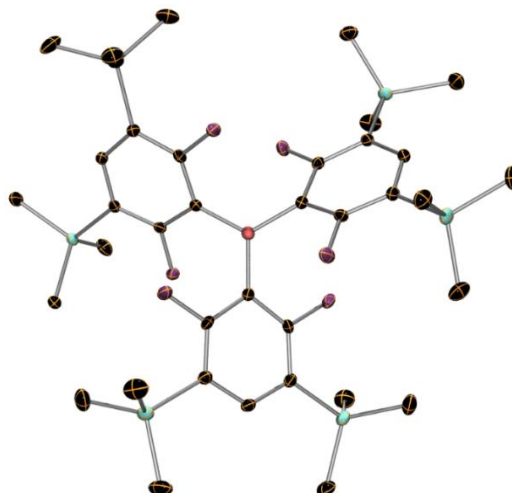
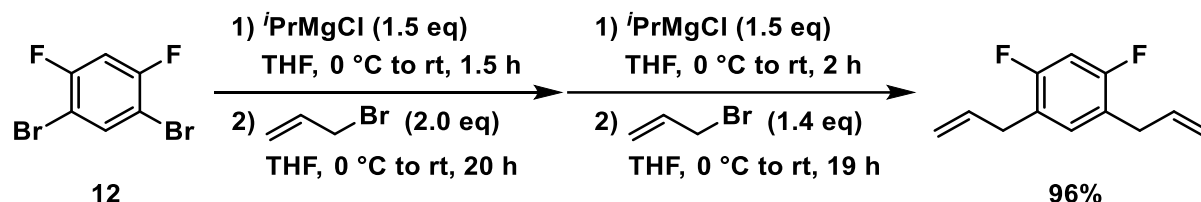


Figure 3.S1. Molecular structure of **B**⁵ with ellipsoids set at 30% probability. H atoms and solvated C₆H₁₄ are omitted for clarity.

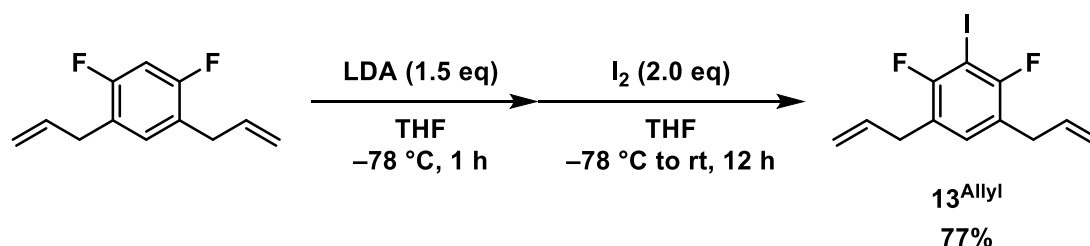
3.5.4. Synthesis of Tris(2,6-difluoro-3,5-diallyl)borane

• Synthesis of 1,5-diallyl-2,4-difluorobenzene



A THF solution of *i*PrMgCl (2.0 M, 22.5 mL, 45.0 mmol) was slowly added to a THF solution of 1,5-dibromo-2,4-difluorobenzene (0.3 M, 8.2 g, 30.0 mmol) at 0 °C. After stirring at room temperature for 1.5 h, allyl bromide (5.1 mL, 60.3 mmol) was added at 0 °C and the resultant solution was stirred for 20 h at room temperature. Subsequently, to the resultant solution, a THF solution of *i*PrMgCl (2.0 M, 22.5 mL, 45.0 mmol) was slowly added followed by stirring for 2 h. The second portion of allyl bromide (3.6 mL, 42.6 mmol) was added to the resultant solution at 0 °C and stirred at room temperature for 19 h. Then, saturated NH₄Cl aq. (15.0 mL) was added. The mixture was concentrated *in vacuo*, and then the organic layer was extracted with hexane (100.0 mL × 3), washed with water (20.0 mL × 3) and brine (20.0 mL × 3), and dried over Na₂SO₄. After removal of all volatiles *in vacuo*, 1,5-diallyl-2,4-difluorobenzene was afforded as a colorless liquid (5.6 g, 28.8 mmol, 96%). This product was used in the next step without further purification, while an analytically pure compound can be obtained by distillation at 70 °C *in vacuo* (ca. 0.2 mmHg). ¹H NMR (400 MHz, CDCl₃): δ 6.98 (t, ⁴J_{H,F} = 8.6 Hz, 1H, Ar-*H*), 6.75 (t, ³J_{H,F} = 9.6 Hz, 1H, Ar-*H*), 5.92 (m, 2H, CH₂CH=CH₂), 5.06 (m, 4H, CH₂CH=CH₂), 3.34 (d, *J* = 6.4 Hz, 4H, CH₂CH=CH₂). ¹³C{¹H} NMR (101 MHz, C₆D₆): δ 159.7 (dd, ¹J_{C,F} = 247.5 Hz, ³J_{C,F} = 12.1 Hz), 135.9, 132.1 (q, *J* = 5.7 Hz), 122.8 (m), 116.2 (m), 103.6 (m), 32.7. ¹⁹F NMR (376 MHz, CDCl₃): δ -121.1 (t, *J* = 9.4 Hz, 2F). HRMS (EI⁺): *m/z* Calcd for C₁₂H₁₂F₂ 194.0907, found 194.0902.

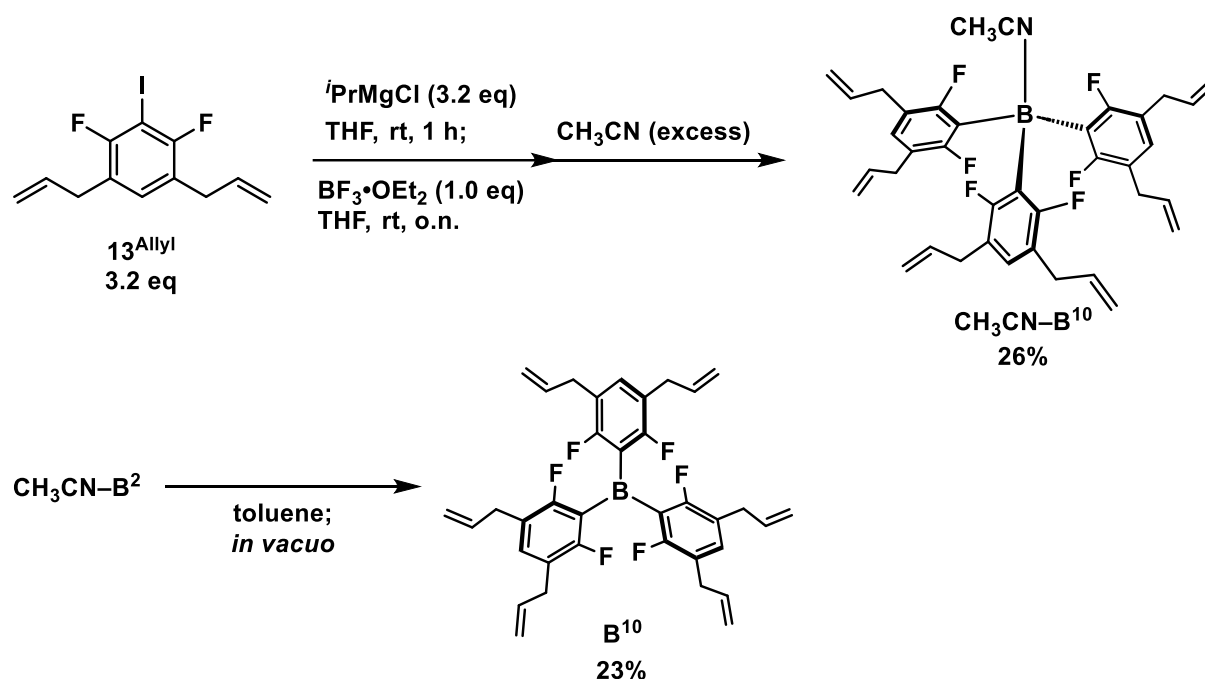
• Synthesis of 1,5-diallyl-2,4-difluoro-3-iodobenzene (**13**^{Allyl})



A THF solution of diisopropylamine (0.4 M, 6.1 mL, 43.5 mmol) was slowly added to a hexane solution of *n*BuLi (1.6 M, 27.2 mL, 43.5 mmol) at -78 °C. After stirring at -78 °C for 1 h, the resultant solution was slowly added to a THF solution of 1,5-diallyl-2,4-difluorobenzene (0.2 M, 5.6 g, 29.0 mmol) at -78 °C. After stirring at -78 °C for 1 h followed by addition of a THF solution of I₂ (0.4 M, 14.6 g, 58.0 mmol), the resultant mixture was allowed to warm to room temperature and then stirred for additional 12 h. After diluted with saturated Na₂S₂O₃ aq. (50.0 mL), the mixture was poured into water (100.0 mL) and the organic layer was extracted with hexane (100.0 mL × 2) and Et₂O (100.0 mL × 1), washed with brine (50.0 mL × 3), and dried

over Na₂SO₄. After removal of all volatiles at 95 °C *in vacuo* (ca. 0.2 mmHg), the residue was fractionally distilled at 170 °C under the identical pressure to afford 1,5-diallyl-2,4-difluoro-3-iodobenzene as a colorless liquid (7.1 g, 22.2 mmol, 77%). ¹H NMR (400 MHz, C₆D₆): δ 6.59 (t, ⁴J_{H,F} = 8.2 Hz, 1H, Ar-*H*), 5.65 (m, 2H, CH₂CH=CH₂), 4.89 (m, 4H, CH₂CH=CH₂), 3.03 (d, *J* = 6.4 Hz, 4H, CH₂CH=CH₂). ¹³C{¹H} NMR (101 MHz, C₆D₆): δ 159.3 (dd, ¹J_{C,F} = 245.4 Hz, ³J_{C,F} = 5.1 Hz), 135.4, 131.9 (q, ³J_{C,F} = 5.4 Hz), 123.5 (m), 116.6 (m), 71.6 (t, *J* = 30.3 Hz), 33.1 (t, ³J_{C,F} = 4.0 Hz). ¹⁹F NMR (376 MHz, C₆D₆): δ -102.0 (d, ⁴J_{H,F} = 7.5 Hz, 2F). HRMS (EI⁺): *m/z* Calcd for C₁₂H₁₁F₂I 319.9874, found 319.9883.

• Synthesis of tris(2,6-difluoro-3,5-diallyl)borane (**B**¹⁰)



A THF solution of 1,5-diallyl-2,4-difluoro-3-iodobenzene (0.2 M, 2.0 g, 6.3 mmol) was slowly added to a THF solution of *i*PrMgCl (2.0 M, 3.2 mL, 6.3 mmol) at room temperature. The reaction mixture was then stirred at room temperature for 1 h, and then BF₃·OEt₂ (0.3 mL, 2.0 mmol) was added quickly at room temperature. After stirring at room temperature overnight, the reaction mixture was concentrated *in vacuo*. The residue was extracted with hexane through a Celite pad and all volatiles were removed *in vacuo*, affording oily crude **B**¹⁰. Then, an enough amount of CH₃CN was added and the reaction mixture was stirred at room temperature for 15 min. Subsequently, all volatiles were completely removed *in vacuo* (note: azeotropic removal with toluene may be effective) to yield a crude mixture including a white solid of CH₃CN-**B**¹⁰. *n*-Pentane was then added to the residue followed by vigorous stirring at room temperature for 20 min, resulting into a precipitation of a white solid of CH₃CN-**B**¹⁰ that was filtered and dried *in vacuo* to afford analytically pure CH₃CN-**B**¹⁰ as a white solid. CH₃CN-**B**¹⁰ was additionally obtained by recrystallization from the filtrate solution at -30 °C, followed by washing with *n*-pentane (cooled to -30 °C prior to use), filtration, and removal of volitions *in vacuo*. Eventually, CH₃CN-**B**¹⁰ was isolated in total 26% yield (320.8 mg, 0.5 mmol). A single crystal of CH₃CN-**B**¹⁰ suitable for SC-XRD analysis was obtained by recrystallization at 15 °C from its hot hexane solution. After dissolving CH₃CN-**B**¹⁰ in toluene, removal of all volatiles *in vacuo* resulted in the isolation of **B**¹⁰ as a liquid (265.1 mg, 0.4 mmol, 23%). CH₃CN-**B**¹⁰: ¹H NMR (400 MHz, CD₃CN): δ 6.89 (t,

$^4J_{\text{H,F}} = 8.2$ Hz, 3H, Ar-*H*), 5.92 (m, 6H, $\text{CH}_2\text{CH}=\text{CH}_2$), 4.98 (m, 12H, $\text{CH}_2\text{CH}=\text{CH}_2$), 3.24 (d, $J = 6.0$ Hz, 12H, $\text{CH}_2\text{CH}=\text{CH}_2$), 1.96 (s, CH_3CN). **^{11}B NMR** (128 MHz, CD_3CN): δ -9.6. **$^{13}\text{C}\{^1\text{H}\}$ NMR** (101 MHz, CD_3CN): δ 162.8 (dd, $^1J_{\text{C,F}} = 243.4$ Hz, $^3J_{\text{C,F}} = 15.2$ Hz), 137.7, 130.5 (d, $^3J_{\text{C,F}} = 4.0$ Hz), 122.4 (m), 115.9, 33.7. Resonances of the C_{ipso} with respect to the boron atom were not observed. **^{19}F NMR** (376 MHz, CD_3CN): δ -113.9 (d, $^4J_{\text{H,F}} = 7.5$ Hz, 6F). **B^{10} : ^1H NMR** (400 MHz, C_6D_6): δ 6.93 (t, $^4J_{\text{H,F}} = 8.2$ Hz, 3H, Ar-*H*), 5.75 (m, 6H, $\text{CH}_2\text{CH}=\text{CH}_2$), 4.94 (m, 12H, $\text{CH}_2\text{CH}=\text{CH}_2$), 3.13 (d, $J = 6.4$ Hz, 12H, $\text{CH}_2\text{CH}=\text{CH}_2$). **^{11}B NMR** (128 MHz, C_6D_6): Not observed. **$^{13}\text{C}\{^1\text{H}\}$ NMR** (101 MHz, C_6D_6): δ 161.6 (dd, $^1J_{\text{C,F}} = 249.5$ Hz, $^3J_{\text{C,F}} = 11.1$ Hz), 136.3, 135.9, 122.7 (m), 116.3, 32.9. Resonances of the C_{ipso} with respect to the boron atom were not observed. **^{19}F NMR** (376 MHz, C_6D_6): δ -110.0 (d, $^4J_{\text{H,F}} = 7.5$ Hz, 6F). **Crystal data** for $2(\text{C}_{38}\text{H}_{36}\text{BF}_6\text{N})$ ($M = 1262.98$): orthorhombic, space group $P2_12_12$ (#18), $a = 38.5825(7)$ Å, $b = 20.2669(3)$ Å, $c = 8.77509(14)$ Å, $\alpha = 90^\circ$, $\beta = 90^\circ$, $\gamma = 90^\circ$, $V = 6861.6(2)$ Å³, $Z = 4$, $T = -150$ °C, $\mu(\text{Cu K}\alpha) = 0.774$ mm⁻¹, $D_{\text{calcd}} = 1.223$ g/cm³, 95439 reflections measured ($8.142^\circ \leq 2\theta \leq 136.468^\circ$), 12569 unique ($R_{\text{int}} = 0.0840$, $R_{\text{sigma}} = 0.0439$) which were used in all calculations. Solvated molecule of toluene was squeezed. The final R_1 was 0.0522 ($I \geq 2\sigma(I)$) and wR_2 was 0.1510 (all data).

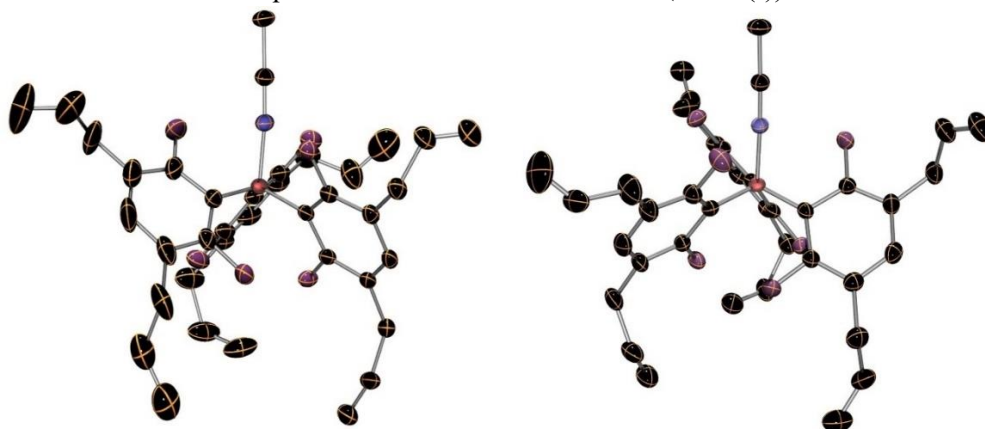


Figure 3.S2. Molecular structures of $\text{CH}_3\text{CN}-\text{B}^{10}$ with ellipsoids set at 30% probability. H atoms and disordered atoms are omitted for clarity.

3.5.5. The Reaction between B^n and $\text{Et}_3\text{P}=\text{O}$ ($n = 5, 10$, and 11)

General: A J. Young tube was charged with a CH_2Cl_2 solution of $\text{Et}_3\text{P}=\text{O}$ (0.02 M, 0.01 mmol), B^n ($n = 5, 10$, and 11) (0.03 mmol, 3.0 equiv.) and capillary with CD_2Cl_2 as an external standard. Then, measurement of the ^{31}P and ^{11}B NMR spectroscopy was conducted. Acceptor numbers (ANs) were calculated according to the literature and summarized in Table 3.S2.^{S4}

Table 3.S2. Comparison of Lewis acidity of B^n ($n = 5, 10$, and 11) based on the Gutmann-Beckett method.

B^n	B^5	B^{10}	B^{11}
δ_{P}	72.6	71.7	72.9
δ_{B}	-0.4	-0.3	-1.4
AN	70	68	70

Crystallization of $\text{Et}_3\text{P}=\text{O}-\text{B}^5$: A colorless crystal of $\text{Et}_3\text{P}=\text{O}-\text{B}^5$, suitable for SC-XRD analysis, was obtained from an Et_2O solution of B^5 (121.1 mg, 0.2 mmol) and $\text{Et}_3\text{P}=\text{O}$ (20.2 mg, 0.2 mmol) at -30 °C. **Crystal data** for $\text{C}_{42}\text{H}_{72}\text{BF}_6\text{OPSi}_6$ ($M = 917.31$): orthorhombic, $Pbcn$ (#60), $a = 26.8457(6)$ Å, $b = 22.1039(6)$ Å, $c =$

20.4822(5) Å, $\alpha = 90^\circ$, $\beta = 90^\circ$, $\gamma = 90^\circ$, $V = 12154.0(5)$ Å³, $Z = 8$, $T = -150$ °C, $\mu(\text{Cu K}\alpha) = 1.899$ mm⁻¹, $D_{\text{calcd}} = 1.003$ g/cm³, 47215 reflections measured ($6.742^\circ \leq 2\theta \leq 136.5^\circ$), 11107 unique ($R_{\text{int}} = 0.0925$, $R_{\text{sigma}} = 0.0896$) which were used in all calculations. The final R_1 was 0.0660 ($I \geq 2\sigma(I)$) and wR_2 was 0.1814 (all data).

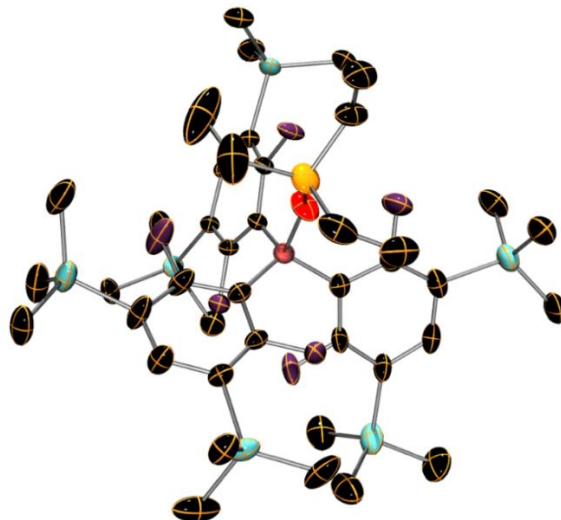
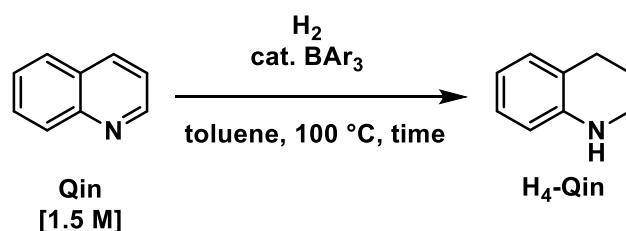


Figure 3.S3. Molecular structure of Et₃P=O–B⁵ with ellipsoids set at 30% probability. H atoms and disordered atoms are omitted for clarity.

3.5.6. Hydrogenation of quinoline (Qin)

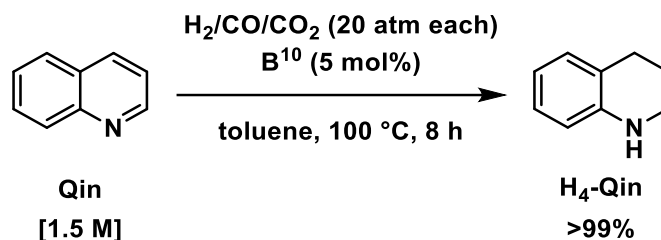
• Hydrogenation of Qin using H₂



BAr ₃	H ₂ (atm)	BAr ₃ amount (mol%)	time	yield
B ⁵	10	5	8	42%
B ¹⁰	10	5	8	>99%
B ¹⁰	20	2	24	87%
B ¹¹	10	5	8	20%
B(C ₆ F ₅) ₃	10	5	8	no reaction

General Procedure: A 30.0 mL autoclave was charged with **Qin**, **Bⁿ** ($n = 5, 10$, and 11), tetradecane (an internal standard), and toluene. Once sealed, the autoclave was pressurized with H₂ and heated 100 °C. After degassed at room temperature, the yield of **H₄-Qin** was determined by GC analysis.

• Hydrogenation of Qin using a gaseous mixture of H₂/CO/CO₂



A 30 mL autoclave was charged with **Qin** (263.2 mg, 2.0 mmol), **B¹⁰** (59.8 mg, 0.1 mmol; 5 mol%), tetradecane (142.5 mg; an internal standard), and toluene (1.3 mL). Once sealed, the autoclave was pressurized with H₂/CO/CO₂ (20 atm each) and heated 100 °C for 8 h. After degassed at room temperature, **H₄-Qin** was given in >99% in GC analysis.

3.5.7. Theoretical studies

• Computational details

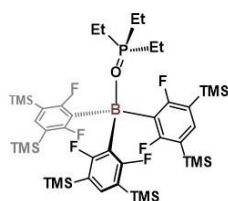
Quantum chemical calculations were performed with the ORCA 5.0.3 program package.^{S5} Gas-phase equilibrium structures have been obtained on the PBEh-3c/Def2-SVP^{S6} level of theory, which was also applied for the frequency analysis to verify that these structures have no imaginary frequency. According to the benchmarked studies for the thermochemistry of Lewis adducts in vacuum,^{S7} and my own investigation using Gaussian 16 (Revision C.01) software,^{S8} the DSD-PBEP86^{S9} double hybrid density functional with the minimally augmented ma-Def2-QZVPP^{S10} basis set with D3BJ^{S11} dispersion correction was employed for the single-point calculations. Also, the resolution-of-identity^{S12} (“RI-“) and chain of spheres “RIJCOSX” approximation with Def2/J^{S13} and Def2-QZVPP/C^{S14} auxiliary sets were applied. Implicit solvation models were adopted with the keyword of “CPCMC(CH₂Cl₂)” when required.^{S15} The reported Gibbs free energies were calculated at 298.15 K. These calculations involve a certain margin of error.

The deformation energies (*E*_{DEF}) were obtained by computing the single point energies (RI-DSD-PBEP86-D3BJ/ma-Def2-QZVPP) of triarylboranes in the structures of each LB–BAr₃ adducts, and subtraction from the energies in the relaxed states.^{S16}

The analyses on the quantum theory of the atoms in molecules were carried out using AIMAll program (Version 19.10.12),^{S17} in which the wave functional files were prepared based on the SCF densities obtained at the PBEPBE/ma-Def2-QZVPP level of theory.

• Method optimization

Geometrical parameters for the theoretically optimized gas-phase structures of Et₃P=O–**B⁵** using the Def2-SVP basis set were compared with the parameters obtained by SC-XRD analysis (Figure 3.S4). As a result, I found that the PBEh-3c functional successfully reproduce the results of SC-XRD analysis. Given the PBEh-3c/Def2-mSVP level of theory, a benchmarked theory shown by ref S16, exhibited nearly identical but slightly deviated results, I used the PBEh-3c/Def2-SVP level in this work.



	Gaussian Rev16C									ORCA v5.0.3	
	XRD	B3LYP-D3	PBE0	M06-2X	wB97X-D	B3LYP	M06L	PBE1	PBEh	PBEh-3c	PBEh-3c/def2-mSVP
O-B	1.554	1.552	1.569	1.543	1.549	1.562	1.573	1.550	1.552	1.538	1.537
P-O	1.494	1.544	1.556	1.542	1.538	1.537	1.537	1.538	1.538	1.524	1.528
B-O-P	149.74	140.33	143.39	139.31	140.87	150.81	142	145.32	144.92	147.55	145.96
B-C	1.638	1.637	1.649	1.633	1.637	1.651	1.627	1.642	1.641	1.639	1.632
B-C	1.638	1.637	1.649	1.633	1.638	1.65	1.622	1.642	1.641	1.637	1.632
B-C	1.64	1.638	1.649	1.64	1.64	1.652	1.634	1.644	1.643	1.64	1.633
O-B-C	104.25	105.18	104.32	104.79	105.28	104.4	102.76	104.66	104.63	105.49	105.56
O-B-C	107.15	110.61	110.15	110.11	110.26	109.45	109.45	109.87	109.85	109.91	109.1
O-B-C	107.51	105.13	105.09	105.15	104.8	105.02	104.05	105.16	105.16	104.88	104.76
C-B-C	105.16	103.76	104.59	105.78	104.84	105.87	108.27	105.04	105.09	105.65	106.96
C-B-C	116.05	115.62	115.77	115.19	115.4	115.05	115.21	115.42	115.45	114.32	114.13
C-B-C	116.15	116.11	116.33	115.32	115.85	116.44	116.05	116.15	116.11	116.22	115.83
O-P-C	106.35	106.32	106	106.85	106.38	106.92	106.67	106.52	106.55	107.57	107.17
O-P-C	111.1	109.81	110.36	109.33	109.98	110.7	110.44	110.38	110.31	111.04	111.25
O-P-C	113.5	115.84	116.26	115.78	115.66	114.47	115.48	115.25	115.28	114.91	115.8
C-P-C	106.65	109.58	109.79	109.6	109.64	109.99	109.1	109.86	109.87	108.66	108.32
C-P-C	108.52	108.85	108.4	108.37	108.73	108.63	107.78	108.51	106.2	106.76	106.57
C-P-C	110.59	106.32	105.85	106.74	106.33	106.03	107.15	106.2	108.5	107.66	107.43

Selected bond lengths in Å and angles in ° for $\text{Et}_3\text{P}=\text{O}-\text{B}^n$ ($n = 5, 10$, and 11)

Figure 3.S4. Results of the calculation method optimization.

• Conformer exploration on $\text{LB}-\text{B}^n$ complexes

I conducted a conformer searching for $\text{LB}-\text{B}^{10}$ adducts at the PBE0/Def2-SVP, gas-phase level using Gaussian 16 (Revision C.01) otherwise noted. When the certain conformers were found to be energetically identical at the PBE0/Def2-SVP, I further computed their energies at the PBEh-3c/Def2-SVP level and used the conformers with the smallest Gibbs energies for discussions.

In the case of $\text{Et}_3\text{P}=\text{O}-\text{B}^5$, I found an energetically nearly identical conformer having B-O-P angle of 175.7° as shown in Figure 3.S5, albeit the optimized structure has the corresponding angle of 147.6° (as reproduced from the SC-XRD result). I concluded the latter is optimal based on the calculation at the RI-DSD-PBEP86-D3BJ/ma-Def2-QZVPP//PBEh-3c/Def2-SVP, CPCMC(CH_2Cl_2) level of theory.

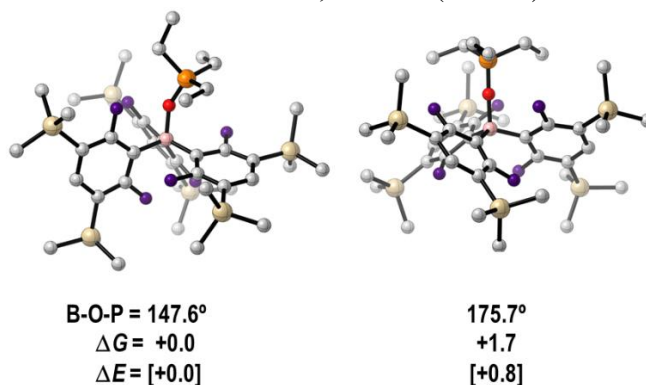
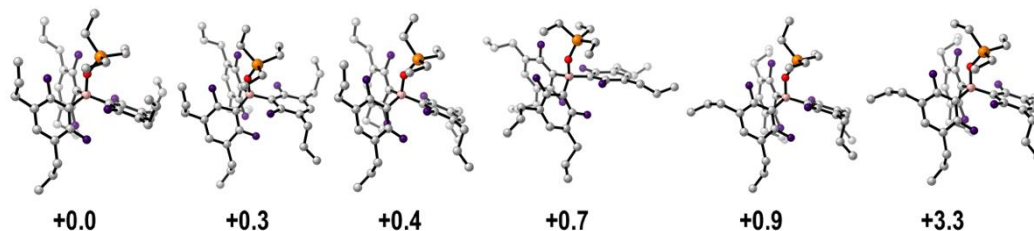


Figure 3.S5. Selected conformers found for $\text{Et}_3\text{P}=\text{O}-\text{B}^5$.

In the cases using B^{10} , several conformers were found in all $\text{LB}-\text{B}^{10}$ adducts, as exemplified in Figure 3.S6.

(A) $\text{LB} = \text{Et}_3\text{P}=\text{O}$



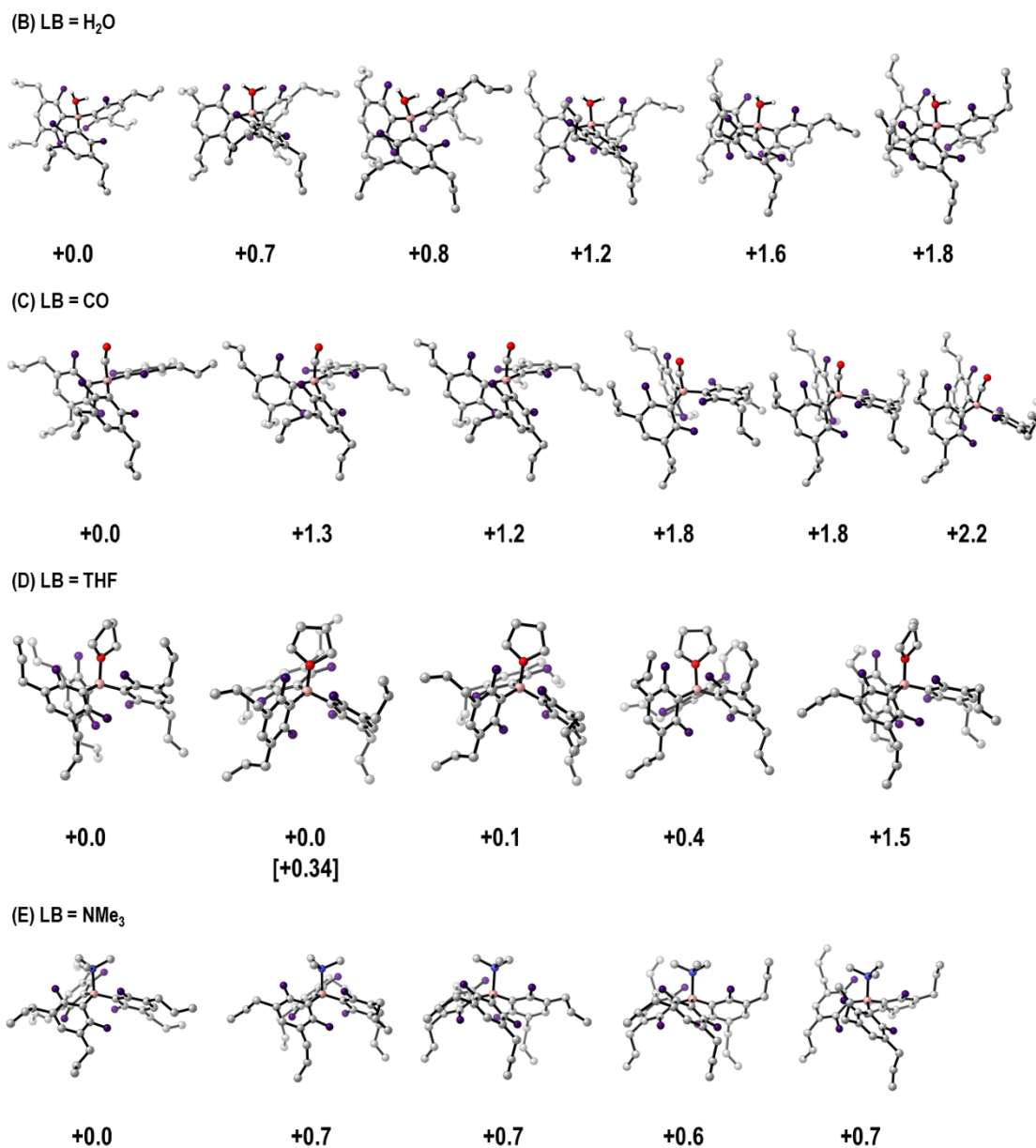
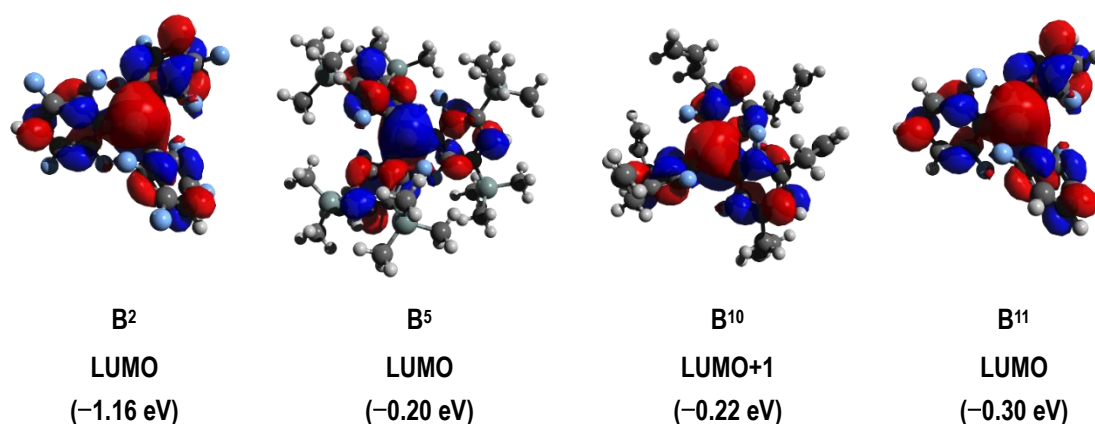


Figure 3.S6. Selected conformers found for LB-B¹⁰. A result computed at the PBEh-3c/Def2-SVP level is shown in a square bracket.

• Selected frontier molecular orbitals

Selected frontier molecular orbitals including the p orbitals of the boron, calculated at the RI-DSD-PBEP86-D3BJ/ma-Def2-QZVPP//PBEh-3c/Def2-SVP level, are shown in Table 3.S3.

Table 3.S3. LUMO(+1) of B², B⁵, B¹⁰, and B¹¹



• **Comparison of the percent buried volume (% V_{Bur}) and structural parameters around the boron centers**

The steric size of TMS and allyl groups were compared using 2,6-F₂-3,5-R₂-BH₂ (R = TMS or allyl) as model substrates, based on their values of % V_{Bur} that were calculated using the program SambVca 2.1.^{S18} In the case of R = allyl, several conformers were confirmed, and % V_{Bur} were calculated for each of them. The final % V_{Bur} for R = allyl was determined by taking the Boltzmann distribution into the account, as shown in Figure 3.S7.

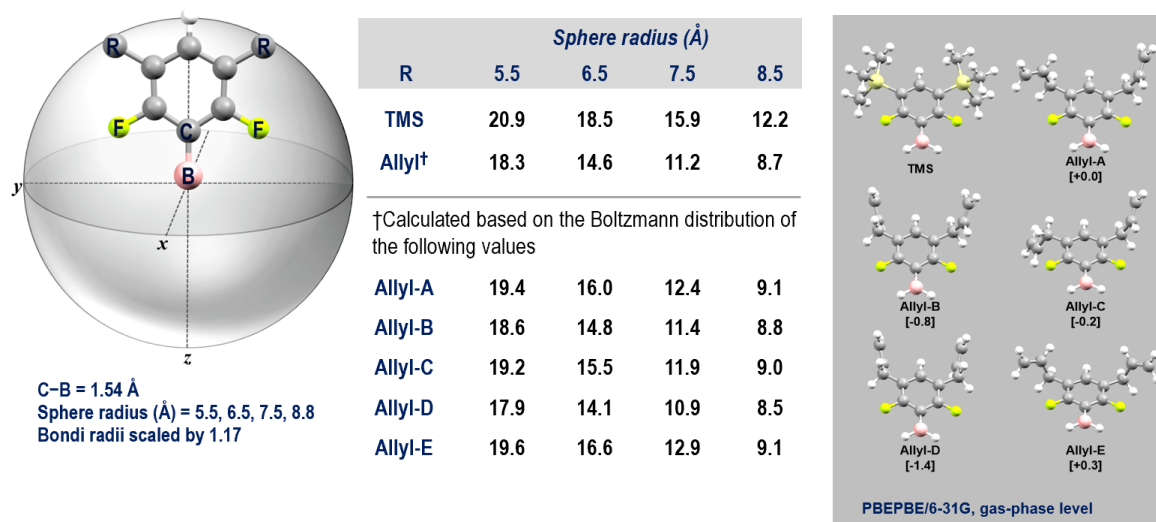


Figure 3.S7. Values of % V_{Bur} calculated for 2,6-F₂-3,5-R₂-BH₂ (R = TMS or allyl).

As shown in Figure 3.S8, I also compared the structural parameters around the boron centers between **Bⁿ** and Et₃P=O-**Bⁿ** ($n = 5, 10, \text{ and } 11$), which clarified a negligible buttressing effect under the present conditions.

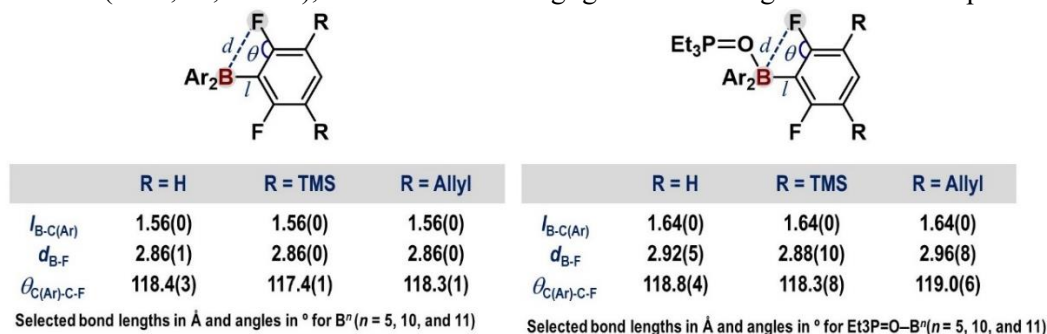


Figure 3.S8. Selected structural parameters around the boron centers in **Bⁿ** and Et₃P=O-**Bⁿ** ($n = 5, 10, \text{ and } 11$).

• **Comparison of geometrical parameters and energies among LB-Bⁿ adducts (*n* = 2–5, 10, and 11)**

From the optimized geometrical parameters, I obtained the following two indices for the evaluation of the degree of geometrical deviation from the ideal tetrahedral geometry around the boron center: (i) $\tau_8(\text{B}) = \{360 - (\alpha + \beta)/141 \times \beta/\alpha\}$, where α and β are the largest and second largest C–B–C angles;^{S19} (ii) a tetrahedral character (THC),^{S20} calculated by the following equation ($\theta = \text{X–B–C}$, X = O or C; $n = 1 - 6$):

$$\text{THC} = \left[1 - \frac{\sum_{n=1-6} |109.5 - \theta_n|}{27} \right] \times 100$$

When the boron center adopts ideal tetrahedral geometry, both $\tau_8(\text{B})$ and THC provide each 1.0 and 100 as their maximum, and smaller values thus suggest that the boron atom adopts more distorted tetrahedral geometry. Results for THF-Bⁿ adducts (*n* = 2–4) are summarized in Figure 3.S9. Results for Et₃P=O (Figure 3.S10), H₂O (Figure 3.S11), CO (Figure 3.S12), THF (Figure 3.S13), and NMe₃ (Figure 3.S14) are summarized below.

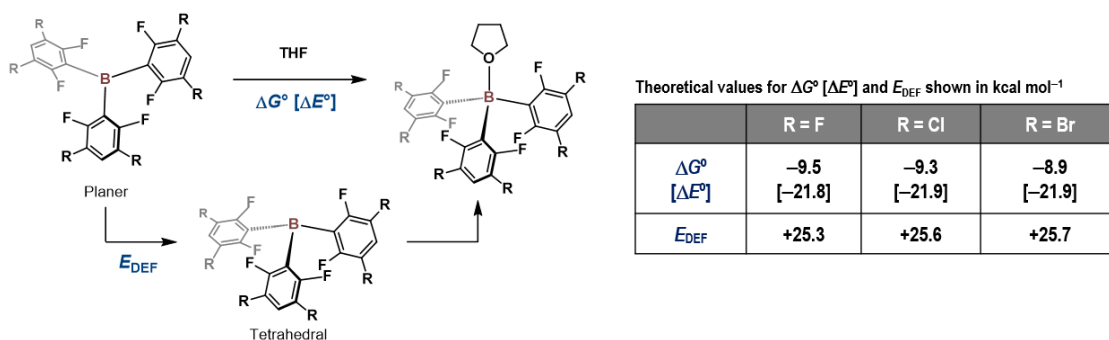


Figure 3.S9. Selected and energies for THF-Bⁿ (*n* = 2–4).

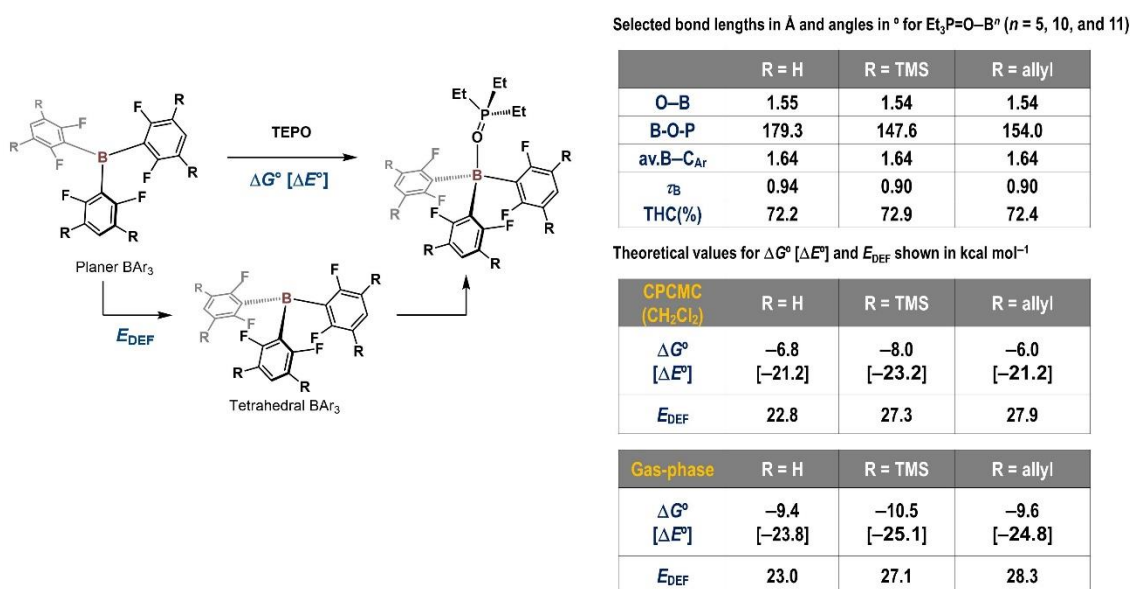
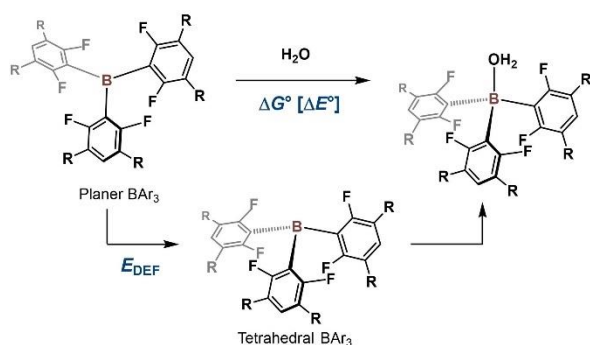


Figure 3.S10. Selected geometrical parameters and energies for Et₃P=O-Bⁿ (*n* = 5, 10, and 11).



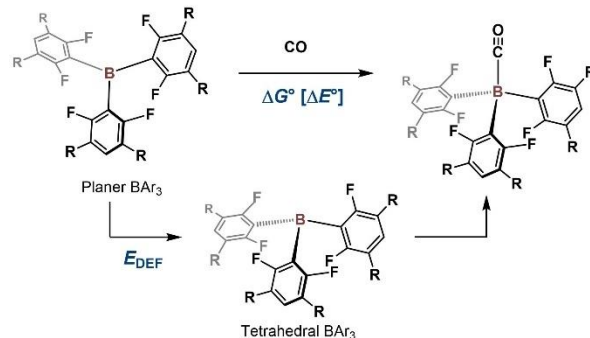
Selected bond lengths in Å and angles in ° for $\text{H}_2\text{O}-\text{B}^n$ ($n = 5, 10$, and 11)

	R = H	R = TMS	R = allyl
O–B	1.65	1.66	1.65
av.B–C _{Ar}	1.62	1.62	1.62
τ_{B}	0.91	0.90	0.91
THC(%)	62.1	60.6	61.1

Theoretical values for ΔG° [ΔE°] and E_{DEF} shown in kcal mol^{−1}

	R = H	R = TMS	R = allyl
ΔG° [ΔE°]	−0.2 [−11.7]	+1.2 [−10.2]	+1.7 [−8.6]
E_{DEF}	17.1	17.3	19.4

Figure 3.S11. Selected geometrical parameters and energies for $\text{H}_2\text{O}-\text{B}^n$ ($n = 5, 10$, and 11).



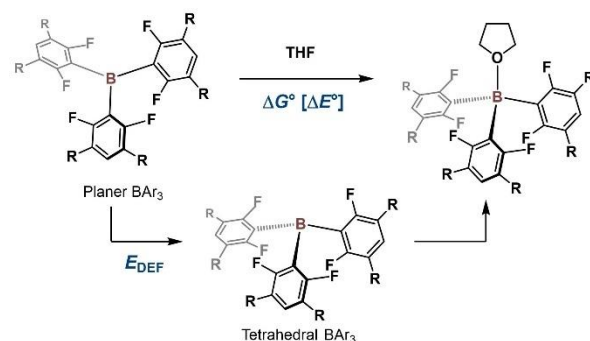
Selected bond lengths in Å and angles in ° for $\text{OC}-\text{B}^n$ ($n = 5, 10$, and 11)

	R = H	R = TMS	R = allyl
O–B	1.63	1.62	1.63
av.B–C _{Ar}	1.63	1.63	1.63
τ_{B}	0.90	0.88	0.92
THC(%)	59.5	63.0	60.4

Theoretical values for ΔG° [ΔE°] and E_{DEF} shown in kcal mol^{−1}

	R = H	R = TMS	R = allyl
ΔG° [ΔE°]	+2.6 [−8.4]	+3.0 [−8.1]	+3.8 [−5.9]
E_{DEF}	15.9	17.7	18.3

Figure 3.S12. Selected geometrical parameters and energies for $\text{OC}-\text{B}^n$ ($n = 5, 10$, and 11).



Selected bond lengths in Å and angles in ° for $\text{THF}-\text{B}^n$ ($n = 5, 10$, and 11)

	R = H	R = TMS	R = allyl
O–B	1.65	1.63	1.64
av.B–C _{Ar}	1.63	1.63	1.63
τ_{B}	0.90	0.90	0.90
THC(%)	68.8	67.7	68.4

Theoretical values for ΔG° [ΔE°] and E_{DEF} shown in kcal mol^{−1}

	R = H	R = TMS	R = allyl
ΔG° [ΔE°]	−4.9 [−17.0]	−4.2 [−17.5]	−3.8 [−16.5]
E_{DEF}	24.0	24.4	26.1

Figure 3.S13. Selected geometrical parameters and energies for $\text{THF}-\text{B}^n$ ($n = 5, 10$, and 11).

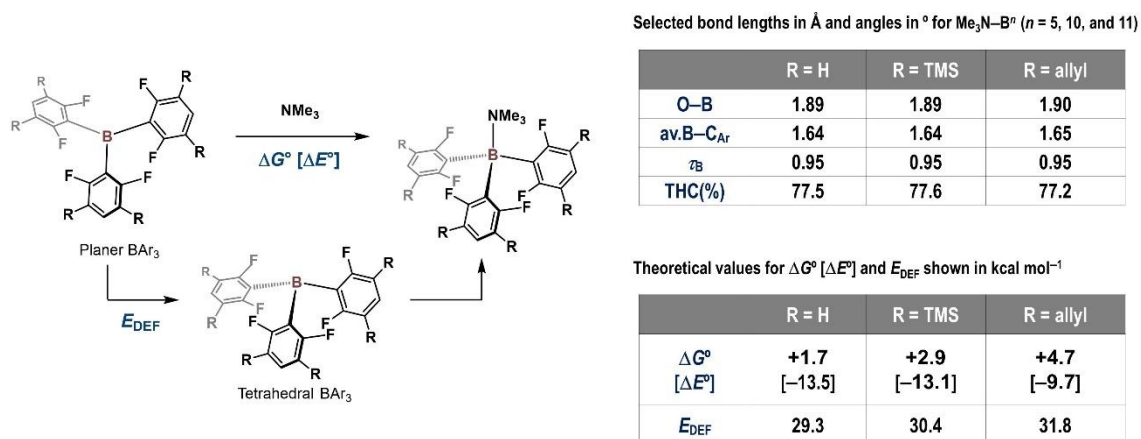


Figure 3.S14. Selected geometrical parameters and energies for $\text{Me}_3\text{N}-\text{B}^n$ ($n = 5, 10, \text{ and } 11$).

• AIM analysis

Selected NCIs confirmed by the AIM analysis for $\text{Et}_3\text{P}=\text{O}-\text{B}^n$ are shown in Figures 3.S15–17, clearly showing the participation of NCIs between *ortho*-F atoms and $\text{Et}_3\text{P}=\text{O}$ moieties in all cases ($n = 5, 10, \text{ and } 11$). On the other hand, NCIs are confirmed between $\text{Et}_3\text{P}=\text{O}$ moieties and *meta*-TMS ($n = 5$) or *meta*-allyl ($n = 10$) groups. Moreover, in the case of B^5 , NCIs are also confirmed between TMS groups.

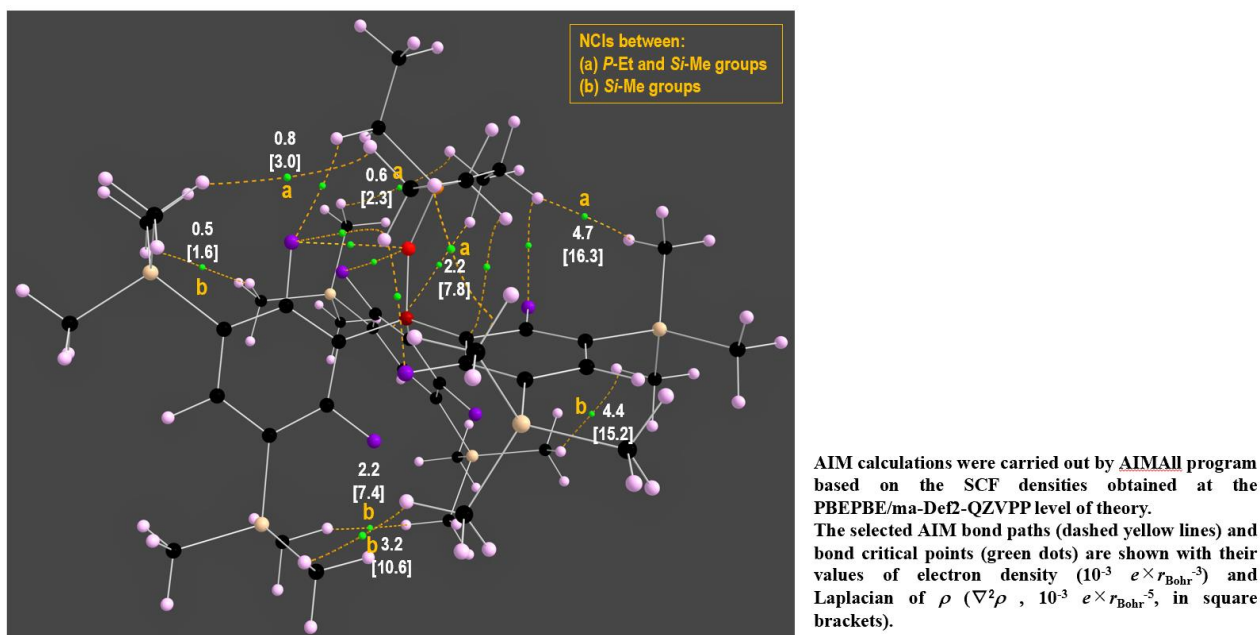
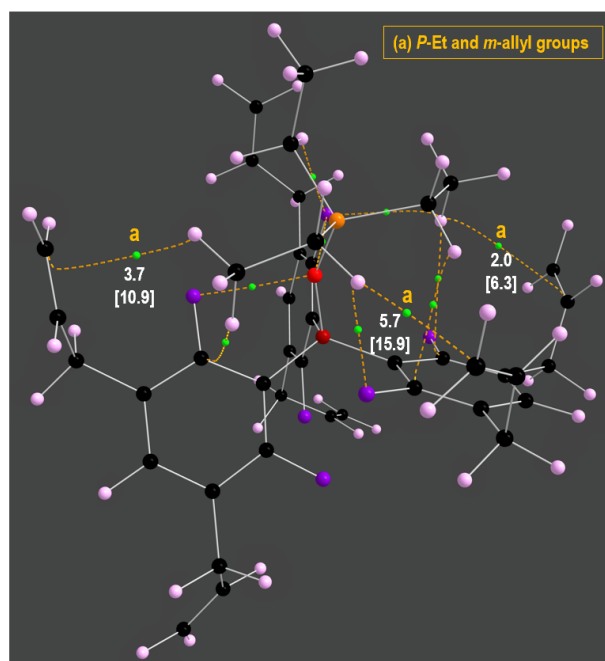
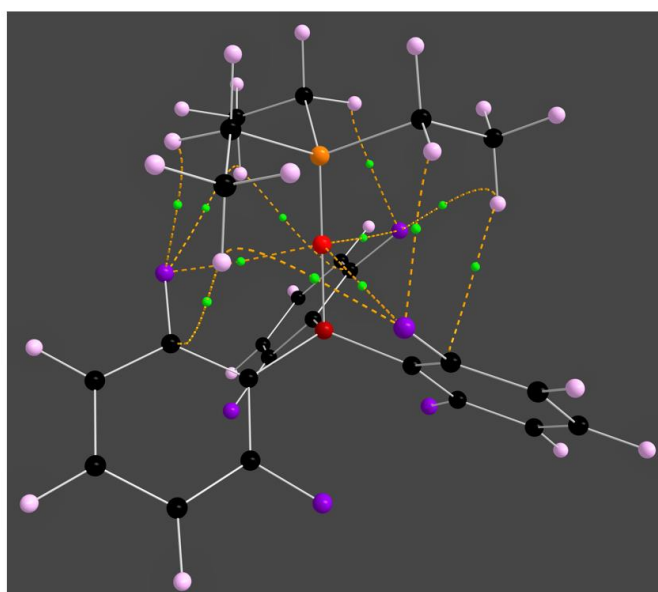


Figure 3.S15. Selected NCIs found in $\text{Et}_3\text{P}=\text{O}-\text{B}^5$.



AIM calculations were carried out by AIMAll program based on the SCF densities obtained at the PBE/PBE/ma-Def2-QZVPP level of theory. The selected AIM bond paths (dashed yellow lines) and bond critical points (green dots) are shown with their values of electron density ($10^{-3} e \times r_{\text{Bohr}}^{-3}$) and Laplacian of ρ ($\nabla^2 \rho$, $10^{-3} e \times r_{\text{Bohr}}^{-5}$, in square brackets).

Figure 3.S16. Selected NCIs found in $\text{Et}_3\text{P}=\text{O}-\mathbf{B}^{10}$.



AIM calculations were carried out by AIMAll program based on the SCF densities obtained at the PBE/PBE/ma-Def2-QZVPP level of theory. The selected AIM bond paths (dashed yellow lines) and bond critical points (green dots) are shown.

Figure 3.S17. Selected NCIs found in $\text{Et}_3\text{P}=\text{O}-\mathbf{B}^{11}$.

Table 3.S4. Summary of AIM parameters for $\text{Et}_3\text{P}=\text{O}-\mathbf{B}^5$

BCP #	Name	Atoms	Rho	DelSqRho	G	V	DI(A/B)
1	BCP1	F5 - F6	0.007599	0.042653	0.008368	-0.006072	0.030875
2	BCP2	C11 - C30	0.32187	-0.965735	0.118839	-0.479111	1.335723
3	BCP3	P1 - O8	0.215388	1.052477	0.437984	-0.612849	0.661326
4	BCP4	O8 - F9	0.013223	0.070757	0.014431	-0.011174	0.056078
5	BCP5	C35 - C46	0.243213	-0.597679	0.062487	-0.274394	1.027293
6	BCP6	H37 - H100	0.004679	0.01632	0.003119	-0.002158	0.0098

7	BCP7	F4 - C10	0.267513	0.069779	0.4443	-0.871156	0.760392
8	BCP8	F4 - H37	0.00838	0.036231	0.007267	-0.005476	0.024966
9	BCP9	F6 - C12	0.011184	0.048328	0.009922	-0.007762	0.033646
10	BCP10	C12 - C14	0.320007	-0.958409	0.116401	-0.472405	1.321564
11	BCP11	C13 - C19	0.3244	-0.984975	0.118952	-0.484149	1.345839
12	BCP12	Si3 - C57	0.1219	0.173959	0.12268	-0.201871	0.437668
13	BCP13	F7 - C11	0.01389	0.058128	0.012354	-0.010176	0.050352
14	BCP14	P1 - C35	0.181376	-0.302218	0.114713	-0.304981	0.660567
15	BCP15	C12 - B124	0.157971	-0.180416	0.122452	-0.290007	0.411207
16	BCP16	C35 - H37	0.280088	-1.054313	0.046666	-0.356909	0.931232
17	BCP17	C10 - C12	0.319791	-0.95826	0.116573	-0.472711	1.3044
18	BCP18	F5 - C13	0.271437	0.079375	0.45515	-0.890457	0.765289
19	BCP19	Si3 - C65	0.123155	0.171222	0.123505	-0.204204	0.448467
20	BCP20	C11 - B124	0.159969	-0.19818	0.121269	-0.292082	0.414196
21	BCP21	C11 - C13	0.320403	-0.961791	0.114899	-0.470245	1.295306
22	BCP22	Si3 - C73	0.123007	0.17154	0.123409	-0.203932	0.445833
23	BCP23	H76 - H92	0.003172	0.010642	0.001958	-0.001255	0.009465
24	BCP24	F7 - C14	0.272506	0.066975	0.454632	-0.892521	0.768571
25	BCP25	C65 - H67	0.274324	-1.005877	0.051048	-0.353566	0.986805
26	BCP26	H45 - H67	0.002207	0.00736	0.001323	-0.000806	0.007217
27	BCP27	F6 - C15	0.272693	0.071751	0.45617	-0.894401	0.765484
28	BCP28	C16 - B124	0.159849	-0.203819	0.119947	-0.290849	0.412288
29	BCP29	C16 - C20	0.318935	-0.95154	0.115871	-0.469627	1.317066
30	BCP30	C15 - C23	0.32105	-0.967064	0.115671	-0.473107	1.330406
31	BCP31	C46 - H48	0.283471	-1.085057	0.044243	-0.359749	0.934178
32	BCP32	C15 - C16	0.32009	-0.959453	0.115292	-0.470446	1.314938
33	BCP33	C24 - C30	0.320254	-0.962405	0.115489	-0.471579	1.328199
34	BCP34	C21 - C24	0.314364	-0.921875	0.111365	-0.453199	1.408302
35	BCP35	O8 - F17	0.013011	0.065465	0.013527	-0.010688	0.056831
36	BCP36	C21 - H22	0.288492	-1.12723	0.04297	-0.367748	0.928459
37	BCP37	C10 - C18	0.322987	-0.977075	0.117867	-0.480002	1.340056
38	BCP38	Si3 - C19	0.120154	0.194212	0.124465	-0.200377	0.421386
39	BCP39	C57 - H60	0.272657	-0.990776	0.052416	-0.352526	0.99904
40	BCP40	O8 - B124	0.117893	0.566996	0.220381	-0.299014	0.26884
41	BCP41	F9 - C20	0.26935	0.072267	0.448966	-0.879865	0.766326
42	BCP42	C19 - C21	0.31293	-0.916049	0.109916	-0.448844	1.390634
43	BCP43	Si2 - C23	0.120192	0.19219	0.12414	-0.200232	0.423311
44	BCP44	P1 - C32	0.181017	-0.30049	0.114626	-0.304375	0.656937

45	BCP45	C23 - C28	0.313878	-0.919961	0.110819	-0.451628	1.403488
46	BCP46	C20 - C25	0.322279	-0.973597	0.116969	-0.477338	1.33712
47	BCP47	C14 - C31	0.320787	-0.966718	0.115026	-0.471731	1.323878
48	BCP48	C18 - C26	0.312377	-0.913062	0.1095	-0.447265	1.38956
49	BCP49	C26 - C31	0.314843	-0.9254	0.111398	-0.454146	1.407181
50	BCP50	C26 - H27	0.288863	-1.131019	0.042508	-0.367772	0.9262
51	BCP51	C25 - C28	0.313377	-0.917835	0.110351	-0.450161	1.397724
52	BCP52	C28 - H29	0.288455	-1.127214	0.042838	-0.367479	0.927993
53	BCP53	F17 - C30	0.263791	0.082742	0.439104	-0.857522	0.757513
54	BCP54	C90 - H91	0.272979	-0.99437	0.051899	-0.352391	0.999553
55	BCP55	F17 - H34	0.008571	0.039805	0.007891	-0.00583	0.027924
56	BCP56	C32 - H33	0.277749	-1.035703	0.047173	-0.353273	0.949424
57	BCP57	C24 - Si119	0.120968	0.193414	0.125212	-0.202071	0.425757
58	BCP58	C32 - H34	0.280653	-1.058856	0.046589	-0.357891	0.935921
59	BCP59	C35 - H36	0.276062	-1.016944	0.049538	-0.353312	0.95633
60	BCP60	C73 - H75	0.271985	-0.985137	0.052799	-0.351881	1.00452
61	BCP61	C32 - C38	0.244295	-0.602822	0.06204	-0.274785	1.033233
62	BCP62	C77 - Si119	0.122361	0.174514	0.123283	-0.202939	0.438902
63	BCP63	C38 - H39	0.281124	-1.061681	0.04698	-0.35938	0.952894
64	BCP64	C38 - H40	0.280375	-1.052684	0.047787	-0.358745	0.950636
65	BCP65	F17 - H72	0.003865	0.016814	0.003129	-0.002054	0.010991
66	BCP66	C38 - H41	0.279897	-1.049488	0.047733	-0.357837	0.951072
67	BCP67	Si2 - C42	0.122984	0.170996	0.123296	-0.203844	0.445363
68	BCP68	C42 - H43	0.274259	-1.005063	0.051281	-0.353828	0.992238
69	BCP69	C42 - H44	0.272007	-0.985399	0.052781	-0.351912	1.004993
70	BCP70	C42 - H45	0.272806	-0.992394	0.052159	-0.352416	0.997425
71	BCP71	C16 - H48	0.002878	0.009345	0.001729	-0.001122	0.006227
72	BCP72	C46 - H47	0.279653	-1.047482	0.047961	-0.357793	0.952996
73	BCP73	C46 - H49	0.280687	-1.057653	0.047487	-0.359387	0.955038
74	BCP74	P1 - C50	0.180707	-0.306678	0.112482	-0.301633	0.670383
75	BCP75	C12 - H51	0.007843	0.024777	0.00503	-0.003866	0.015076
76	BCP76	F7 - H72	0.005568	0.023831	0.004638	-0.003318	0.019801
77	BCP77	C50 - H51	0.278645	-1.047869	0.045654	-0.353275	0.932701
78	BCP78	C50 - H52	0.275396	-1.012351	0.049548	-0.352184	0.957511
79	BCP79	Si2 - C53	0.121853	0.173735	0.12259	-0.201746	0.437122
80	BCP80	C53 - H54	0.27273	-0.99122	0.052413	-0.35263	0.99774
81	BCP81	C53 - H55	0.272249	-0.986823	0.052857	-0.35242	1.001883
82	BCP82	C53 - H56	0.272588	-0.990229	0.052455	-0.352468	0.999684

83	BCP83	C57 - H58	0.272606	-0.990174	0.052473	-0.352489	0.998738
84	BCP84	C57 - H59	0.272229	-0.986882	0.052785	-0.35229	1.002117
85	BCP85	Si2 - C61	0.122885	0.171544	0.123257	-0.203629	0.446366
86	BCP86	C61 - H62	0.272587	-0.990276	0.052512	-0.352592	1.001381
87	BCP87	C61 - H63	0.271998	-0.984884	0.052901	-0.352023	1.004458
88	BCP88	H64 - H103	0.004412	0.015181	0.002846	-0.001897	0.009261
89	BCP89	C61 - H64	0.274986	-1.009591	0.051407	-0.355211	0.982425
90	BCP90	C65 - H66	0.272042	-0.985653	0.052746	-0.351905	1.005083
91	BCP91	C65 - H68	0.272802	-0.992022	0.052299	-0.352604	1.003428
92	BCP92	H70 - H122	0.000846	0.00296	0.000512	-0.000285	0.002674
93	BCP93	C50 - C69	0.243863	-0.601806	0.062589	-0.27563	1.028761
94	BCP94	C69 - H70	0.279988	-1.050007	0.047978	-0.358459	0.950693
95	BCP95	C69 - H71	0.280928	-1.059588	0.047239	-0.359375	0.948157
96	BCP96	C69 - H72	0.284343	-1.089509	0.044965	-0.362308	0.928942
97	BCP97	C73 - H74	0.274686	-1.008306	0.051218	-0.354512	0.989162
98	BCP98	C73 - H76	0.272662	-0.99062	0.052466	-0.352587	0.996497
99	BCP99	C77 - H78	0.272945	-0.993359	0.052214	-0.352767	0.997845
100	BCP100	C77 - H79	0.272194	-0.986408	0.052866	-0.352333	1.001894
101	BCP101	C77 - H80	0.272784	-0.991923	0.052314	-0.35261	0.998185
102	BCP102	C81 - H82	0.272916	-0.993582	0.051916	-0.352227	1.000166
103	BCP103	C81 - Si119	0.122532	0.170362	0.122657	-0.202724	0.444957
104	BCP104	C81 - H83	0.273938	-1.000984	0.051971	-0.354188	0.996383
105	BCP105	C81 - H84	0.272076	-0.985628	0.05278	-0.351968	1.0048
106	BCP106	C18 - Si85	0.120003	0.193521	0.124192	-0.200005	0.421261
107	BCP107	C86 - Si125	0.122158	0.173732	0.122915	-0.202396	0.438509
108	BCP108	C86 - H87	0.27235	-0.98816	0.05261	-0.352259	1.001116
109	BCP109	C86 - H88	0.272494	-0.989268	0.052564	-0.352445	0.998953
110	BCP110	C86 - H89	0.27289	-0.992825	0.052238	-0.352683	0.997881
111	BCP111	C90 - Si125	0.123814	0.170886	0.124148	-0.205574	0.450462
112	BCP112	C90 - H92	0.275031	-1.011274	0.050977	-0.354772	0.983318
113	BCP113	C90 - H93	0.272056	-0.985717	0.052769	-0.351968	1.004231
114	BCP114	Si85 - C94	0.122495	0.174546	0.12343	-0.203223	0.44015
115	BCP115	C94 - H95	0.272435	-0.988784	0.052622	-0.35244	1.000926
116	BCP116	C94 - H96	0.272883	-0.9929	0.052173	-0.352571	0.996504
117	BCP117	C94 - H97	0.272628	-0.990577	0.05245	-0.352544	0.999194
118	BCP118	Si85 - C98	0.121662	0.170817	0.121803	-0.200902	0.440546
119	BCP119	C98 - H99	0.272236	-0.986817	0.052912	-0.352527	1.002293
120	BCP120	C98 - H100	0.273617	-0.997921	0.052273	-0.354026	0.990592

121	BCP121	Si85 - C102	0.124081	0.172476	0.124762	-0.206406	0.450467
122	BCP122	C98 - H101	0.272508	-0.989789	0.052368	-0.352184	1.001352
123	BCP123	C102 - H103	0.27474	-1.009039	0.051021	-0.354301	0.98255
124	BCP124	C102 - H104	0.273117	-0.995393	0.051961	-0.35277	0.997129
125	BCP125	C102 - H105	0.27212	-0.986729	0.052602	-0.351886	1.004225
126	BCP126	H47 - H110	0.00063	0.002259	0.000386	-0.000207	0.001689
127	BCP127	C25 - Si106	0.120625	0.193087	0.12477	-0.201269	0.424358
128	BCP128	Si106 - C107	0.121981	0.170542	0.1221	-0.201564	0.441474
129	BCP129	C107 - H108	0.272214	-0.986747	0.052699	-0.352085	1.004136
130	BCP130	C107 - H109	0.272659	-0.990608	0.052444	-0.352539	1.00356
131	BCP131	C115 - H116	0.271926	-0.984491	0.052822	-0.351766	1.005151
132	BCP132	C107 - H110	0.273798	-0.999495	0.052133	-0.354139	0.995747
133	BCP133	Si106 - C111	0.122171	0.174308	0.123039	-0.202501	0.438127
134	BCP134	C111 - H112	0.272749	-0.991575	0.052327	-0.352547	0.997724
135	BCP135	C111 - H113	0.272668	-0.990939	0.052374	-0.352483	0.998905
136	BCP136	C111 - H114	0.272327	-0.987599	0.052809	-0.352518	1.002256
137	BCP137	Si106 - C115	0.123049	0.170656	0.123291	-0.203918	0.446917
138	BCP138	H82 - H117	0.000476	0.001559	0.000264	-0.000139	0.002061
139	BCP139	C115 - H117	0.274388	-1.005825	0.051308	-0.354072	0.992489
140	BCP140	C115 - H118	0.272973	-0.993688	0.05209	-0.352603	1.002324
141	BCP141	Si119 - C120	0.122073	0.171095	0.122309	-0.201843	0.442161
142	BCP142	C120 - H121	0.272849	-0.992385	0.052168	-0.352433	1.002088
143	BCP143	C120 - H122	0.273697	-0.997917	0.052539	-0.354557	0.99654
144	BCP144	C120 - H123	0.272246	-0.987146	0.052664	-0.352115	1.004387
145	BCP145	C31 - Si125	0.119379	0.191116	0.123057	-0.198335	0.419291
146	BCP146	H71 - C126	0.002188	0.007783	0.001398	-0.00085	0.006745
147	BCP147	Si125 - C126	0.122423	0.171566	0.122785	-0.202678	0.443419
148	BCP148	C126 - H127	0.272227	-0.986492	0.052918	-0.352459	1.002069
149	BCP149	C126 - H128	0.274191	-1.003904	0.051522	-0.354021	0.992373
150	BCP150	C126 - H129	0.272293	-0.987911	0.052471	-0.35192	1.002731

Table 3.S5. Summary of AIM parameters for Et₃P=O–B¹⁰.

BCP #	Name	Atoms	Rho	DelSqRho	G	V	DI(A B)
1	BCP1	P1 - O6	0.215857	1.155459	0.459399	-0.629934	0.57308
2	BCP2	C64 - C90	0.268391	-0.775435	0.061746	-0.317351	0.999327
3	BCP3	O6 - F7	0.013702	0.072353	0.015061	-0.012034	0.056905
4	BCP4	F2 - C8	0.274422	0.296517	0.515877	-0.957626	0.723424
5	BCP5	F3 - C10	0.011091	0.049421	0.010211	-0.008066	0.034101

6	BCP6	C10 - C12	0.328275	-1.06574	0.115913	-0.498261	1.305878
7	BCP7	F4 - C9	0.011445	0.052045	0.010891	-0.008771	0.036101
8	BCP8	C12 - C29	0.334407	-1.098205	0.112144	-0.498839	1.30724
9	BCP9	C10 - B51	0.159423	-0.107943	0.143308	-0.313602	0.356082
10	BCP10	F15 - C28	0.269172	0.305927	0.506528	-0.936573	0.71771
11	BCP11	C8 - C10	0.329052	-1.06723	0.11559	-0.497988	1.335148
12	BCP12	F3 - C11	0.27043	0.306625	0.509372	-0.942088	0.714654
13	BCP13	C9 - B51	0.161281	-0.131966	0.140995	-0.314982	0.356227
14	BCP14	C9 - C11	0.32933	-1.070385	0.114417	-0.49643	1.313693
15	BCP15	F5 - C12	0.265979	0.318581	0.502334	-0.925023	0.711229
16	BCP16	F4 - C13	0.268921	0.313359	0.507618	-0.936897	0.717518
17	BCP17	C14 - B51	0.161526	-0.130078	0.141556	-0.315632	0.359427
18	BCP18	C14 - C18	0.330283	-1.072402	0.117406	-0.502912	1.335588
19	BCP19	F2 - C14	0.013418	0.058139	0.012379	-0.010223	0.049398
20	BCP20	C13 - C14	0.328528	-1.064859	0.113968	-0.494151	1.307557
21	BCP21	C12 - H35	0.006944	0.021781	0.004463	-0.003482	0.017065
22	BCP22	O6 - F15	0.013163	0.072924	0.014972	-0.011712	0.053127
23	BCP23	C9 - C28	0.327989	-1.058792	0.115955	-0.496608	1.325239
24	BCP24	C8 - C16	0.330871	-1.082368	0.10732	-0.485233	1.283582
25	BCP25	C11 - C17	0.332922	-1.090379	0.110434	-0.493462	1.303241
26	BCP26	F7 - C18	0.263514	0.330831	0.499612	-0.916515	0.710674
27	BCP27	C16 - C64	0.26391	-0.74881	0.061482	-0.310166	0.982298
28	BCP28	C22 - C28	0.332233	-1.088072	0.109413	-0.490844	1.293051
29	BCP29	C17 - C19	0.328201	-1.056451	0.108137	-0.480387	1.356535
30	BCP30	C19 - H20	0.290472	-1.175238	0.041678	-0.377166	0.954426
31	BCP31	C13 - C21	0.33424	-1.097587	0.111802	-0.498001	1.311928
32	BCP32	C19 - C22	0.328587	-1.057081	0.108963	-0.482197	1.366123
33	BCP33	C18 - C23	0.332221	-1.088834	0.109342	-0.490892	1.29215
34	BCP34	C16 - C24	0.329473	-1.061854	0.109496	-0.484455	1.372779
35	BCP35	C24 - C29	0.326949	-1.050238	0.107123	-0.476806	1.348065
36	BCP36	C24 - H25	0.290438	-1.175162	0.041613	-0.377015	0.955105
37	BCP37	C21 - C26	0.328068	-1.05673	0.107736	-0.479654	1.350863
38	BCP38	C23 - C26	0.329225	-1.060265	0.109492	-0.48405	1.371055
39	BCP39	C26 - H27	0.290552	-1.17575	0.041715	-0.377367	0.954121
40	BCP40	P1 - C30	0.18595	-0.244008	0.138939	-0.338879	0.592135
41	BCP41	F7 - H31	0.008518	0.040055	0.008018	-0.006022	0.026219
42	BCP42	C30 - H31	0.285839	-1.127922	0.04437	-0.37072	0.946521
43	BCP43	C33 - H34	0.279996	-1.073275	0.048667	-0.365653	0.970246

44	BCP44	C30 - H32	0.282375	-1.097699	0.045928	-0.36628	0.960451
45	BCP45	P1 - C33	0.185497	-0.241722	0.138634	-0.337698	0.598324
46	BCP46	C33 - H35	0.283171	-1.105514	0.045018	-0.366415	0.946856
47	BCP47	C30 - C36	0.252786	-0.687093	0.058891	-0.289556	1.027642
48	BCP48	C36 - H37	0.285914	-1.128323	0.04556	-0.373201	0.956567
49	BCP49	C36 - H38	0.284616	-1.115323	0.04671	-0.372251	0.95451
50	BCP50	C36 - H39	0.285028	-1.117941	0.046785	-0.373056	0.954092
51	BCP51	C8 - H42	0.004267	0.014188	0.002759	-0.001972	0.009719
52	BCP52	F7 - H42	0.005425	0.024985	0.004794	-0.003342	0.015451
53	BCP53	C33 - C40	0.252155	-0.685987	0.059602	-0.290701	1.021142
54	BCP54	C40 - H41	0.284964	-1.118302	0.046672	-0.37292	0.954032
55	BCP55	C40 - H42	0.289797	-1.162402	0.042949	-0.376499	0.933476
56	BCP56	C40 - H43	0.285572	-1.124003	0.046309	-0.373619	0.955778
57	BCP57	P1 - C44	0.186492	-0.247782	0.138899	-0.339743	0.595527
58	BCP58	F5 - H45	0.008115	0.037053	0.007418	-0.005572	0.02283
59	BCP59	C44 - H45	0.28529	-1.122655	0.044371	-0.369405	0.940192
60	BCP60	C44 - H46	0.280083	-1.072277	0.049237	-0.366542	0.96865
61	BCP61	C28 - H50	0.005862	0.018168	0.003667	-0.002793	0.015854
62	BCP62	C44 - C47	0.251468	-0.681494	0.05963	-0.289634	1.020393
63	BCP63	H48 - C77	0.003702	0.010949	0.002085	-0.001434	0.013769
64	BCP64	H45 - C97	0.005654	0.01589	0.003224	-0.002475	0.022609
65	BCP65	C47 - H48	0.285569	-1.123569	0.045898	-0.372689	0.946688
66	BCP66	C97 - H99	0.29016	-1.175638	0.042294	-0.378498	0.980271
67	BCP67	C47 - H49	0.284881	-1.118428	0.046816	-0.373239	0.960167
68	BCP68	C95 - C97	0.364004	-1.22834	0.14852	-0.604126	1.818516
69	BCP69	C47 - H50	0.289064	-1.156757	0.042868	-0.374925	0.932646
70	BCP70	O6 - B51	0.113436	0.65142	0.230713	-0.298571	0.221772
71	BCP71	C23 - C52	0.263975	-0.749017	0.060975	-0.309204	0.984137
72	BCP72	C52 - H53	0.284974	-1.121103	0.044458	-0.369193	0.930065
73	BCP73	C52 - H54	0.283763	-1.108098	0.045979	-0.368983	0.929676
74	BCP74	C21 - C55	0.263589	-0.747758	0.061012	-0.308963	0.982075
75	BCP75	C55 - H56	0.284954	-1.121461	0.044282	-0.368929	0.927386
76	BCP76	C55 - H57	0.285827	-1.124117	0.045557	-0.372143	0.933002
77	BCP77	C17 - C58	0.263611	-0.747556	0.061014	-0.308917	0.982083
78	BCP78	C58 - H59	0.284749	-1.119318	0.044559	-0.368947	0.928188
79	BCP79	C58 - H60	0.285705	-1.12303	0.045638	-0.372033	0.933191
80	BCP80	C22 - C61	0.263893	-0.748434	0.061141	-0.30939	0.983688
81	BCP81	C61 - H62	0.286228	-1.131554	0.043896	-0.370681	0.929456

82	BCP82	C61 - H63	0.283959	-1.109674	0.045979	-0.369377	0.931388
83	BCP83	C64 - H65	0.284296	-1.11211	0.045992	-0.370012	0.933242
84	BCP84	C64 - H66	0.287139	-1.139181	0.04351	-0.371815	0.928976
85	BCP85	C29 - C67	0.263833	-0.748191	0.061283	-0.309613	0.983018
86	BCP86	C67 - H68	0.284252	-1.112426	0.045743	-0.369593	0.931634
87	BCP87	C67 - H69	0.286934	-1.137669	0.043515	-0.371448	0.92919
88	BCP88	C58 - C70	0.268952	-0.778908	0.061765	-0.318256	1.001112
89	BCP89	C70 - H71	0.291541	-1.187291	0.039468	-0.375758	0.954571
90	BCP90	C70 - C72	0.364742	-1.233052	0.149088	-0.606439	1.835258
91	BCP91	C72 - H73	0.288341	-1.160713	0.042587	-0.375353	0.976817
92	BCP92	C72 - H74	0.290544	-1.179158	0.04201	-0.378809	0.981573
93	BCP93	C61 - C75	0.269185	-0.780322	0.062075	-0.31923	1.000343
94	BCP94	C75 - H76	0.289944	-1.171754	0.040838	-0.374614	0.958466
95	BCP95	C75 - C77	0.364445	-1.230846	0.148857	-0.605426	1.821349
96	BCP96	C97 - H98	0.289569	-1.172957	0.041355	-0.375948	0.970052
97	BCP97	C77 - H78	0.28928	-1.169853	0.041761	-0.375984	0.972548
98	BCP98	C77 - H79	0.289745	-1.171586	0.042729	-0.378354	0.981543
99	BCP99	C52 - C80	0.269426	-0.78172	0.061889	-0.319208	1.000783
100	BCP100	C80 - H81	0.290586	-1.17814	0.040275	-0.375084	0.958991
101	BCP101	C80 - C82	0.364841	-1.2335	0.149048	-0.606471	1.826344
102	BCP102	C82 - H83	0.288384	-1.161228	0.042563	-0.375433	0.974995
103	BCP103	C82 - H84	0.290132	-1.175155	0.042458	-0.378705	0.982699
104	BCP104	C55 - C85	0.269082	-0.779759	0.061866	-0.318672	1.001437
105	BCP105	C85 - H86	0.291361	-1.185269	0.039739	-0.375795	0.955873
106	BCP106	C85 - C87	0.364728	-1.232995	0.149063	-0.606374	1.834817
107	BCP107	C87 - H88	0.288421	-1.161475	0.042519	-0.375407	0.976548
108	BCP108	C87 - H89	0.290447	-1.178143	0.042131	-0.378798	0.981995
109	BCP109	H42 - C90	0.002025	0.006261	0.001145	-0.000724	0.004853
110	BCP110	C90 - H91	0.289278	-1.165039	0.04154	-0.374341	0.960614
111	BCP111	C90 - C92	0.364919	-1.233826	0.149286	-0.607029	1.827557
112	BCP112	C92 - H93	0.290185	-1.178859	0.040874	-0.376463	0.969623
113	BCP113	C92 - H94	0.290524	-1.179289	0.04199	-0.378803	0.980982
114	BCP114	C67 - C95	0.268933	-0.778749	0.062156	-0.319	1.000391
115	BCP115	C95 - H96	0.289607	-1.168711	0.041008	-0.374194	0.95938

Table 3.S6. Summary of AIM parameters for Et₃P=O–B¹¹.

BCP #	Name	Atoms	Rho	DelSqRho	G	V	DI(A B)
1	BCP1	F4 - H37	0.006625	0.028752	0.005612	-0.004037	0.021725

2	BCP2	F2 - O8	0.011648	0.059697	0.012231	-0.009537	0.048049
3	BCP3	F7 - H39	0.003922	0.018323	0.003394	-0.002208	0.009922
4	BCP4	P1 - O8	0.216852	1.16701	0.462486	-0.63322	0.662457
5	BCP5	P1 - C28	0.180713	-0.306331	0.112835	-0.302253	0.657618
6	BCP6	F4 - O8	0.011596	0.059424	0.012173	-0.00949	0.047729
7	BCP7	F7 - O8	0.011932	0.061002	0.012522	-0.009794	0.049531
8	BCP8	P1 - C35	0.180717	-0.306307	0.112853	-0.302282	0.657275
9	BCP9	O8 - B9	0.110448	0.576365	0.212903	-0.281714	0.250586
10	BCP10	F2 - C10	0.268653	0.086143	0.450512	-0.879489	0.767252
11	BCP11	C14 - C15	0.319858	-0.95818	0.115092	-0.469728	1.316938
12	BCP12	C10 - C15	0.319572	-0.95563	0.116752	-0.472412	1.310365
13	BCP13	C10 - C11	0.327197	-1.005712	0.115232	-0.481891	1.322136
14	BCP14	C13 - C14	0.32538	-0.997915	0.112404	-0.474288	1.31012
15	BCP15	C10 - H32	0.005384	0.0167	0.003276	-0.002376	0.015047
16	BCP16	C11 - C12	0.32005	-0.962481	0.111209	-0.463038	1.380485
17	BCP17	C12 - C13	0.321721	-0.970519	0.112553	-0.467736	1.395442
18	BCP18	F3 - C14	0.279335	0.080074	0.472676	-0.925335	0.781902
19	BCP19	B9 - C15	0.160771	-0.201766	0.121549	-0.29354	0.415422
20	BCP20	F6 - C15	0.0133	0.055384	0.011731	-0.009615	0.050887
21	BCP21	F3 - C16	0.013251	0.055216	0.011684	-0.009564	0.050251
22	BCP22	C17 - H39	0.005357	0.016618	0.003258	-0.002361	0.014977
23	BCP23	F5 - C22	0.013308	0.05538	0.011729	-0.009614	0.05061
24	BCP24	B9 - C16	0.160918	-0.201401	0.121839	-0.294028	0.416089
25	BCP25	C35 - H37	0.279422	-1.04754	0.047089	-0.356062	0.942058
26	BCP26	F4 - C17	0.268593	0.087171	0.45062	-0.879447	0.766653
27	BCP27	C16 - C21	0.319888	-0.958297	0.115167	-0.469909	1.318546
28	BCP28	C16 - C17	0.319668	-0.956445	0.116736	-0.472583	1.309397
29	BCP29	C17 - C18	0.32737	-1.006612	0.115406	-0.482465	1.322791
30	BCP30	C20 - C21	0.325252	-0.997307	0.112268	-0.473863	1.309264
31	BCP31	C18 - C19	0.319931	-0.961902	0.111108	-0.462692	1.379567
32	BCP32	C19 - C20	0.321809	-0.970927	0.112631	-0.467995	1.396282
33	BCP33	F5 - C21	0.279441	0.0799	0.472875	-0.925775	0.781958
34	BCP34	B9 - C22	0.161059	-0.202213	0.121854	-0.294261	0.416095
35	BCP35	F6 - C23	0.279371	0.081091	0.47299	-0.925707	0.781833
36	BCP36	C22 - C27	0.319724	-0.956609	0.116811	-0.472775	1.310469
37	BCP37	C22 - C23	0.320068	-0.95941	0.115204	-0.470261	1.317067
38	BCP38	C23 - C24	0.32544	-0.998283	0.112462	-0.474494	1.310252
39	BCP39	F7 - H44	0.006761	0.029416	0.005749	-0.004145	0.022009

40	BCP40	C26 - C27	0.327195	-1.005661	0.115255	-0.481925	1.322087
41	BCP41	C24 - C25	0.321699	-0.97036	0.112549	-0.467688	1.395458
42	BCP42	C25 - C26	0.319983	-0.962057	0.111181	-0.462877	1.380441
43	BCP43	F7 - C27	0.26852	0.086941	0.450406	-0.879077	0.766732
44	BCP44	F2 - H30	0.006545	0.028406	0.005539	-0.003976	0.021491
45	BCP45	C28 - H29	0.275246	-1.010218	0.049583	-0.35172	0.963136
46	BCP46	C28 - C31	0.243419	-0.599429	0.062521	-0.2749	1.028116
47	BCP47	C28 - H30	0.279357	-1.046983	0.047107	-0.35596	0.94224
48	BCP48	F4 - H32	0.004148	0.019425	0.003611	-0.002365	0.010595
49	BCP49	C31 - H32	0.283926	-1.088325	0.044223	-0.360528	0.92901
50	BCP50	C31 - H33	0.280553	-1.055406	0.047768	-0.359388	0.956035
51	BCP51	C11 - H55	0.285274	-1.105853	0.044134	-0.364731	0.956453
52	BCP52	C12 - H56	0.287656	-1.125723	0.042607	-0.366644	0.961019
53	BCP53	C31 - H34	0.280674	-1.054995	0.047832	-0.359412	0.951723
54	BCP54	C35 - H36	0.275272	-1.010492	0.049562	-0.351747	0.963375
55	BCP55	C35 - C38	0.24332	-0.598857	0.06249	-0.274695	1.027744
56	BCP56	C38 - H41	0.280661	-1.054865	0.04784	-0.359395	0.951715
57	BCP57	C38 - H39	0.283885	-1.087974	0.044237	-0.360468	0.92926
58	BCP58	C38 - H40	0.280596	-1.055769	0.047766	-0.359474	0.955948
59	BCP59	P1 - C42	0.180743	-0.306535	0.112844	-0.302321	0.656654
60	BCP60	F2 - H46	0.00405	0.018964	0.00352	-0.002298	0.010263
61	BCP61	C27 - H46	0.005397	0.016767	0.003293	-0.002394	0.015476
62	BCP62	C42 - H43	0.275282	-1.010542	0.049575	-0.351785	0.963262
63	BCP63	C42 - H44	0.279463	-1.047765	0.047097	-0.356136	0.941854
64	BCP64	C42 - C45	0.243382	-0.599188	0.06251	-0.274817	1.027671
65	BCP65	C45 - H46	0.283911	-1.088108	0.044251	-0.360529	0.929027
66	BCP66	C45 - H47	0.280536	-1.055291	0.047769	-0.35936	0.956035
67	BCP67	C45 - H48	0.280667	-1.054946	0.047827	-0.359391	0.951569
68	BCP68	C18 - H49	0.285283	-1.105937	0.044131	-0.364745	0.956435
69	BCP69	C19 - H50	0.287662	-1.125797	0.042596	-0.366641	0.960997
70	BCP70	C20 - H51	0.286005	-1.112662	0.04342	-0.365006	0.954315
71	BCP71	C26 - H52	0.285275	-1.105805	0.04415	-0.364751	0.956541
72	BCP72	C25 - H53	0.287656	-1.125708	0.042614	-0.366655	0.961101
73	BCP73	C24 - H54	0.285997	-1.112611	0.04343	-0.365013	0.954438
74	BCP74	C13 - H57	0.286013	-1.112702	0.043433	-0.365042	0.954423

3.5.8. References for supporting information

- S1. (a) L. Greb, C.-G. Daniliuc, K. Bergander, J. Paradies, *Angew. Chem. Int. Ed.* **2013**, 52, 5876. (b) T. A. Gazis, B. A. J. M. Thaker, D. Willcox, D. M. C. Ould, J. Wenz, J. M. Rawson, M. S. Hill, T. Wirth, R. L.

- Melen, *Chem. Commun.* **2020**, 56, 3345.
- S2. K. Murakami, K. Hirano, H. Yorimitsu, K. Oshima, *Angew. Chem. Int. Ed.* **2008**, 47, 5833.
- S3. T. D. Yarwood, A. J. Waring, P. L. Coe, *J. Fluorine Chem.* **1996**, 78, 113.
- S4. M. A. Beckett, G. C. Strickland, J. R. Holland, K. S. Varma, *Polymer* **1996**, 37, 4629.
- S5. F. Neese, F. Wennmohs, U. Becker, C. Riplinger, *J. Chem. Phys.* **2020**, 152, 224108.
- S6. (a) S. Grimme, J. G. Brandenburg, C. Bannwarth, A. Hansen, *J. Chem. Phys.* **2015**, 143, 054107. (b) A. T. Cavasin, A. Hillisch, F. Uellendahl, S. Schneckener, A. H. Göller, *J. Chem. Inf. Model.* **2018**, 58, 1005.
- S7. (a) P. Erdmann, L. Greb, *ChemPhysChem* **2021**, 22, 935. (b) P. Erdmann, J. Leitner, J. Schwarz, L. Greb, *ChemPhysChem* **2020**, 21, 987.
- S8. Gaussian 16, Revision C.01, M. J. Frisch, G. W. Trucks, H. B. Schlegel, G. E. Scuseria, M. A. Robb, J. R. Cheeseman, G. Scalmani, V. Barone, G. A. Petersson, H. Nakatsuji, X. Li, M. Caricato, A. V. Marenich, J. Bloino, B. G. Janesko, R. Gomperts, B. Mennucci, H. P. Hratchian, J. V. Ortiz, A. F. Izmaylov, J. L. Sonnenberg, D. Williams-Young, F. Ding, F. Lipparini, F. Egidi, J. Goings, B. Peng, A. Petrone, T. Henderson, D. Ranasinghe, V. G. Zakrzewski, J. Gao, N. Rega, G. Zheng, W. Liang, M. Hada, M. Ehara, K. Toyota, R. Fukuda, J. Hasegawa, M. Ishida, T. Nakajima, Y. Honda, O. Kitao, H. Nakai, T. Vreven, K. Throssell, J. A. Montgomery, Jr., J. E. Peralta, F. Ogliaro, M. J. Bearpark, J. J. Heyd, E. N. Brothers, K. N. Kudin, V. N. Staroverov, T. A. Keith, R. Kobayashi, J. Normand, K. Raghavachari, A. P. Rendell, J. C. Burant, S. S. Iyengar, J. Tomasi, M. Cossi, J. M. Millam, M. Klene, C. Adamo, R. Cammi, J. W. Ochterski, R. L. Martin, K. Morokuma, O. Farkas, J. B. Foresman, and D. J. Fox, Gaussian, Inc., Wallingford CT, 2016.
- S9. S. Kozuch, J. M. Martin, *Phys. Chem. Chem. Phys.* **2011**, 13, 20104.
- S10. J. Zheng, X. Xu, D. G. Truhlar, *Theor. Chem. Acc.* **2011**, 128, 295.
- S11. (a) A. D. Becke, E. R. Johnson, *J. Chem. Phys.* **2005**, 122, 154104. (b) S. Grimme, J. Antony, S. Ehrlich, H. Krieg, *J. Chem. Phys.* **2010**, 132, 154104. (c) E. R. Johnson, A. D. Becke, *J. Chem. Phys.* **2005**, 123, 024101. (d) S. Grimme, S. Ehrlich, L. Goerigk, *J. Comput. Chem.* **2011**, 32, 1456.
- S12. K. Eichkorn, O. Treutler, H. Öhm, M. Häser, R. Ahlrichs, *Chem. Phys. Lett.* **1995**, 242, 652.
- S13. F. Weigend, *Phys. Chem. Chem. Phys.* **2006**, 8, 1057.
- S14. a) H-La, Hf-Rn: A. Hellweg, C. Hättig, S. Höfener, W. Klopper, *Theor. Chem. Acc.* **2007**, 117, 587; b) Ce-Lu: J. Chmela, M. E. Harding, *Mol. Phys.* **2018**, 116, 1523.
- S15. V. Barone, M. Cossi, *J. Phys. Chem. A* **1998**, 102, 1995.
- S16. P. Erdmann, L. Greb, *Angew. Chem. Int. Ed.* **2022**, 61, e202114550.
- S17. AIMAll (Version 19.10.12), Todd A. Keith, TK Gristmill Software, Overland Park KS, USA, 2019 (aim.tkgristmill.com)
- S18. SambVca 2.0: <https://www.molnac.unisa.it/OMtools/sambvca2.0/>. L. Falivene, R. Credendino, A. Poater, A. Petta, L. Serra, R. Oliva, V. Scarano, L. Cavallo, *Organometallics*, **2016**, 35, 2286.
- S19. M. H. Reineke, M. D. Sampson, A. L. Rheingold, C. P. Kubiak, *Inorg. Chem.* **2015**, 54, 3211.
- S20. (a) H. Höpfl, *J. Organomet. Chem.* **1999**, 581, 129. (b) S. Toyota, M. Ōki, *Bull. Chem. Soc. Jpn.* **1992**, 65, 1832.

Conclusion

In this thesis, I have discussed the strategies for generation of frustrated Lewis pairs (FLPs) from classical Lewis adduct (CLAs) induced by conformational isomerization. FLPs have been often reported to decompose quickly under ambient conditions, which should restrict their facile use in organic synthesis. It should be thus worthwhile to develop a strategy to generate FLPs from CLAs effectively, because such a 'frustration revival strategy' can further expand the utility and applications of FLPs in organic chemistry. In the context of the frustration revival strategy, our group has developed the thermal revival system of FLPs from *N*-phosphine-oxide-substituted imidazolylienes (PoxIm)s–borane adduct by rotation of the *N*-phosphinoyl moiety. However, details on reaction mechanisms for the generation of FLP species from the PoxIm–borane adduct remained unclear.

In Chapter 1, I have studied the detailed reaction mechanism on revival of FLPs from PoxIm–borane adducts. The detailed mechanistic studies revealed that FLPs are generated through the steric repulsion between carbene and borane induced by the rotation of phosphinoyl moiety. The rotation occurs after borane was transferred to oxygen from carbene, and the heterolytic cleavage of H₂ proceeds between carbene and borane.

In Chapter 2, I focused on the conformational isomerization of triarylboranes, as Lewis Acids, comprising FLPs and CLAs. I have then developed a strategy to control and modify their Lewis acidity by focusing on remote back strain to regulate the generation of FLPs and perform the FLP-catalyzed hydrogenation of carbonyl compounds using a 1:1:1 molar ratio of gaseous mixture of H₂, CO, and CO₂. The hydrogenation reaction proceeded efficiently when using the combination of B(2,6-F₂-3,5-R₂-C₆H)₃ (R = Cl and Br) and 4-methyltetrahydropyran (MTHP) to generate FLPs.

In Chapter 3, the remote back strain has been clarified by experimental and theoretical studies. As a result, remote back strain is consist of steric repulsion and NCIs generated between *meta*-substituents on Ar groups in triarylborane. In addition, hydrogenation of quinoline with a 1:1:1 molar ratio of gaseous mixture of H₂, CO, and CO₂ has been successfully demonstrated by employing triarylborane designed with the concept of remote back strain.

From these studies, I am confident that the approaches to FLPs from classical Lewis adducts CLAs can broaden the scope and applications of FLPs in organic chemistry. I trust that the increased utility and applications of FLPs as catalysts and activators for small molecules would significantly advance the progress of organic chemistry.

List of Publications

1. “A Boron-Transfer Mechanism Mediating the Thermally Induced Revival of Frustrated Carbene–Borane Pairs from Their Shelf-Stable Adducts”
Yoichi Hoshimoto, Mahiro Sakuraba, Takuya Kinoshita, Masaki Ohbo, Manussada Ratanasak, Jun-ya Hasegawa, Sensusuke Ogoshi
Commun. Chem. **2021**, 4, 137.
2. “Remote Back Strain: A Strategy for Modulating the Reactivity of Triarylboranes”
Mahiro Sakuraba, Taichi Morishita, Taiki Hashimoto, Sensusuke Ogoshi, Yoichi Hoshimoto
Synlett **2023**, 34, 2187.
3. “Strategic Use of Crude H₂ for the Catalytic Reduction of Carbonyl Compounds”
Mahiro Sakuraba, Sensusuke Ogoshi, Yoichi Hoshimoto
Tetrahedron Chem, DOI: 10.1016/j.tchem.2023.100059.

Supplementary Publications

1. “Complexation between MOTf (M = Li and Na) and *N*-Phosphine Oxide-substituted Imidazolyliidenes via Coordination of the *N*-Phosphoryl Groups”
Takuya Kinoshita, Mahiro Sakuraba, Yoichi Hoshimoto, Sensusuke Ogoshi
Chem. Lett. **2019**, 48, 230-233.